University of Silesia
Faculty of Science and Technology
PhD thesis

Transport properties of disordered quantum chains with many-body interactions

Author:
Maciej Kozarzewski
no. 8283

PhD supervisor:
prof. dr hab. Marcin Mierzejewski

Katowice 2020

Słowa kluczowe: numerical methods, MBL,

Ja niżej podpisany: Maciej Kozarzewski,

autor pracy dyplomowej pt.

"Transport properties of disordered quantum chains with many-body interactions"

Numer albumu: 8283

Student Wydziału Nauk Ścisłych i Technicznych Uniwersytetu Śląskiego w Katowicach Kierunku Fizyka

Oświadczam, że ww. praca dyplomowa:

- została przygotowana samodzielnie

- nie narusza praw autorskich w rozumieniu ustawy z dnia 4 lutego 1994 r. o prawie autorskim i prawach pokrewnych (tekst jednolity Dz.U. z 2006 r. nr 90, poz.631, z późn. zm.) oraz dóbr osobistych chronionych prawem cywilnym,

- nie zawiera danych i informacji, które uzyskałem w sposób niedozwolony, - nie była podstawą nadania dyplomu uczelni wyższej lub tytułu zawodowego, ani mnie, ani innej osobie.

Oświadczam, że wyrażam zgodę na przetwarzanie mojej pracy dyplomowej, a także na przechowywanie jej w celach realizowanej procedury antyplagiatowej w bazie cyfrowej Systemu Antyplagiatowego.

Oświadczam również, że treść pracy zapisanej na przekazanym przeze mnie nośniku elektronicznym jest identyczna z treścią zawartą w wydrukowanej wersji pracy.

Jestem świadomy odpowiedzialności karnej za składanie fałszywego oświadczenia.

Abstract

Many-body localized (MBL) systems have recently attracted a lot of attention. It was known that they exhibit many unusual behaviours but for a long time they were a subject of only theoretical (or numerical) research. Few years ago it became possible to create such systems in laboratory and experimentally verify their properties, at the same time stimulating more theoretical works.

This dissertation concerns transport properties of one dimensional MBL systems. We focus on 1D system of spinless fermions with disorder driven by external magnetic field. That field causes Bloch oscillations but we show that for strong disorder the frequency is constant and independent of any other parameters. Moreover, the current decay is a result of destructive interference of currents flowing between the neighboring sites. Interestingly, those local currents do not exhibit any signs of damping, indicating that MBL prevented that system from heating.

Then we switch to spin-$\frac{1}{2}$ systems, namely disordered Hubbard model. There is an ongoing discussion whether the disorder in charge sector can cause full localization. We create an effective spin model assuming that charges are frozen. Within this effective model we show that full MBL cannot exist without introducing disorder also in spin sector. We investigate the energy transport and find that it is supressed. While we cannot exclude that it is a finite-size effect, it still contrasts with the relatively fast spin relaxation.

Abstrakt

Systemy z lokalizacją wielociałową (ang. many-body localization, w skrócie MBL) zyskały ostatnio dużo uwagi. Już wcześniej wiedziano, że wykazują one wiele nietypowych zachowań, ale przez długi czas były tematem jedynie teoretycznych (lub numerycznych) badań. Kilka lat temu możliwe stało się tworzenie takich układów w laboratorium i eksperymentalne zweryfikowanie ich własności, co z kolei stymulowało powstawanie kolejnych prac teoretycznych.

Rozprawa dotyczy własności transportowych jednowymiarowych układów MBL. Skupiamy się na jednowymiarowym układzie bezspinowych fermionów z nieporządkiem, do którego przyłożono zewnętrzne pole magnetyczne. To pole wywołuje oscylacje Blocha, ale pokazujemy, że dla silnego nieporządku ich częstotliwość jest stała i niezależna od pozostałych parametrów. Co więcej, zanik prądu jest wynikiem destruktywnej interferencji prądów płynących między sąsiednimi węzłami. Co ciekawe, te lokalne prądy nie wykazują żadnego tłumienia, co wskazuje na to, że MBL zapobiega nagrzewaniu się takich układów.

Następnie przenosimy się do układów ze spinem $\frac{1}{2}$, konkretnie modelu Hubbarda z nieporządkiem. Trwa ciągła dyskusja na temat tego, czy nieporządek w sektorze ładunków może wywołać pełną lokalizację. Tworzymy efektywny model spinowy zakładając, że ładunki są nieruchome. W ramach modelu efektywnego pokazujemy, że faktycznie pełna lokalizacja nie jest możliwa bez wprowadzania dodatkowego nieporządku w sektorze spinowym. Badamy też transport energii i okazuje się, że jest on stłumiony. Wprawdzie nie możemy wykluczyć, że jest to efekt skończonego rozmiaru układu, ale i tak kontrastuje to z relatywnie szybką relaksacją spinu.

Contents

Chapter 1

Introduction

Band theory successfully describes electrical properties of various solid state materials. It can be derived basing on a few different models, probably most known being nearly-free electron model or tight binding model. Independently of the details, in order to predict the band structure it is necessary to make a few simplifications. Typically we assume the thermodynamic limit, i.e. an infinite (or at least macroscopic) size of a system so that the bands are sufficiently densely filled with energy levels and we can treat them as continuous. We require the material to be homogeneous, so we have to be careful with applications of band theory if there are for example doping particles. Another interesting example is what can happen if we consider boundary conditions in more detail. In the recent years in experiments we observed topological insulators [1] - materials that conduct on the surface but not in the bulk. The last assumption we mention here is the perturbative character of many-body interactions.

1.1 Mott insulators

In 1937 an article was written stating that certain transition-metal oxides are insulators although the band theory predicted that they should be conductors [2]. It was later explained by Mott [3] on the example of NiO that Coulomb repulsion of 3d electrons leads to formation of the energy gap. As the insulating properties depend on the ratio between interactions and hopping integral, it was hinted that perhaps at higher

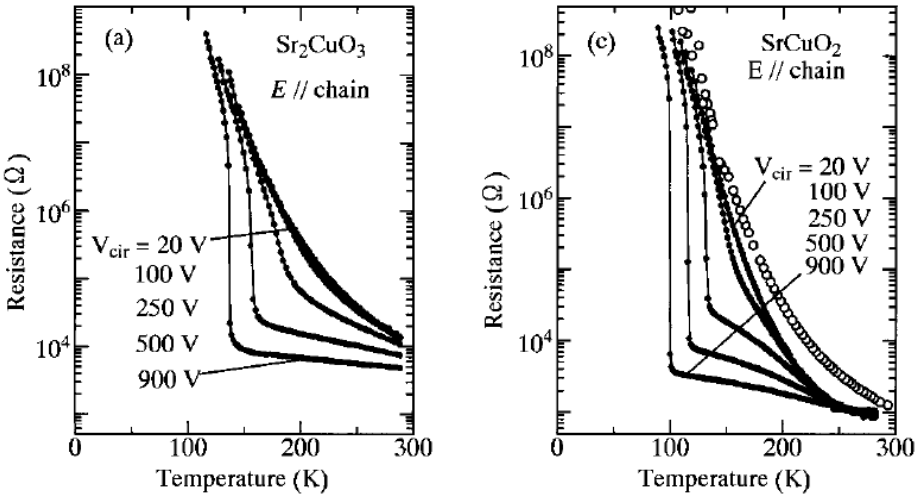

Figure 1.1: Resistance of a sample as a function of temperature for various voltages V_{cir}. Taken from Phys. Rev. B, **62** 7015 (2000).

temperatures such materials could became metals or semi-conductors. This opened entire research direction focused on the metal-insulator transition that occurs when some parameters are varied. One of the first experiments on Sr_2CuO_3 and $SrCuO_2Y$ were performed in 2000 [4]. It is of a particular interest as those compounds were effectively one-dimensional, like most systems that are investigated numerically. Authors subjected samples to external electric field in the form of short pulses (to minimize Joule heating) while changing temperature. It was observed that below some critical temperature the measured sample resistance increased by several orders of magnitude as a result of applied external field and this transition was more abrupt for stronger fields (up to 900V). Other metal-insulator transition experiments were performed in subsequent years [5] [6] [7] with similar results.

1.2 Anderson localization

Another example of a system that escapes the description of the band theory is an Anderson insulator first described in 1958 [8]. Anderson studied a single particle in three dimensional (3D) lattice with disorder and various forms of hopping terms. Disorder enters as random shifts within range $[-W, W]$ to the on-site energies. Hopping, denoted

as $V(r)$, was not restricted to the nearest neighbors. It was found that if $V(r)$ decays faster than $1/r^3$ and the ratio of interaction to disorder strengths is above some critical value, the system undergoes a transition from diffusive phase into localized one. This problem was later studied in 1D and 2D to find that there is no phase transition - all states are localized for arbitrarily small disorder W [9].

One dimensional case can be analytically proven to localize, but for higher dimensions only approximate solutions exist. Anderson localization in 2D and 3D was a subject of numerical simulations as early as in 1977 [10, 11] that confirmed theoretical predictions and additionally allowed for precise investigation of the critical disorder strength.

Consider following single particle tight binding Anderson model

$$H = -t_h \sum_j (c^\dagger_{j+1} c_j + H.c.) + \sum_j \epsilon_j c^\dagger_j c_j, \tag{1.1}$$

where disorder enters as ϵ_j which are random numbers drawn from a uniform distribution in the range $[-W, W]$. In one dimension, it can be solved to find that all eigenstate wavefunctions are bound to some specific regions of the system and beyond them they decay exponentially. The rate of decay is summarized in a factor we now call Anderson localization length ξ and depends on the disorder strength W. In general, in such localized systems diffusion on distances larger than ξ is suppressed. Presence of the disorder causes particle to localize despite that in the classical understanding it has sufficient energy to freely move within the system. Additionally, if the disorder is strong enough, even the quantum tunneling is unlikely, resulting in the wavefunctions being localized.

Anderson localization was observed in the experiments with photons [12, 13, 14, 15, 16]. Photons are particularly appealing as they do not interact with each other and their diffusion through disordered material obeys the same laws as the charge current flowing in a resistor. In [12] the disorder was created by using powder of a semiconductor (gallium arsenide). Authors measured transmission coefficient vs thickness of the scattering material for different sizes of powder particles. In normal conditions they are inversely proportional to each other. However once the average diameter of a particle was decreased below $1\mu m$ the relation changed to exponential decay as expected for

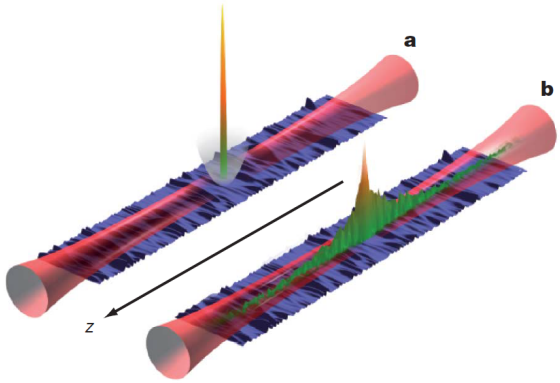

Figure 1.2: On **a** Bose-Einstein condensate (BEC) is trapped in magnetic field. On **b** the trap is switched off and the particles are free to diffuse in the system. Taken from Nature volume **453**, pages 891–894 (2008).

the localized phase, which means that material stopped "conducting" light.

Anderson localization was also observed in systems with matter particles [17, 18, 19]. While in general it is difficult (or impossible) to eliminate interactions between particles, it can be mitigated by lowering their density [19]. In this particular experiment, particles are trapped in some place in the system. The disorder was realised by using optical speckle field [20]. At $t = 0$ the trap is switched off and the particles are allowed to spread over the lattice. During this process, authors were directly measuring their density by irradiating the atoms and capturing fluorescing image. In the localized phase it was clearly visible that particles remained close to the original site, and their distribution followed exponential decay. It was possible to estimate the localization length exactly like it was defined few paragraphs earlier.

Additionally, Anderson localization was found in other systems such as microwaves [21] or even sound waves [22].

1.3 Many-body localization

The topic of adding interactions to Anderson insulator was already studied in [23]. In general, it is expected that interactions create a possibility for information exchange within the system even if the mobility of individual particles is greatly reduced (or not

possible). Because of this, we encounter a transition from ergodic phase into localized one, depending on the ratio between disorder and interactions.

Combining interactions and disorder takes us to the many-body localization (MBL) phenomenon. It is believed that MBL systems are the only generic physical systems that do not thermalize [24, 25]. Perhaps the best studied case is the following Heisenberg model with random magnetic field

$$H = J \sum_i \bar{S}_i \bar{S}_{i+1} + \sum_i \epsilon_i S_i^z, \tag{1.2}$$

where ϵ_i are drawn from a uniform distribution $[-W, W]$. This model can be mapped on the interacting spinless fermions model using the Jordan-Wigner transformation [26].

$$H = t_h \sum_j (c_{j+1}^\dagger c_j + c_j^\dagger c_{j+1}) + V \sum_j \hat{n}_j \hat{n}_{j+1} + \sum_j \hat{n}_j \epsilon_j, \tag{1.3}$$

where $t_h = \frac{J}{2}$ and $V = J$. If we take $V = 0$, the model reduces to Anderson insulator which has all states localized. By increasing the interactions the system changes from MBL to ergodic. On the other hand, with fixed V, for $W = 0$ the system is integrable and by increasing the disorder the system transits to MBL phase.

This MBL transition was originally investigated in [27] and later in [28, 29, 30] using the method called level statistics. If we define $\delta_n = E_{n+1} - E_n$ and

$$r_n = \frac{min(\delta_n, \delta_{n+1})}{max(\delta_n, \delta_{n+1})}, \tag{1.4}$$

it can be shown that there are two special cases for which the average over all energy levels $r = \langle r_n \rangle$ can be calculated. Ergodic systems have Wigner-Dyson statistics with numerically established value of $r \approx 0.5307$ [31] while in the limit of strong disorder (i.e. in the MBL regime) it changes to Poisson distribution with $r = 2\ln(2) - 1 \approx 0.3863$. Originally, the transition to MBL phase was considered to occur for $W \approx 3.5$ [29]. The exact position of the transition is still debated to this day, as shown in numerous works for various Hamiltonians [32, 33, 34, 35] and for disorder distributions other than uniform [36]. However, for uniformly distributed disorder, most of the time we can expect the transition to be somewhere around $W = 3$ or $W = 4$. While we focused here on 1D systems, there are also works that confirm the existence of MBL phase in

higher dimensions [37]. The level statistics method became very useful for the purpose of finding MBL transitions, and is still being studied [38, 39].

In the rest of this section we will discuss the most characteristic properties of MBL phase.

1.3.1 Absence of thermalization

In statistical physics we consider a physical system coupled to external reservoir so they can both exchange energy. Such system evolves in time towards thermal state where it reaches thermal equilibrium with the environment. This process erases the information about the initial conditions. System's thermal state can be entirely described by macroscopic parameters such as pressure, temperature, etc. as opposed to having to fully specify the initial quantum state of every particle or the initial many-body wave-function.

On the other hand, an isolated quantum system undergoes unitary time evolution which preserves the information about the initial conditions. What we do here is that we focus on a specific part of the system, treating the rest as the environment. If we define some few-body observables on that part, then we can ask if the memory of the initial conditions is "visible" in measurements of those observables. By "few-body" we mean an operator acting on $n \ll N$ particles, much smaller than total number of particles N.

Eigenstate thermalization hypothesis (ETH) introduced in [40, 41] formulates two conditions on the matrix elements of an observable expressed in the eigenbasis of a Hamiltonian. It states that diagonal elements $\langle n|\hat{O}|n\rangle = O(E)$ are smooth function of the eigenstate energy E and $O(E)$ matches the microcanonical expectation value of that observable at energy E. On the other hand, off-diagonal elements are functions of average energy and difference between energy levels $\langle m|\hat{O}|n\rangle = f_O((E_m + E_n)/2, E_m - E_n)R_{mn}$ multiplied by random number with zero mean and unit variance. They are not only much smaller than diagonal elements but also they exponentially vanish in the limit of infinite system size and for long time evolution their contributions tend to cancel out. While there is no formal proof of ETH, it was tested numerically in various

systems [42, 43, 44, 45].

In the Anderson model, lack of thermalization is associated with the fact that strong disorder prevents diffusive transport so the two parts of the system cannot exchange energy in any way. Later it was confirmed that localization occurs also in the interacting systems [24] hence they also will not thermalize. Because MBL retain information of initial conditions such systems are appealing candidates to be used in quantum computers [46].

1.3.2 Entanglement entropy

If we divide the system into two disjoint parts A and B then in the pure state $|n\rangle$ we can calculate following reduced density matrix $\rho_A = Tr_B(|n\rangle \langle n|)$ by tracing over subsystem B. Then the von Neumann entropy is defined as $S(|n\rangle) = -Tr(\rho_A \ln \rho_A)$. For high temperature in the ETH phase, entanglement entropy (EE) exhibits volume scaling with the size of the subsystem A [47, 48]. On the other hand, MBL systems have much smaller EE with different, area scaling [49, 50]. Obviously, previous statements hold only if $L_A \ll L_B$ as otherwise the entropy scaling would start to saturate. Those properties can be observed in experiments and in theory could be used to distinguish the two phases [51, 52].

Another aspect of entanglement entropy in the context of MBL is its change in time. For Anderson model, it is quickly bounded by a constant but for interacting systems we observe unbounded logarithmic growth of entropy [48, 53, 54, 55, 56, 57]. Once again, it assumes infinite system size as otherwise the growth will be limited to a finite value. The anomalously slow growth of entropy is also connected to the fact that localization prevents transport in the system. While the unbounded logarithmic growth was mainly observed in numerical simulations, for some kinds of systems it was possible to predict this behaviour theoretically [55], at least in the limit of weak interactions.

1.3.3 Local integrals of motion

The anomalous properties of MBL phase can be best explained by the presence of local integrals of motion (LIOM) and what comes from it, many local conservation laws. We consider following local operator I_α, in literature often called "logical bit" or "l-bit" [58, 59]. The name originates from the fact that it has binary spectrum. It was suggested that now we can rewrite MBL Hamiltonian using l-bits in the form of a series expansion

$$H = h_0 + \sum_\alpha h_\alpha I_\alpha + \sum_{\alpha,\beta} h_{\alpha,\beta} I_\alpha I_\beta + \sum_{\alpha,\beta,\gamma} h_{\alpha,\beta,\gamma} I_\alpha I_\beta I_\gamma + \dots . \tag{1.5}$$

All I_α commute with each other and with the Hamiltonian. The set is complete meaning that every many-body eigenstate can be uniquely labeled with eigenvalues of each I. It is worth noting that practical construction of such operators is non-trivial [60, 61, 62]. Every of I_α is itself localized so if we take a pair of I_α, I_β then the coupling between them in equation (1.5) decays exponentially with distance.

Using the concept of LIOMs, one can explain most of the intriguing phenomena of the MBL. The lack of thermalization comes from the fact that every observable will have overlap with some of the I_α. Because of this states that would be thermal in ETH phase, in MBL will differ by the eigenvalues of I_α. Entanglement entropy is influenced only by the few LIOMs localized near the point that divides the system into A and B parts, explaining area-law scaling. Similarly, the slow growth of entropy is because of the exponentially decaying interactions between LIOMs. In the Appendix A, we show numerical construction of LIOMs in MBL systems.

1.3.4 Optical conductivity

Optical condictivity, $\sigma(\omega)$, is a generalisation of electrical conductivity for arbitrary frequency ω. It can be measured experimentally using optical spectroscopy. It is formally defined as straightforwardly as

$$\langle J(\omega) \rangle = \sigma(\omega) E(\omega), \tag{1.6}$$

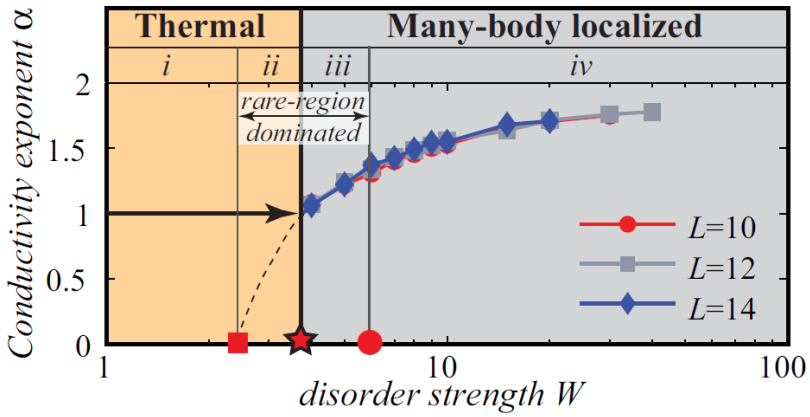

Figure 1.3: *ac* conductivity exponent α vs disorder strength. We can distinguish four regimes here: (i) the diffusive thermal phase, (ii) the subdiffusive thermal phase (only in 1D), (iii) "MBL-Griffiths" regime, (iv) "MBL-Mott" regime. Taken from Phys. Rev. B **92**, 104202 (2015).

where J is the current and E is electrical field. From Kubo's linear response theory for temperatures $T > 0$ we obtain following form of $\sigma(\omega)$ [63, 64, 65, 66]

$$\sigma(\omega) = \frac{1 - e^{-\beta\omega}}{L\omega} \mathrm{Re} \int_0^\infty e^{i\omega t} \langle J(t) J(0) \rangle dt, \tag{1.7}$$

where J is the current operator either in spin or charge sector and L is the system size. Of particular interest is the low frequency region, where it was observed that conductivity behaves like $\sigma(\omega) = \sigma_0 + \xi \mid \omega \mid^\alpha$ where $\alpha \leq 2$ which is difficult to be explained theoretically. Several numerical studies [65, 66, 67, 68] have been performed in this topic finding that $\alpha \approx 1$ in thermal phase while growing towards 2 in the localized phase [69] but the exact ω dependence of $\sigma(\omega)$ remains largely an open question. Near the phase transition the transport is dominated by the ergodic regions with relatively low degree of disorder ("MBL-Griffiths"). In previously mentioned works, it was also shown that for large disorder in the limit $\omega \to 0$, the dynamical conductivity goes to zero indicating vanishing *d.c.* transport [70]. We will refer to this result later in chapter 3.

Additionally, sub-diffusive transport was observed even in the ergodic phase [64]. It was shown that local spin density correlation function (similarily one can use charge

density correlations) $C_S = \langle S_t^z(0) S_t^z(t) \rangle$ decays sublinearly in time $C_S \sim t^{-\alpha}$. Further studies suggest that transport can already become sub-diffusive, while still having a long way to MBL transition [71].

1.4 Disordered Hubbard model

In the context of MBL, spinful fermions gained less interest than spinless systems (as Heisenberg model can be mapped to such). However recent experimental works focused on a disordered Hubbard model or its variations [72, 73, 74]. We will now briefly discuss the first of those papers.

Since truly random potential is difficult to create in laboratory, disorder was created by interference of two incommensurate optical lattices. While formally the disorder should be uncorrelated with itself, it turns out that if the system is large enough it does not matter. This conclusion was previously confirmed in theoretical studies on quasiperiodic systems [75, 76]. The resulting model realised in the experiment [72] is known as Andre-Aubry model.

$$H = -t_h \sum_{i,\sigma} (c^\dagger_{i+1,\sigma} c_{i,\sigma} + H.c.) + U \sum_i \hat{n}_{i,\uparrow} \hat{n}_{i,\downarrow} + \Delta \sum_{i,\sigma} cos(2\pi\beta i + \phi) \hat{n}_{i,\sigma}. \tag{1.8}$$

In the experiment, the initial state was prepared in such a way that "particles" occupied only evenly indexed sites. The authors introduced an intuitively interpretable way to measure the level of localization, called imbalance

$$I = \frac{N_e - N_o}{N_e + N_o}, \tag{1.9}$$

where N_e is the average number of particles on even sites while, N_o, on odd sites. It has three special values: 1 if all particles stayed on even sites, -1 if they perfectly moved into odd sites, or 0 if particles diffused uniformly within entire system. Such imbalance definition can be easily generalised for the case of any initial placement and number of particles. From the experiment, we observe that when one increases disorder strength, then the long time value of imbalance gets closer to one indicating that more particles remained in their original positions.

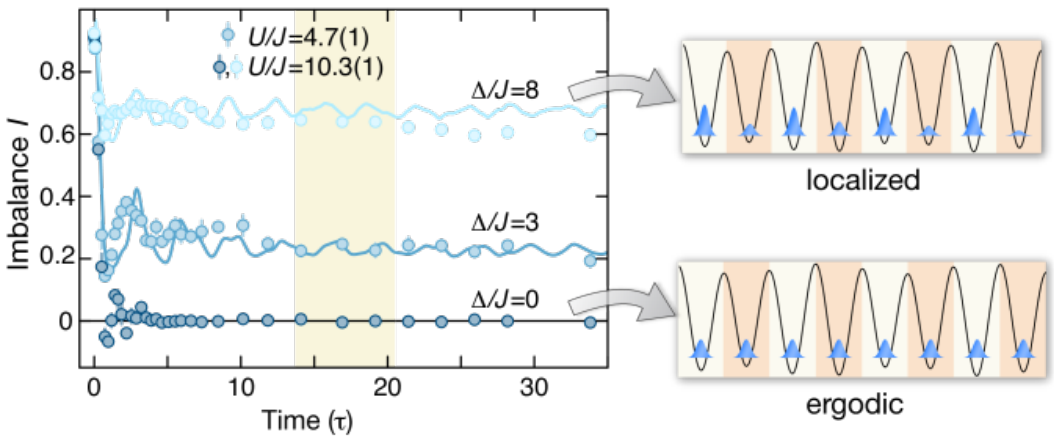

Figure 1.4: Imbalance vs time in evolution of the Andre-Aubry model. For larger values of Δ/J the stationary value of imbalance is non-zero indicating localization. Taken from Science **349**, 842 (2015).

The MBL transition in the disordered Hubbard model was already studied in [77]. Their model is slightly different as they introduce second nearest neighbor hopping to make the Hamiltonian non-integrable. Also they introduce weak random magnetic field coupled to spins to break aformentioned SU(2) symmetry. They use the level statistics approach [28] to find the necessary disorder required to cause localization. From their work we see that for spin-spin interactions, $U = 1$, the disorder strength $W = 10$ is already sufficient to fully localize the system. They also numerically simulate the previously described experiment calculating the imbalance and observe the same behaviour.

Usually the disorder is coupled only to charge degrees of freedom. Recently it was evidenced that it is not enough to cause full MBL [78] meaning that only charges are localized while spins are not. Similar conclusions were achieved in our work [79] using LIOMs approach (more details can be found in Appendix A). Unless one includes also random magnetic field, spins will not be localized. It was suggested in several works [80, 81, 82, 83] that the lack of localization in such systems is due to the SU(2) spin rotation symmetry. In chapter 4 we show that spin transport in such system is subdiffusive. Subdiffusion was reported in several theoretical works [68, 71, 84, 85, 86, 87] while at the same time showing that in disordered spin systems we can also find

anomalous diffusion regime, depending on the studied timescale. On the other hand, the energy transport in disordered Hubbard model seems to be largely suppressed [88].

1.5 Motivation and structure of the thesis

The research work described in this thesis concerns transport properties of many-body localized systems, namely anomalous transport properties of spinless systems, apparent lack of full localization and the absence of energy transport in disordered Hubbard model.

In the first chapter we have just covered an introduction to strongly correlated systems, focusing on many-body localization. We briefly discussed most important topics like the lack of thermalization, local integrals of motion or transport properties.

Second chapter presents numerical methods used for time evolution and finding the initial states. While most of them are well known, in some cases we created a custom adaptation of them to better suit our research. We also recall the overall concept of averaging over disorder.

Third chapter concerns systems of spinless fermions subjected to strong external field. We investigate the current flowing in the system depending on the strength of the disorder. We show theoretically that in MBL phase the current oscillates with characteristic frequency independent of all other parameters.

Fourth chapter focuses on disordered Hubbard model. It was shown before that disorder coupled to charges apparently cannot localize spins. We create an effective model of such system which enables us to theoretically prove that hypothesis.

Fifth chapter continues to investigate spin systems but this time, we focus on the energy transport. Using previously derived effective model we show that energy transport is suppressed, which is then confirmed in full Hubbard model.

There is also an Appendix A in which we briefly summarize the LIOM approach for deciding whether given system exhibits full MBL behaviour or not. Because it is not directly related to transport properties, it was not included as separate chapter.

Chapters 3, 4, 5 and Appendix A are based on following publications, respectively

- M. Kozarzewski, P. Prelovšek, M. Mierzejewski, *"Distinctive response of many-body localized systems to strong electric field"* Phys. Rev. B **93**, 235151 (2016),
- M. Kozarzewski, P. Prelovšek, M. Mierzejewski, *"Spin Subdiffusion in the Disordered Hubbard Chain"* Phys. Rev. Lett. **120**, 246602 (2018) Editor's Suggestion,
- M. Kozarzewski, M. Mierzejewski, P. Prelovšek, *"Suppressed energy transport in the strongly disordered Hubbard chain"* Phys. Rev. B **99**, 241113(R) (2019),
- M. Mierzejewski, M. Kozarzewski, P. Prelovšek, *"Counting local integrals of motion in disordered spinless-fermion and Hubbard chains"* Phys. Rev. B **97**, 064204 (2018).

Chapter 2

Methods

2.1 Numerical simulations

In condensed matter physics, system is usually defined by a Hamiltonian H. In general, it looks as follows

$$H = H_{single-particle} + H_{interactions}, \tag{2.1}$$

which is a sum of single-particle Hamiltonian and a term describing interaction between particles. One could try solving Schrödinger's equations for many-particle wavefunction but the interactions make that procedure difficult, if not impossible in most cases. More convenient approach is to move to occupation number formalism known as the second quantization formalism [89]. In order to create Hamiltonian matrix, we have to choose a basis. Typically we stay with positional basis where we simply enumerate all possible combinations of placing N particles on L sites. Since we only consider systems with fixes nuber of particles, we can use combinatorial number system [90] as mapping between combinations and their indices. After combining individual operators into Hamiltonian matrix almost all of its elements are zeros, so it would be inefficient to store all of them. There exist several formats for storing sparse matrices [91], we used compressed-row storage format (CRS).

Once we have Hamiltonian, we can pick initial state. In this thesis we are usually interested in the high-temperature behaviour. We can either calculate the target energy of the system knowing $\beta = \frac{1}{T}$ if we need some specific temperature, or simply set all

elements of a state vector to random values and then normalize it. In the second case we get state corresponding to temperature that is undefined but high. Next section covers the topic of finding eigenstates of a matrix in more detail.

Finally we perform time evolution of a system to calculate expectation values of some observables. In a few cases, we wanted to get stationary values (at infinite time) so we used exact diagonalization. However usually we use step by step numerical time evolution, either Runge-Kutta (RK) 4th order or Chebyshev polynomial expansion. Since our Hamiltonians contain randomness, every time we calculate time dependence of an observable, it will be different, depending on the particular values of the random numbers that were chosen. This is why we repeat every simulation with another realisations of disorder and average the results at the end. If we use sufficient number of realisations, our results will depend only on the parameters controlling the randomness.

2.2 Ground states

2.2.1 Exact diagonalization

Diagonalization of a matrix H is a process of finding such orthogonal matrix V that

$$V^{-1}HV = D, \tag{2.2}$$

where matrix D is diagonal. Typical approach to this problem is to use QR algorithm [92, 93, 94]. In each step we perform QR decomposition of matrix $H_k = Q_k R_k$ ($H_0 = H$) where Q_k is orthogonal and R_k is upper triangular. Then we calculate $H_{k+1} = R_k Q_k$. It can be shown that

$$H_{k+1} = R_k Q_k = Q_k^{-1} Q_k R_k Q_k = Q_k^T H_k Q_k, \tag{2.3}$$

which means that with each step we orthogonally transform the original matrix and H_k matrices converge to diagonal form. In practical implementations QR algorithm is not used directly because of its high computational cost $O(n^3)$. For symmetric matrices (such as real-valued Hamiltonians) we first perform orthogonal reduction of the original matrix to the tridiagonal form. For non-symmetrical matrices we can reduce them to

upper-Hessenberg form. Two possible methods for tridiagonalization use either Givens rotations or Householder reflections [95], both being orthogonal.

Having tridiagonal matrix, we could now apply QR algorithm to find its eigenvalues and eigenvectors as now the method's cost dropped down to $O(n)$ (or $O(n^2)$ for upper-Hessenberg form). The straightforward application of QR algorithm suffers from poor convergence in the case of degenerate eigenvalues, which requires special shifts of the matrix which can get complicated in real application [96]. For this thesis QR algorithm was not used, instead we developed custom software specifically for finding states of the system in the H eigenvector basis at given time, effectively fusing several computation steps into a single one.

2.2.2 Eigenvalues of tridiagonal matrix

To calculate eigenvalues of a tridiagonal matrix we can define following Sturm's sequence [97] of characteristic polynomials

$$\begin{aligned} P_0(\lambda) &= 1 \\ P_1(\lambda) &= \alpha_1 - \lambda \\ P_i(\lambda) &= (\alpha_i - \lambda)\, P_{i-1}(\lambda) - \beta_i^2 P_{i-2}(\lambda), \end{aligned} \tag{2.4}$$

where λ is the eigenvalue. The $\alpha_{1,2,3,\dots}$ are matrix elements on the main diagonal, while $\beta_{1,2,3,\dots}$ on the first off-diagonal, with $\beta_1 = 0$ (like in equation (2.9)). For given λ we can calculate values of all polynomials and count the number of sign changes between two consecutive polynomials. Interesting fact is that now the number of sign changes is equal to the number of eigenvalues smaller than λ. So using simple bisection algorithm [98] we can quickly find the desired eigenvalue with very high accuracy. Such direct application of Sturm sequence has one drawback - the values can go beyond the range of computer floating-point number representation. To mitigate this problem it is advised to define following sequence

$$Q_i(\lambda) = \frac{P_i(\lambda)}{P_{i-1}(\lambda)}. \tag{2.5}$$

Then

$$\begin{aligned} Q_1(\lambda) &= \alpha_1 - \lambda \\ Q_i(\lambda) &= (\alpha_i - \lambda) - \tfrac{\beta_i^2}{Q_{i-1}(\lambda)}. \end{aligned} \tag{2.6}$$

It can be seen that now instead of counting sign changes of P_i we have to count the number of negative Q_i-s.

2.2.3 Inverse iteration

Once we have eigenvalues of tridiagonal matrix the problem of finding eigenvectors is much easier. Most of the time, we only want to find the eigenstates once, use for some calculations and then discard. It is not necessary (and for big matrices not possible) to calculate all of them at the same time. Because of that we decided to use inverse iteration [99] instead of QR algorithm. This method is very fast converging (just a few steps are needed). We start from vector $|\phi_0\rangle$ which can be either a random vector - or better - an approximation of an eigenvector (if available). Then we proceed by calculating

$$|\phi_{i+1}\rangle = \frac{(H - \lambda I)^{-1} |\phi_i\rangle}{c_i}, \tag{2.7}$$

where H is the studied Hamiltonian, I is unit matrix. c_i is a constant added to keep the norm of the vector in allowable range, in this case it is set to $c_i = \| |\phi_i\rangle \|$ as our state vectors should be normalized anyway. We can get rid of calculating an inverse matrix by rewriting the equation in the following form

$$(H - \lambda I) |\phi_{i+1}\rangle = \frac{1}{c_i} |\phi_i\rangle . \tag{2.8}$$

Now we have tridiagonal system of linear equations to solve, for which we can use Thomas algorithm [100] to get the desired eigenvector.

With exact arithmetic inverse iteration automatically returns vectors that are orthogonal to each other. But because of numerical round-off errors it is unavoidable that for eigenvalues which are too close to each other the according eigenvectors would not be orthogonal. In such case additional re-orthogonalization step is required. Fortunately it turns out that those problematic vectors do not have to be fully orthogonalized against all previous vectors but only against those of them that have sufficiently close eigenvalues. We took advantage of this fact in our implementation. Finally, we have to transform the obtained vector back to the original basis $|\psi\rangle = V |\phi\rangle$ where $|\phi\rangle$ is

the tridiagonal matrix eigenvector and V is the transformation that tridiagonalized the original matrix.

2.2.4 Lanczos method

For systems with large number of states, the previous method fails in the first step - Householder reduction to tridiagonal form - as the entire dense matrix cannot be stored in computer memory. However sometimes we do not need the entire energy spectrum but only a small fraction of it. Basic example of such method is power iteration. If we want to find eigenvector of H associated with its largest eigenvalue we can take random vector $|\phi_0\rangle$ and repeatably calculate $|\phi_{k+1}\rangle = H|\phi_k\rangle$. More sophisticated solution is Lanczos method [101]. It can be applied to Hermitian matrices to partially diagonalize it. We are looking for an orthonormal matrix V such that $T = V^T H V$, where H is our initial Hamiltonian matrix and T is the resulting tridiagonal matrix of form

$$T = \begin{bmatrix} \alpha_1 & \beta_2 & & & & 0 \\ \beta_2 & \alpha_2 & \beta_3 & & & \\ & \beta_3 & \alpha_3 & \beta_4 & & \\ & & \beta_4 & \dots & \dots & \\ & & & \dots & \alpha_{n-1} & \beta_n \\ 0 & & & & \beta_n & \alpha_n \end{bmatrix} \tag{2.9}$$

Rearranging the original equation, we get $VT = HV$. We put $|\phi_i\rangle$ for i-th column of matrix V

$$H|\phi_i\rangle = \beta_i|\phi_{i-1}\rangle + \alpha_i|\phi_i\rangle + \beta_{i+1}|\phi_{i+1}\rangle\,. \tag{2.10}$$

As $|\phi_1\rangle$ we can take some already known eigenvector (if available) or a normalized random vector. We can multiply from the left side by $\langle\phi_i|$ to get

$$\langle\phi_i|H|\phi_i\rangle = \langle\phi_i|\beta_i|\phi_{i-1}\rangle + \langle\phi_i|\alpha_i|\phi_i\rangle + \langle\phi_i|\beta_{i+1}|\phi_{i+1}\rangle\,. \tag{2.11}$$

Since the matrix V is orthonormal we know that the only non-zero dot product in this equation is $\langle\phi_i \mid \phi_i\rangle = 1$

$$\alpha_i = \langle\phi_i|H|\phi_i\rangle\,. \tag{2.12}$$

In order to obtain $|\phi_{i+1}\rangle$ and β_{i+1} we need to rewrite the equation (2.10) in the following form

$$\beta_{i+1} |\phi_{i+1}\rangle = H |\phi_i\rangle - \beta_i |\phi_{i-1}\rangle - \alpha_i |\phi_i\rangle , \tag{2.13}$$

$$|\phi_{i+1}\rangle = \frac{1}{\beta_{i+1}} \left(H |\phi_i\rangle - \beta_i |\phi_{i-1}\rangle - \alpha_i |\phi_i\rangle\right) . \tag{2.14}$$

Since we want to obtain normalized vectors $|\phi_i\rangle$

$$|\psi_{i+1}\rangle = H |\phi_i\rangle - \beta_i |\phi_{i-1}\rangle - \alpha_i |\phi_i\rangle , \tag{2.15}$$

then $\beta_{i+1} = \| |\psi_{i+1}\rangle \|$ and $|\phi_{i+1}\rangle = \frac{1}{\beta i+1} |\psi_{i+1}\rangle$. In theory, if we continue such iterations until $\beta_i = 0$ we would get full orthogonal reduction of a matrix like the one obtained by one of previously mentioned methods. In typical applications, we terminate after some predefined number of iterations. In both cases, one may encounter the problem of the matrix V not being exactly orthogonal because of the numerical errors (same problem as in Gram–Schmidt process). In such case additional re-orthogonalization step is required, either partial or full [102]. After we obtained the tridiagonal matrix, we proceed just as in the previous two sections to find its eigenvectors. The difference is that to restore them to the original basis we have to apply the transformation V created in the Lanczos method. Usually it is not practical to store V in memory but it is easier to recalculate it using the original starting vector $|\phi_1\rangle$.

Another variant, known as microcanonical Lanczos method, can be used to find a state with target energy E. We apply Lanczos method not to the Hamiltonian but to a matrix $(H - EI)^2$. Since it commutes with H they have common set of eigenvectors.

$$\left(H^2 - 2HEI + E^2 I\right) |\phi\rangle = \left(E_0^2 - 2E_0 E + E^2\right) |\phi\rangle = \left(E_0 - E\right)^2 |\phi\rangle , \tag{2.16}$$

Lanczos method will find the state with the lowest energy, which is zero in this case. Such eigenvector corresponds to the state with energy E of the original Hamiltonian. Additionally this method can be used to perform time evolution [103, 104, 105].

2.3 Time evolution

2.3.1 Runge-Kutta 4th order

For time-dependent Hamiltonians investigated in this thesis, classic Runge-Kutta 4th order method [106] proved out to be the fastest and most accurate. Equations for solving time-dependent Schrödinger equation $i\hbar\frac{d}{dt}|\psi(t)\rangle = H(t)|\psi(t)\rangle$ and $|\psi(t_0)\rangle = |\psi_0\rangle$ look like the following

$$\begin{aligned} |k_1\rangle &= \Delta t H(t_n)|\psi(t_n)\rangle \\ |k_2\rangle &= \Delta t H(t_n + \tfrac{\Delta t}{2})(|\psi(t_n)\rangle + \tfrac{1}{2}|k_1\rangle) \\ |k_3\rangle &= \Delta t H(t_n + \tfrac{\Delta t}{2})(|\psi(t_n)\rangle + \tfrac{1}{2}|k_2\rangle) \\ |k_4\rangle &= \Delta t H(t_n + \Delta t)(|\psi(t_n)\rangle + |k_3\rangle), \end{aligned} \tag{2.17}$$

then $|\psi_{n+1}\rangle = |\psi_n\rangle + \frac{1}{6}(|k_1\rangle + 2|k_2\rangle + 2|k_3\rangle + |k_4\rangle)$ and $t_{n+1} = t_n + \Delta t$.

2.3.2 Chebyshev polynomials

On the other hand, the time-independent Schrödinger equation $i\hbar\frac{d}{dt}|\psi\rangle = H|\psi\rangle$ can be analytically solved to obtain

$$|\psi(t)\rangle = e^{-iHt/\hbar}|\psi(0)\rangle = U(t)|\psi(0)\rangle, \tag{2.18}$$

where $U(t)$ is the time evolution operator. The e^x function could now be approximated by its series expansion which could be calculated by repeated $H|\psi\rangle$ actions. This would allow us to create approximation of the operator $U(t)$ and simulate evolution of the system. But in reality e^x series is relatively slow converging, so Chebyshev polynomials expansion of $U(t)$ can be used instead [107]. Chebyshev polynomials $T_k(x)$ of the first kind are solutions of differential equation

$$(1-x^2)\frac{d^2y}{dx^2} - x\frac{dy}{dx} + k^2 y = 0 \tag{2.19}$$

for $k = 0, 1, 2, 3, ...$ [108]. Polynomials $T_k(x)$ form an orthogonal set with the inner product defined as following

$$\int_{-1}^{1} \frac{T_m(x)T_n(x)}{\sqrt{1-x^2}}dx = \begin{cases} 0, \ m \neq n \\ \pi/2, \ m = n \neq 0 \\ \pi, \ m = n = 0 \end{cases} . \tag{2.20}$$

We look for a series expansion of a function $f(s)$

$$f(x) = \sum_{k=1}^{\infty} c_k T_k(s). \tag{2.21}$$

To calculate the coefficients c_k we calculate the inner product of $T_m(x)$ and $f(x)$

$$\int_{-1}^{1} \frac{T_m(x)f(x)}{\sqrt{1-x^2}}dx = \int_{-1}^{1} \frac{T_m(x)\left[\sum_{k=1}^{\infty} c_k T_k(x)\right]}{\sqrt{1-x^2}}dx, \tag{2.22}$$

and for $f(H) = e^{-iHt/\hbar}$ we get following solution

$$c_k = (-i)^k a_k J_k(\tau), \tag{2.23}$$

where J_k is a Bessel function of the first kind and k-th order [109]. Because Chebyshev polynomials are defined in [-1,1] range we have to scale both time and Hamiltonian by E_s which is chosen to be the largest eigenvalue of H

$$\tilde{H} = \frac{1}{E_s}H, \quad \tau = E_s t. \tag{2.24}$$

Also there is a recurrence relation which is useful for calculating $T_k(x)$

$$T_{k+1}(x) = 2xT_k(x) - T_{k-1}(x), \tag{2.25}$$

so to calculate any term in the expansion we only need to have two preceding terms.

One trick to increase the accuracy when numerically solving differential equations (applicable also to the RK method) is to take adaptive timestep accordingly to how fast the function is changing. Unfortunately we could not use it here, as the further post-processing of the simulation results would be more problematic if the timestep was not constant. But in Chebyshev polynomial expansion method, we have additional way

to incorporate similar improvement. For each simulation step, the number of elements in the series expansion was variable with the condition on the norm $\|T_k(H)\,|\psi\rangle\,\|$ being below some pre-defined threshold (usually set to 10^{-12} or lower). This way, the program could increase the amount of computation where it was necessary and save time when it was possible, all while maintaning fixed accuracy.

2.3.3 Exact diagonalization

For problems where we would like to know the long time behaviour of a system (or even at infinite time) the previous methods cannot be used. Instead we can reformulate following equation

$$|\psi(t)\rangle = e^{-iHt/\hbar}\,|\psi(0)\rangle\,, \tag{2.26}$$

by switching to the basis of eigenvectors of H.

$$|\psi(t)\rangle = e^{-iHt/\hbar}\sum |n\rangle\,\langle n|\,|\psi(0)\rangle\,, \tag{2.27}$$

where $|n\rangle$ are the eigenvectors of H. Using the fact that $H\,|n\rangle = E_n\,|n\rangle$ it can be further transformed into following form

$$|\psi(t)\rangle = \sum e^{-iE_nt/\hbar}\,|n\rangle\,\langle n|\,|\psi(0)\rangle\,. \tag{2.28}$$

To calculate state at any arbitrary time t we have to solve eigenproblem of the Hamiltonian H and express state vector in the eigenbasis of H. Obviously due to the time and resource constraints it usually can be done only for systems with relatively small number of states.

2.4 Summary

In this chapter we briefly described all numerical methods used in our work starting from the creating state space and Hamiltonian matrix. Then we discussed the procedure of averaging over disorder to get final results independent of the particular disorder realisations. Later we presented three methods for time evolution, workhorse of our research. Which one is used depends on the size of Hilbert space or whether the

Hamiltonian is time dependent or not. Finally we get to the methods for finding ground states which are frequently used in chapter 3. We described a custom implementation of well known QR algorithm and Lanczos method which we used for large Hamiltonians.

Chapter 3

Transport in strong electric field

The results presented in this chapter were previously published in *"Distinctive response of many-body localized systems to strong electric field"*, M. Kozarzewski, P. Prelovšek, M. Mierzejewski, Phys. Rev. B **93**, 235151 (2016)

3.1 Motivation

As it was presented in the introduction chapter, topic of many-body localization (MBL) is full of open questions. One of them is the investigation of ergodic-MBL transition. On the numerical side, we have very useful technique for determining in which phase the system is, using the level statistics [28]. But since it requires calculating the entire energy spectrum, it is not that useful for addressing the main question concerning the properties of an infinite system. This is why there is an ongoing search for other hallmarks of MBL that could be used to distinguish the two phases.

In this chapter we focus on the system driven by strong electric field. We show that in such case, the response is very different depending on disorder strength. In the ergodic phase, the frequency of current oscillations is proportional to the field and current decays due to the Joule heating. On the other hand in the MBL phase, the frequency is constant and does not depend on either field, disorder strengths, or the initial conditions. We show that the physics can be captured by the local model, which later can be used to analytically calculate this characteristic oscillation frequency. From these results we

conclude that in MBL phase, current decay is caused by destructive interference of the local currents while each of them individually undergoes undamped oscillations. This suggests that many-body localization prevents the system from heating.

3.2 Results

3.2.1 Model

We study following model of interacting spinless fermions in a one-dimensional lattice with periodic boundary conditions.

$$H = -t_h \sum_{j=0}^{L-1} (e^{i\phi(t)} c_{j+1}^\dagger c_j + H.c.) + V \sum_{j=0}^{L-1} \hat{n}_j \hat{n}_{j+1} + V' \sum_{j=0}^{L-1} \hat{n}_j \hat{n}_{j+2} + \sum_{j=0}^{L-1} \hat{n}_j \epsilon_j, \qquad (3.1)$$

where $\hat{n}_j = c_j^\dagger c_j$. The number of lattice sites is L and the number of particles is $N = L/2$. Unless specified otherwise, interactions constants are $V = V' = 1$. Last term represents the disorder with ϵ_j being random variables drawn from uniform distribution $[-W, W]$. From now on, this parameter W will control how strong the disorder is. Additionally, after randomizing ϵ we shift them to make $\sum \epsilon_j = 0$. Non zero average value manifests itself only by shifting the energy levels of H by some constant value. While it does not change the behaviour of the system in any way, it complicates the reasoning about the results of simulation, especially when the energy of the system is involved.

The second-nearest neighbor interaction term was added to make the system non-integrable in the case of $W = 0$ [110]. It is not the only possibility. Other choice could be for example adding second-nearest hopping as in [28]. The Hamiltonian is explicitly time-dependent with the introduction of external magnetic flux $\phi(t)$ in the hopping term. Also the hopping integral t is set to 1 and was taken to be energy unit.

Unless stated otherwise, all numerical simulations are repeated many times with different sets of ϵ_j (typically >1000). Then, the results are averaged over the disorder to produce quantities which does not depend on the particular disorder realisations but only on the parameter W.

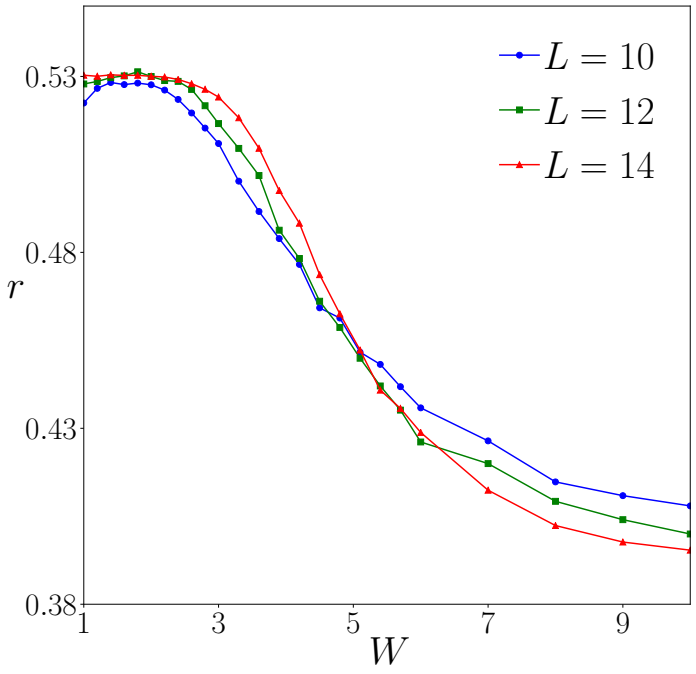

Figure 3.1: The level statistics r as in equation (1.4) vs disorder strength W for systems with $L = 10, 12, 14$ sites.

3.2.2 Level statistics

By increasing disorder strength the system can go from ergodic state to many-body localized but it is not known a-priori where exactly the transition occurs. In order to investigate the MBL transition we repeat the level statistics procedure described in [28, 29, 30]. Due to high computational cost this method is limited to small system sizes up to $L = 14$ but the transition is already visible (figure 3.1). We conclude that for our system with interactions $V = V' = 1$ the transition happens between $W = 3$ and $W = 5$. In the further analysis we take $W = 6$ to have system in the MBL phase.

3.2.3 Time evolution

External field is switched on at $t = 0$. With one exception for *a.c.* driving, the flux is $\phi(t) = Ft$ resulting in a *d.c.* electric field. For the initial state we take high temperature state with energy E_0. In order to get the relation between E_0 and temperature we use

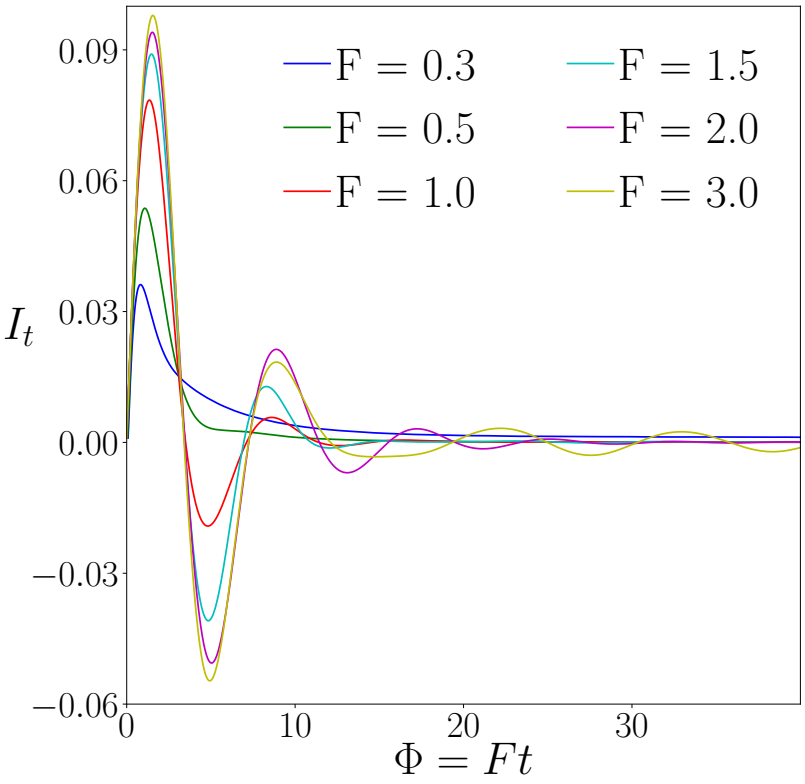

Figure 3.2: Current I_t vs $\phi(t)$ for various fields F and weak disorder $W = 1$.

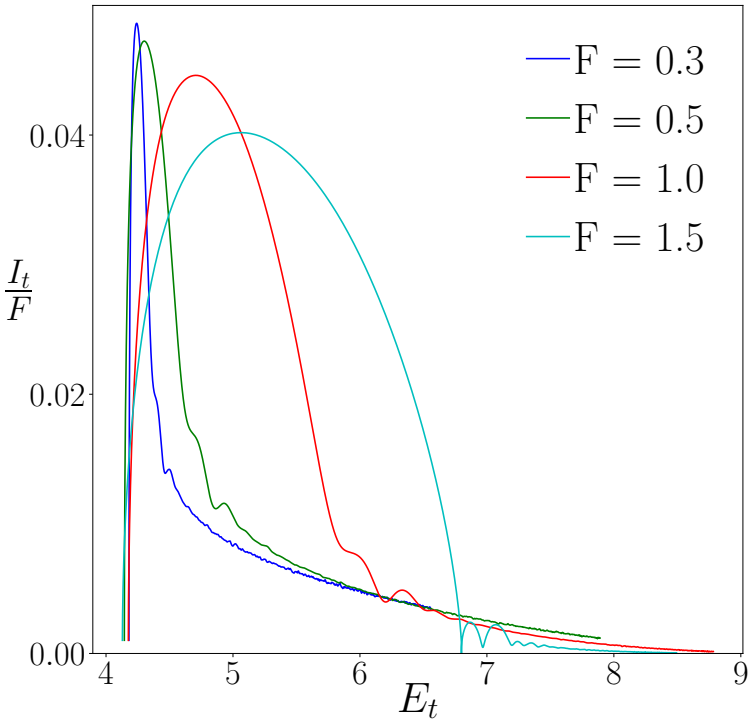

Figure 3.3: Conductivity I_t/F vs total energy E_t for various fields F and disorder $W = 3$ (near MBL transition).

high-T expansion [111] with the form

$$E_0 = L\frac{V+V'}{4} - \beta\frac{8+V^2+V'^2}{4} - \frac{\beta}{4}\sum_i \epsilon_i, \tag{3.2}$$

where $\beta = 1/T$. After calculating target energy E_0 we find appropriate initial state vector using microcanonical Lanczos method (see equation (2.16) in previous chapter). Unless specified otherwise we take $\beta = 0.2$, $V = V' = 1$, $L = 20$, $N = L/2 = 10$. We calculate the total energy $E_t = \langle H(t)\rangle_c$ and particle current $I_t = \langle J(t)\rangle_c$ where operator

$$J(t) = -\frac{d}{d\phi}H(t)/L = \frac{t_h}{L}\sum_{j=0}^{L-1}(ie^{i\phi(t)}c^\dagger_{j+1}c_j + H.c.). \tag{3.3}$$

The $\langle\rangle_c$ symbol means averaging over disorder realisations. The time evolution was carried out using Runge-Kutta 4th order method.

3.2.4 Driving for weak disorder

In general, for weak disorder the current I_t is expected to vanish when $t \to \infty$ because of Joule heating [112]. In figure 3.2 where $W = 1$, we can see that increasing F changes the current response from non-oscillatory decay to Bloch oscillations with the frequency roughly proportional to F. Even for $W = 3$, the system is still in non-MBL phase and can be expected to evolve towards thermal quasiequilibrium state in which instantaneous expectation values of operators will be determined by E_t. In order to filter out the heating, in figure 3.3 conductivity I_t/F was plotted against energy E_t. We can see that for long times the conductivity is uniquely determined by E_t and independent of F.

3.2.5 Memory effects

As it was already stated, MBL systems do not thermalize. A clear example of such effect can be seen in figure 3.4. What we did here is that blue-line shows results for system where the external field was turned on at $t = 0$ and turned off at $t = 5$. Then the system was left to relax to its equilibrium state before switching the field on again at $t = 25$. Just before the second pulse was turned on, we calculated the system energy E.

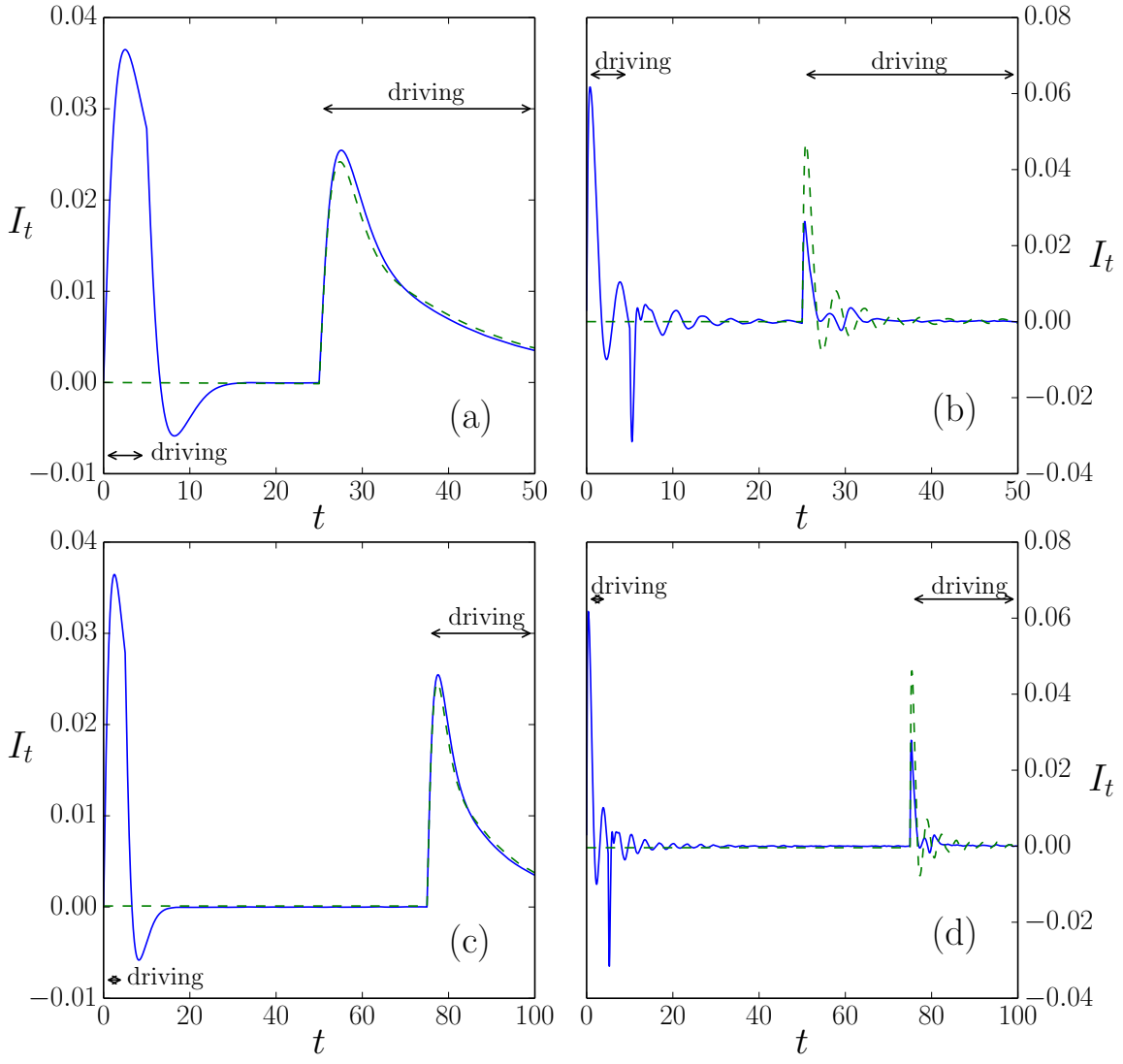

Figure 3.4: Current I_t vs time t. Arrows labelled "driving" mark when the system was subjected to external field ($F \neq 0$). On panels (a) and (c) the disorder was weak $W = 1$ and field $F = 0.3$, while on panels (b) and (d) $W = 6$ and $F = 3$. Top two panels differ from the bottom ones by the time between turning the field on again.

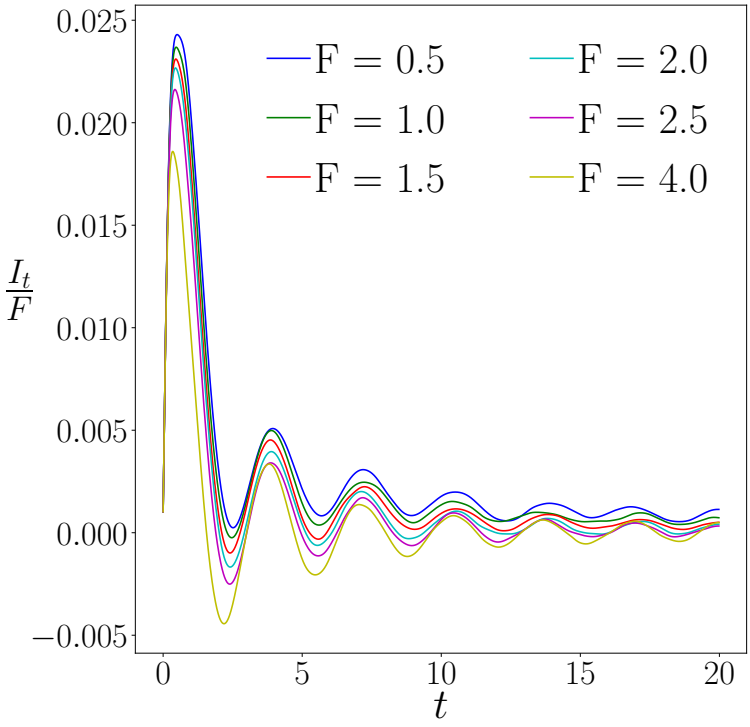

Figure 3.5: Conductivity I_t/F vs time t for various fields F and disorder $W = 6$ (in the MBL phase).

The dashed-line shows results for system was created in a equilibrium microcanonical state with energy E and was excited by the field only once. In panel (a) we can see that for weak disorder $W = 1$ the response of both systems is almost the same while on panel (b), for systems in the MBL, the response strongly depends on the history. On panels (c) and (d) the procedure was repeated but giving much more time for the system to relax from which we see that previous relaxation time was already sufficient. Although we used two states with the same energy, in MBL they are distinguishable (unlike thermal states in ETH phase) by the eigenvalues of local integrals of motion.

3.2.6 Current oscillations

In the MBL phase, we investigate the response to steady driving when changing values of the model parameters. In figure 3.5 we see that for strong disorder the amplitude of the current oscillations is roughly proportional to F while the frequency is constant.

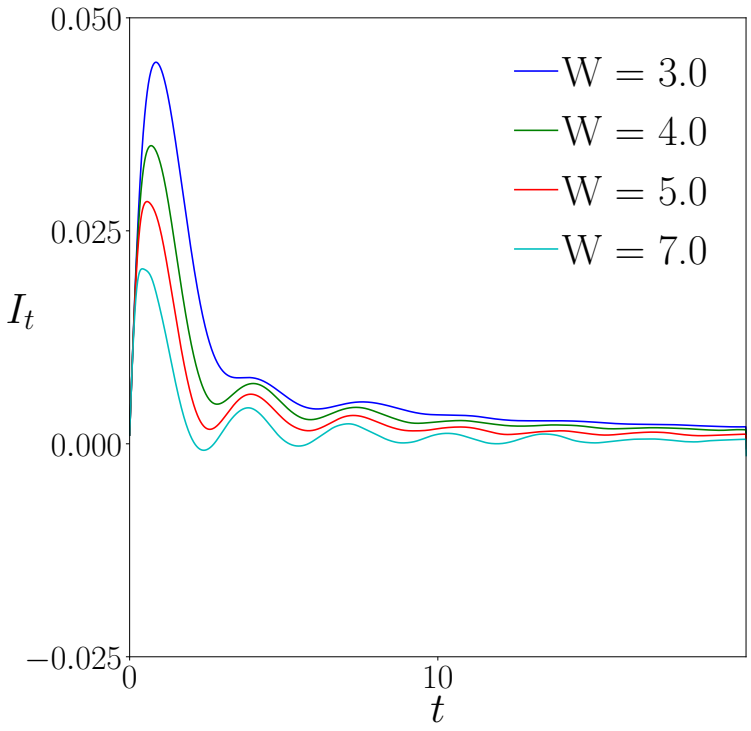

Figure 3.6: Current I_t vs time t for various disorder W and fixed field $F = 1$.

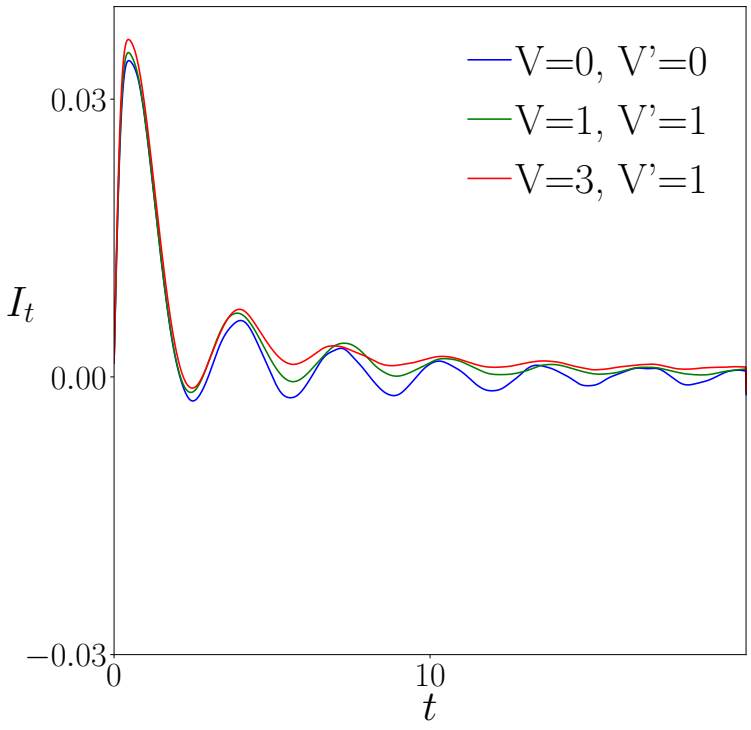

Figure 3.7: Current I_t vs time t for various interactions V, V' and fixed disorder $W = 6$ and field $F = 1.5$.

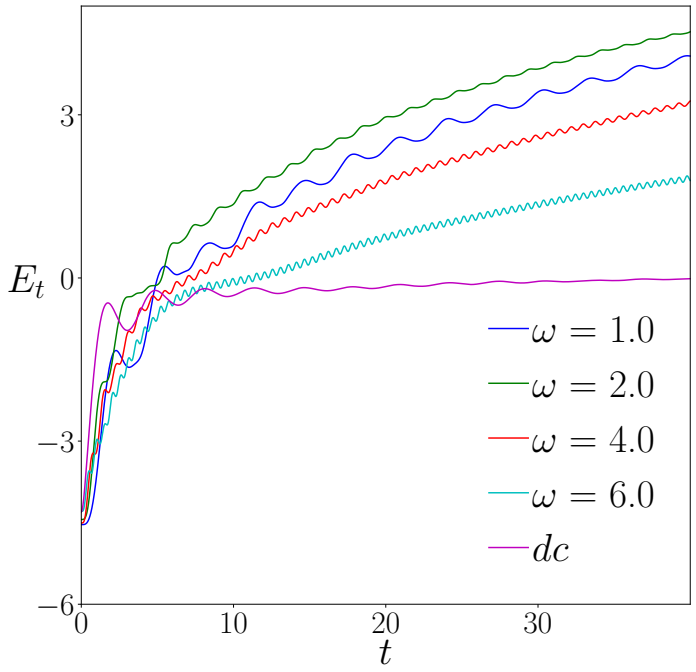

Figure 3.8: Energy E_t vs time t for *a.c.* driving $F(t) = 3\sin(\omega t)$ for various ω and single *d.c.* driving with $F = 3$, all in the MBL phase with $W = 6$.

In figure 3.6 we can see response with various disorder strengths W. While $W = 3$ seems to be slightly too low to cause clear oscillations, larger values reveal the same oscillatory behaviour of the current with frequency independent of W. Finally we check what happens when we change interaction parameters V and V'. In figure 3.7 we see that the difference is in the the decay profile, but the frequency once again does not depend on interactions.

In principle, we could use Fourier transform to calculate the spectrum and get the oscillation frequency. Such approach suggested that frequency is approximately equal 2. However, as the frequency resolution is inversely proportional to the length of the time window, the simulations would have to be carried for much longer times than we could afford in order to get required accuracy. Much more elegant way to get any insight in this topic was to considder *a.c.* driving of the form $F(t) = F\sin(\omega t)$. We expect that the fastest heating would occur when ω will be equal to the natural oscillation frequency which is confirmed in figure 3.8.

Things clear out when we consider local currents flowing between two neighboring

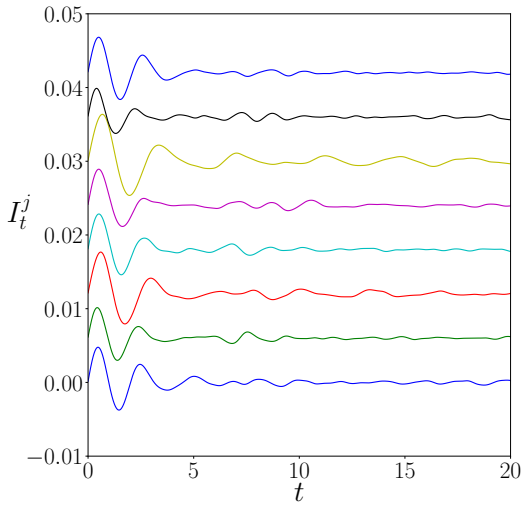

(a) Local currents for weak disorder $W = 1$ and field $F = 3$.

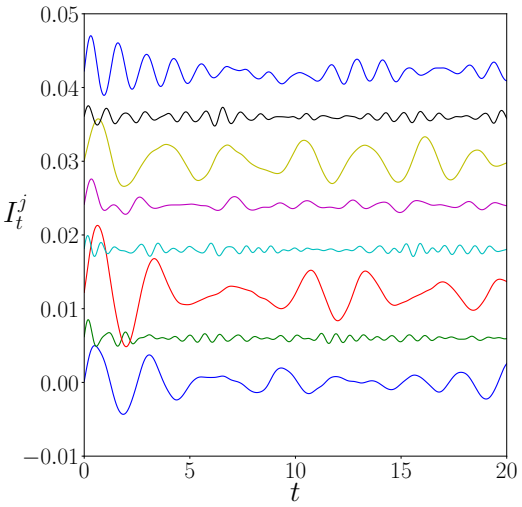

(b) Local currents in MBL phase $W = 6$ and field $F = 3$.

Figure 3.9: Local currents I_t^j on consecutive bonds (shifted vertically for clarity) vs time t. Various lines correspond to various j.

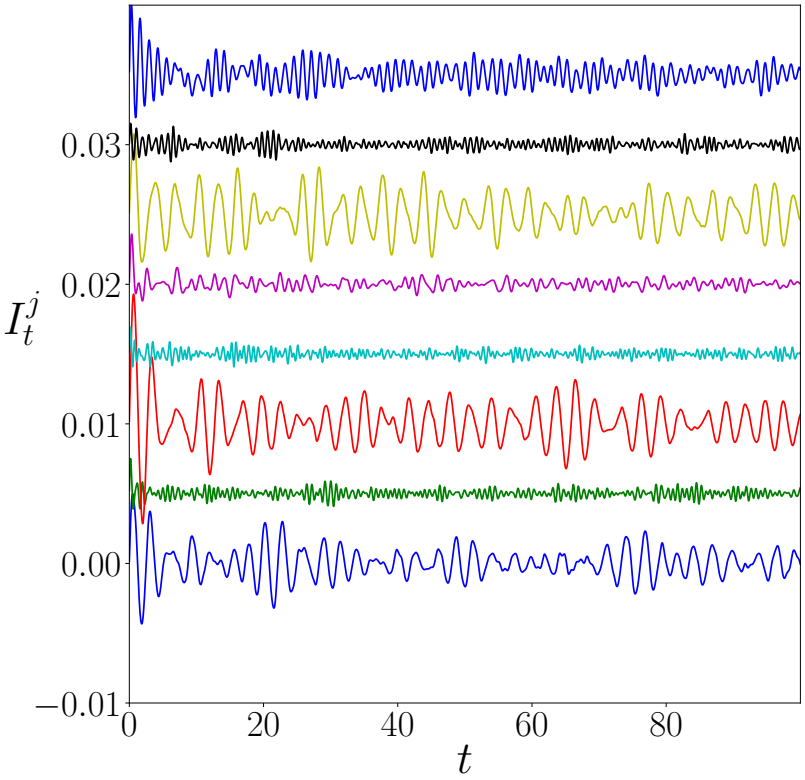

Figure 3.10: The same local currents as in figure 3.9 but for longer times, $W = 6$ and field $F = 3$.

sites

$$I_t^j = \langle ie^{i\phi(t)} c_{j+1}^\dagger c_j + H.c. \rangle, \tag{3.4}$$

noting the absence of averaging over disorder. Also $I_t = \sum_j I_t^j / L$. In the ergodic phase the local currents seem to be correlated with each other and all vanish because of the heating described earlier (figure 3.9a). However, in the MBL phase the currents oscillate with different frequencies and amplitudes, not mentioning that there is no visible decay (figure 3.9b). We also include the same results plotted for longer times (figure 3.10) where it is clear that the oscillations do not vanish even after longer times.

3.2.7 Local model

The mutual independence of local currents I_j^t calculated for various bonds j suggests that we can formulate local two-site model to investigate the systems behaviour. The two-site Hamiltonian has following forms

$$H(t=0) = H_0 = \begin{bmatrix} \epsilon & 1 \\ 1 & -\epsilon \end{bmatrix}, \tag{3.5}$$

$$H(t>0) = H_F = \begin{bmatrix} \epsilon + F & 1 \\ 1 & -\epsilon - F \end{bmatrix}. \tag{3.6}$$

Eigenvalues of H_0 are $\pm\sqrt{1+\epsilon^2} = \pm E_0$, eigenvectors

$$|\phi_\pm\rangle = c_{0\pm} \begin{bmatrix} 1 \\ -\epsilon \pm \sqrt{1+\epsilon^2} \end{bmatrix}, \tag{3.7}$$

while for H_F energies are $\pm\sqrt{(\epsilon+F)^2+1} = \pm E_F$ and eigenvectors

$$|\psi_\pm\rangle = c_{F\pm} \begin{bmatrix} 1 \\ -(F+\epsilon) \pm \sqrt{1+(F+\epsilon)^2} \end{bmatrix}, \tag{3.8}$$

where $c_{0\pm}$ and $c_{F\pm}$ are normalization factors. We use following current operator

$$J_2 = \begin{bmatrix} 0 & i \\ -i & 0 \end{bmatrix}, \tag{3.9}$$

and calculate

$$\langle\phi_\pm| J_2 |\phi_\pm\rangle = \langle\psi_\pm| J_2 |\psi_\pm\rangle = 0, \tag{3.10}$$

$$\langle\phi_\pm| J_2 |\phi_\mp\rangle = \mp i, \tag{3.11}$$

$$\langle\psi_\pm| J_2 |\psi_\mp\rangle = \mp i. \tag{3.12}$$

With tedious but straightforward calculations we derive the inner products

$$\langle\phi_\pm \mid \psi_\pm\rangle = 1 - O(F^2), \tag{3.13}$$

$$\langle\phi_\pm \mid \psi_\mp\rangle = \frac{\pm F}{2(1+\epsilon^2)} + O(F^2). \tag{3.14}$$

Any initial state can be written in the form of density matrix

$$\rho(t=0) = x |\phi_-\rangle \langle\phi_-| + (1-x) |\phi_+\rangle \langle\phi_+| + \alpha |\phi_-\rangle \langle\phi_+| + \bar{\alpha} |\phi_+\rangle \langle\phi_-|, \tag{3.15}$$

where $x \in [0,1]$ is real, while α is complex so it will not cause any problems during time-averaging. Current at time t can be calculated from

$$I(t) = Tr[\rho(t) J_2]. \tag{3.16}$$

Combining two equations above we split the result into four parts $I_{--}, I_{-+}, I_{+-}, I_{++}$. We show only derivation for the first one.

$$I_{--} = x \langle\phi_-| U^+(t) J_2 U(t) |\phi_-\rangle = x \langle\phi_-| e^{iH_F t} J_2 e^{-iH_F t} |\phi_-\rangle. \tag{3.17}$$

To calculate $e^{-iH_F t} |\phi_-\rangle$ we use the identity $|\psi_-\rangle \langle\psi_-| + |\psi_+\rangle \langle\psi_+| = I$.

$$e^{-iH_F t} |\phi_-\rangle = e^{-iH_F t}(|\psi_-\rangle \langle\psi_-| + |\psi_+\rangle \langle\psi_+|) |\phi_-\rangle. \tag{3.18}$$

Using definitions and inner products written previously we have

$$e^{-iH_F t} |\phi_-\rangle = \underbrace{e^{-iH_F t} |\psi_-\rangle}_{e^{iE_F t}|\psi_-\rangle} \underbrace{\langle\psi_- \mid \phi_-\rangle}_{1-O(F^2)} + \underbrace{e^{-iH_F t} |\psi_+\rangle}_{e^{-iE_F t}|\psi_+\rangle} \underbrace{\langle\psi_+ \mid \phi_-\rangle}_{\frac{F}{2(1+\epsilon^2)}+O(F^2)}. \tag{3.19}$$

Combining this with equation (3.12) and simplifying we get

$$I_{--} = x \frac{F}{2(1+\epsilon^2)} \underbrace{i(e^{-2iE_F t} - e^{2iE_F t})}_{2\sin(2E_F t)}. \tag{3.20}$$

We approximate

$$E_F = \sqrt{(\epsilon + F)^2 + 1} \approx E_0 + \frac{\epsilon F}{E_0}, \tag{3.21}$$

assuming that disorder ϵ is much larger than the field F. Thus

$$\sin(2E_F t) = \sin(2tE_0) \underbrace{\cos(2t\frac{\epsilon F}{E_0})}_{\approx 1+O(F^2)} + \cos(2tE_0) \underbrace{\sin(2t\frac{\epsilon F}{E_0})}_{\text{vanishes after averaging}}. \tag{3.22}$$

Finally we obtain the first part of the current

$$I_{--} = x\frac{\sin(2E_0 t)}{E_0^2}F = x\frac{\sin(2\sqrt{1+\epsilon^2}t)}{1+\epsilon^2}F. \tag{3.23}$$

Together with similarily calculated I_{++} we have

$$I_F(t) = (2x-1)\frac{\sin(2\sqrt{1+\epsilon^2}t)}{1+\epsilon^2}F. \tag{3.24}$$

This result explains why the lowest frequencies oscillate with the largest amplitudes. From the other two part I_{-+} and I_{+-} we obtain term that is not proportional to F, which arises if the initial state is not pure ($\alpha \neq 0$)

$$I_0(t) = \alpha \sin(2\sqrt{1+\epsilon^2}t). \tag{3.25}$$

The parameter x can be evaluated within canonical ensemble as probability that system is in state with lower energy $-E_0$

$$x = \frac{e^{\beta E_0}}{e^{\beta E_0} + e^{-\beta E_0}}, \tag{3.26}$$

where $\beta = \frac{1}{kT}$. In this way

$$2x - 1 = \frac{2e^{\beta E_0} - e^{-\beta E_0} - e^{\beta E_0}}{e^{\beta E_0} + e^{-\beta E_0}} = \frac{e^{\beta E_0} - e^{-\beta E_0}}{e^{\beta E_0} + e^{-\beta E_0}} = \tanh(\beta E_0). \tag{3.27}$$

In order to obtain average current in the whole system composed of infinitely many two-site subsystems we perform averaging over disorder

$$\langle I_F(t)\rangle_c = \int_{-W}^{W} f(\epsilon)(2x(\epsilon)-1)\frac{\sin(2\sqrt{1+\epsilon^2}t)}{1+\epsilon^2}F d\epsilon, \tag{3.28}$$

where $f(\epsilon)$ is the disorder distribution. We make following substitution $u = \epsilon^2 t$, thus $d\epsilon = du/(2\sqrt{tu})$ and $\epsilon = \sqrt{\frac{u}{t}}$. We also assume that distributions of $x(\epsilon)$ and $f(\epsilon)$ are symmetric.

$$\langle I_F(t)\rangle_c = 2F\int_0^{W^2 t} f\left(\sqrt{\frac{u}{t}}\right)(2x\left(\sqrt{\frac{u}{t}}\right)-1)\frac{\sin(2\sqrt{1+\frac{u}{t}}t)}{1+\frac{u}{t}}\frac{du}{2\sqrt{tu}}. \tag{3.29}$$

We are interested in the limit of long times, so $x\left(\sqrt{\frac{u}{t}}\right) \approx x(\epsilon = 0)$ (for large disorder the original $x(\epsilon)$ weakly depends on ϵ anyway), $f\left(\sqrt{\frac{u}{t}}\right) \approx f(\epsilon = 0)$, $\sin(2\sqrt{1+\frac{u}{t}}t) \approx \sin(2t+u)$ and $\left(1+\frac{u}{t}\right)\sqrt{t} \approx \sqrt{t}$. Using identity for a sine of a sum, the integral is now split into two symmetric parts $\langle I_F(t)\rangle_c = I_s(t) + I_c(t)$. We show calculations for the former one. Combining all the approximations above with equation (3.29) and simplifying gives

$$I_s(t) = F\frac{\sin(2t)}{\sqrt{t}} f(\epsilon = 0)(2x(\epsilon = 0) - 1)\int_0^\infty \frac{\cos(u)}{\sqrt{u}} du. \tag{3.30}$$

Recalling the two Fresnel integrals

$$\int_0^\infty \frac{\sin(t)}{\sqrt{t}} dt = \int_0^\infty \frac{\cos(t)}{\sqrt{t}} dt = \sqrt{\frac{\pi}{2}}, \tag{3.31}$$

we get

$$I_s(t) \approx F\frac{\sin(2t)}{\sqrt{t}} f(\epsilon = 0)(2x(\epsilon = 0) - 1)\sqrt{\frac{\pi}{2}}. \tag{3.32}$$

The other integral I_c differs only by having $\cos(2t)$ instead $\sin(2t)$. Returning to original $\langle I_F(t)\rangle_c = I_s(t) + I_c(t)$ and noticing that $\sin(2t) + \cos(2t) = \sqrt{2}\sin(2t + \frac{\pi}{4})$ we have

$$\langle I_F(t)\rangle_c = \sqrt{\frac{\pi}{t}} f(\epsilon = 0)(2x(\epsilon = 0) - 1)F \sin\left(2t + \frac{\pi}{4}\right). \tag{3.33}$$

Interestingly, despite all the approximations we made, the resulting function is exactly the same as the result of numerical integration of the original equation (3.28) (except near $t = 0$).

From the latter result, we obtain that in MBL phase the system exhibits the same frequency of oscillations independently on the driving. The decay of current is not due to the Joule heating but because of the destructive interference of individual two-site currents. On figure 3.11 we compare the result of numerical simulations with the current obtained from equation (3.33) assuming uniform distribution of disorder $f(0) = \frac{1}{2W}$ and $x(0) = \frac{1}{2}(1 + \tanh(\beta))$. The local model is too simple to explain the damping but correctly predicts the frequency of oscillations.

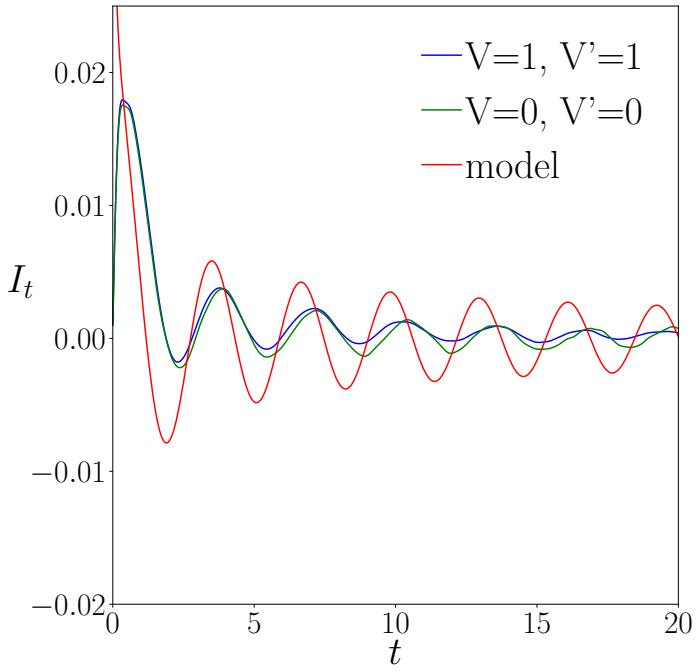

Figure 3.11: Current I_t for $F = 1$, $W = 8$ for the interacting and noninteracting models, compared with result from the local-model in equation (3.33)

3.3 Summary

In this chapter we focused on the t-VW spinless fermions model with external driving as in equation (3.1). The goal was to find out whether ergodic and MBL phases can be distinguished by the systems response to constant external field F.

At first, we used level statistics procedure to clarify how strong disorder is required to push the system into MBL phase (fig 3.1). Then, we performed several numerical simulations changing parameters to establish basic knowledge what impact on the results each parameter has. As expected, we get that in ergodic phase both the frequency of oscillations ω and the current I is proportional to the field F, at least for moderate strengths of F (fig 3.2). We showed that while the system heats up quickly, it always reaches the same thermal state after sufficiently long time (fig 3.3).

On the other hand, in MBL phase, frequency of oscillations seems to be constant, while the current is still proportional to the field (fig 3.5). Additionally, current is inversely proportional to the disorder strength W (fig 3.6). Interactions have relatively

small influence on the results, visible mostly in the current decay profile (fig 3.7). In order to determine the frequency we performed simulation with *a.c.* driving to obtain that resonant frequency $\omega = 2$.

We added calculation of currents on various bonds to our simulations and observed that while in ergodic phase the currents on various bonds are correlated and decay to zero (fig 3.9a), in MBL phase the currents seem to be independent and do not decay, at least not within time scale of the simulations (fig 3.9b). Additionally it was visible that their frequency is inversely proportional to the amplitude.

All those observations enabled us to create a local, two-site model that we solved analytically. Within linear response theory, we obtained the closed-form-equation for each local current (equation (3.24)). It is clear that there is no decay of the amplitude. Then we performed averaging over infinite number of such local models to obtain the current flowing in the full system. The final equation (3.33) correctly explains all the observations we did during numerical simulations - linear proportionality to F, inverse to W, decay as $1/\sqrt{t}$ and constant frequency $\omega = 2$.

We showed that by performing measurements of current response to external field (which can be done in experiments) one can differentiate the ergodic and MBL phases. Also, the *d.c.* driving as shown in fig 3.8 suggests that optical conductivity goes to zero in the limit of $\omega \to 0$ which is consistent with recent findings [69].

Chapter 4

Spin transport in disordered Hubbard chain

The results presented in this chapter were previously published in *"Spin Subdiffusion in the Disordered Hubbard Chain"*, M. Kozarzewski, P. Prelovšek, M. Mierzejewski, Phys. Rev. Lett. **120**, 246602 (2018) Editor's Suggestion

4.1 Motivation

Work presented in this chapter was greatly influenced by article [78] where authors numerically showed that Hubbard model with disorder coupled to charges does not fully localize. Our goal is to provide more arguments for this statement, but from the theoretical point of view.

We derive an effective model based on the assumtpion that charges are completely localized. Our result is that spins indeed remain delocalized and subdiffuse in the system. However, the effective model eliminates all coupling terms between charges and spins so it is likely that charges will also eventually delocalize but for timescales and system sizes inaccesible to numerical simulations (at least at the time of writing this thesis).

4.2 Results

4.2.1 Model

We study Hubbard model with disorder copuled to charge degrees of freedom

$$H = -t_h \sum_{i,\sigma} (c^\dagger_{i+1,\sigma} c_{i,\sigma} + H.c.) + \sum_i \epsilon_i \hat{n}_i + U \sum_i \hat{n}_{i,\uparrow} \hat{n}_{i,\downarrow}, \tag{4.1}$$

where $\hat{n}_i = \hat{n}_{i,\uparrow} + \hat{n}_{i,\downarrow}$ and $\hat{n}_{i,\sigma} = c^\dagger_{i,\sigma} c_{i,\sigma}$ for $\sigma \in \{\uparrow, \downarrow\}$. The system has L sites and N particles, hopping integral $t_h = 1$, total spin projection S^z is zero and each ϵ_i is drawn from uniform distribution in range $[-W, W]$.

4.2.2 Two electrons

The problem of two interacting particles in random potential was already studied in [113] or [114] but in different context and the results are not directly applicable to our considerations. We study the behaviour of the system with two ($N = 2$) electrons with opposite spin projections on system with $L = 16$ sites. The initial state is chosen in such a way that electrons are placed on two different sites separated by some distance d. Then we perform time evolution using exact diagonalization as we want to see what happens in the long-time regime. During the simulation, for each site i we calculate local spin $\langle S_i(t) \rangle = \langle \hat{n}_{i\uparrow} - \hat{n}_{i\downarrow} \rangle$ and the number of particles $\langle n_i(t) \rangle = \langle \hat{n}_{i\uparrow} + \hat{n}_{i\downarrow} \rangle$. In figure 4.1 we can see the time-dependence of both functions for strong disorder $W = 8$. It is clear that charges remain localized but spins oscillate. We generated much more of such plots where we observed that this pattern of spin oscillation is universal. Sometimes it happens that an electron is not localized on a single site but oscillates on two or more sites as can be seen on figure 4.2. Actually the only rare case when the spin oscillations are not visible is when all ϵ_i are randomly assigned to relatively low values so the system does not exhibit any localization.

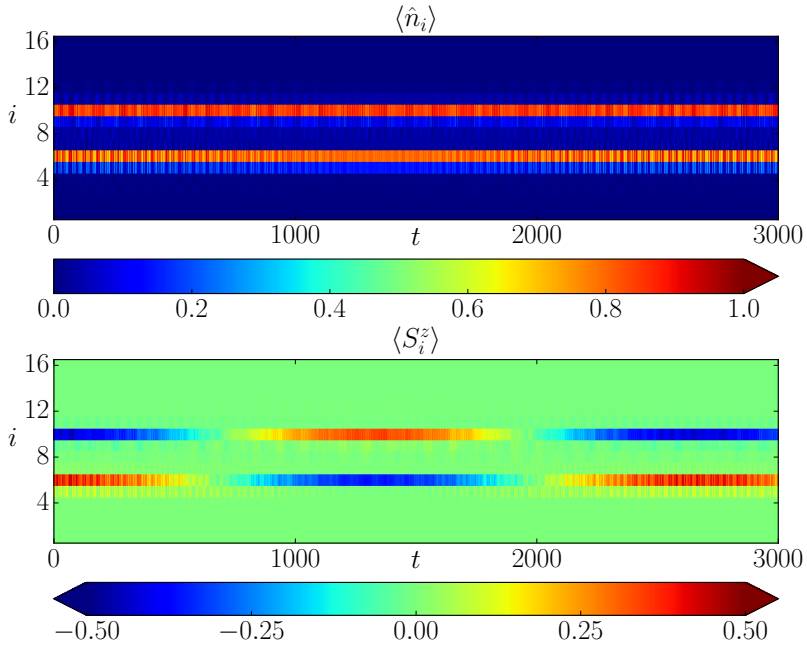

Figure 4.1: Spin $\langle S_i(t) \rangle$ and number of particles $\langle n_i(t) \rangle$ in the disordered Hubbard model for single realisation of ϵ_i-s for $L = 16, W = 8, U = 1$.

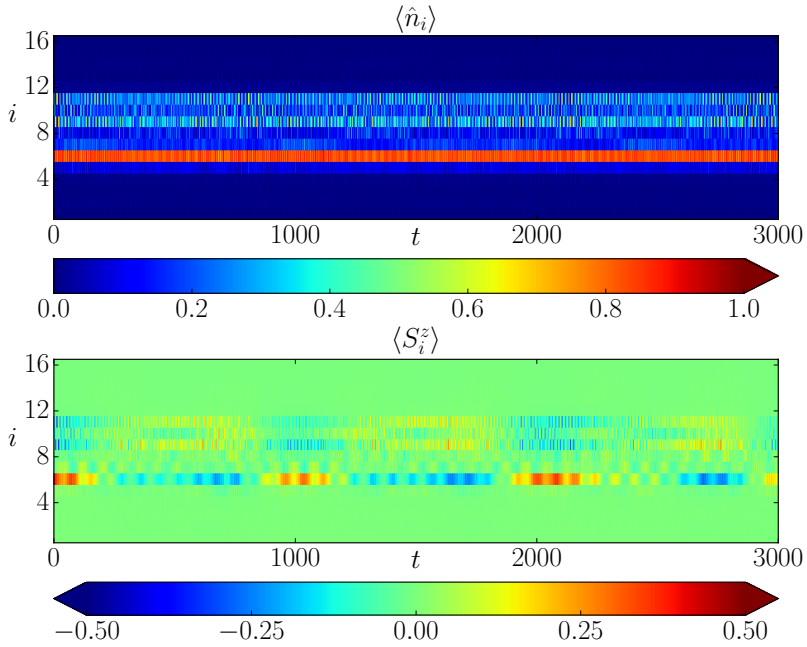

Figure 4.2: Similar to figure 4.1 but this time the upper electron is not localized on a single site so the spin oscillation pattern looks fuzzy.

4.2.3 Effective spin model

Using the observation that charges are essentially frozen we can create effective spin model. In general, we can always diagonalize the noninteracting ($U = 0$) single-particle Hamiltonian from equation (4.1). We introduce operators $\varphi^\dagger_{a\sigma} = \sum_i \phi_{ai} c^\dagger_{i\sigma}$ which create particle with spin σ in the Anderson localized state a. Coefficients ϕ_{ai}, the wave-function of the Anderson state $|o\rangle$, are elements of an (in general) unitary matrix used to change the basis. We can simply invert the relation into the form

$$c^\dagger_{i\sigma} = \sum_a \phi^*_{ai} \varphi^\dagger_{a\sigma}. \tag{4.2}$$

By putting this equation into the interaction term of the Hubbard model we get

$$U \sum_i \hat{n}_{i,\uparrow} \hat{n}_{i,\downarrow} = \frac{U}{2} \sum_\sigma \sum_{aa'bb'} \chi^{ab}_{a'b'} \varphi^\dagger_{a\sigma} \varphi^\dagger_{b\bar{\sigma}} \varphi_{b'\bar{\sigma}} \varphi_{a'\sigma}, \tag{4.3}$$

where

$$\chi^{ab}_{a'b'} = \sum_i \phi^*_{ai} \phi^*_{bi} \phi_{b'i} \phi_{a'i}, \tag{4.4}$$

and $\chi^{ab}_{a'b'}$ is invariant to permutation of indices a, b and a', b'. The $\frac{1}{2}$ factor in equation (4.3) comes from the fact that on the right-hand side we have introduced summation over spin projections.

Now we use an approximation where we neglect all terms that change the occupation of the states in the Anderson basis. Because of this, we are left only with terms where either $a = a', b = b'$ or $a = b', b = a'$ and in both cases $a \neq b$.

$$H_U = \frac{U}{2} \sum_{a \neq b, \sigma} \chi^{ab}_{ab} \left[\varphi^\dagger_{a\sigma} \varphi^\dagger_{b\bar{\sigma}} \varphi_{b\bar{\sigma}} \varphi_{a\sigma} + \varphi^\dagger_{a\sigma} \varphi^\dagger_{b\bar{\sigma}} \varphi_{a\bar{\sigma}} \varphi_{b\sigma} \right]. \tag{4.5}$$

We can now reorder the operators to make the terms more obvious

$$H_U = \frac{U}{2} \sum_{a \neq b, \sigma} \chi^{ab}_{ab} \left[\underbrace{\varphi^\dagger_{a\sigma} \varphi_{a\sigma}}_{\hat{n}_{a\sigma}} \underbrace{\varphi^\dagger_{b\bar{\sigma}} \varphi_{b\bar{\sigma}}}_{\hat{n}_{b\bar{\sigma}}} - \underbrace{\varphi^\dagger_{a\sigma} \varphi_{a\bar{\sigma}}}_{S^+_a} \underbrace{\varphi^\dagger_{b\bar{\sigma}} \varphi_{b\sigma}}_{S^-_b} \right]. \tag{4.6}$$

We use here standard spin operators $S^+_a = \varphi^\dagger_{a\uparrow} \varphi_{a\downarrow}$, $S^-_a = \varphi^\dagger_{a\downarrow} \varphi_{a\uparrow}$ and $S^z_a = \frac{1}{2}(\hat{n}_{a\uparrow} - \hat{n}_{a\downarrow})$. If we now write the summation over spins explicitly we get

$$H_U = U \sum_{a \neq b} \chi^{ab}_{ab} \left[\frac{1}{2} \left(\hat{n}_{a\uparrow} \hat{n}_{b\downarrow} + \hat{n}_{a\downarrow} \hat{n}_{b\uparrow} \right) - \frac{1}{2} \left(S^+_a S^-_b - S^-_a S^+_b \right) \right]. \tag{4.7}$$

Using the relations $\hat{n}_{a\uparrow} = \frac{1}{2}\hat{n}_a + S_a^z$ and $\hat{n}_{a\downarrow} = \frac{1}{2}\hat{n}_a - S_a^z$ it is straightforward to show that

$$H_U = U \sum_{a \neq b} \chi_{ab}^{ab} \left[\frac{1}{4}\hat{n}_a\hat{n}_b \underbrace{- S_a^z S_b^z - \frac{1}{2}\left(S_a^+ S_b^- - S_a^- S_b^+\right)}_{-\bar{S}_a \cdot \bar{S}_b} \right]. \tag{4.8}$$

We also introduce

$$J_{ab} = 2U\chi_{ab}^{ab} = \sum_i \mid \phi_{ai} \mid^2 \mid \phi_{bi} \mid^2, \tag{4.9}$$

so the final effective Hamiltonian is

$$H_U = \frac{1}{2} \sum_{a \neq b} J_{ab} \left(\frac{1}{4}\hat{n}_a\hat{n}_b - \bar{S}_a \cdot \bar{S}_b \right). \tag{4.10}$$

In order to test the approximation we used following procedure: We randomize some set of ϵ_i (the disorder) and choose intial state with two electrons placed at sites j and $j + d$. We perform numerical simulation of such system as described in the previous subsection to extract the oscillation frequency ω_2. Then we numerically diagonalize the noninteracting Hamiltonian to obtain all the ϕ coefficients, pick two states a, b that maximize $\mid \phi_{j,a} \mid^2$ and $\mid \phi_{j+d,b} \mid^2$ and use formula (4.9) to calculate the approximate frequency J_{ab}. The results can be seen in figures 4.3 and 4.4. The correlation is not perfect mainly because in the numerical simulation electrons are not necessarily localized on a single site (as already described). That introduces a lot of noise into the frequency spectrum which makes it very challenging for the software to automatically pick the "correct" frequency. Nevertheless we see that the fit is better for larger d.

In the Anderson model, eigenstates decay exponentially in space when we move from the "center" of localization. In such case, in the limit of low occupancy we can formulate following approximate relation

$$J_{ab} \simeq 2Ue^{-x_{ab}/\lambda}, \tag{4.11}$$

where x_{ab} is the distance between two particles and λ is somehow proportional to the Anderson localization length ξ (the numerical constant is not important here).

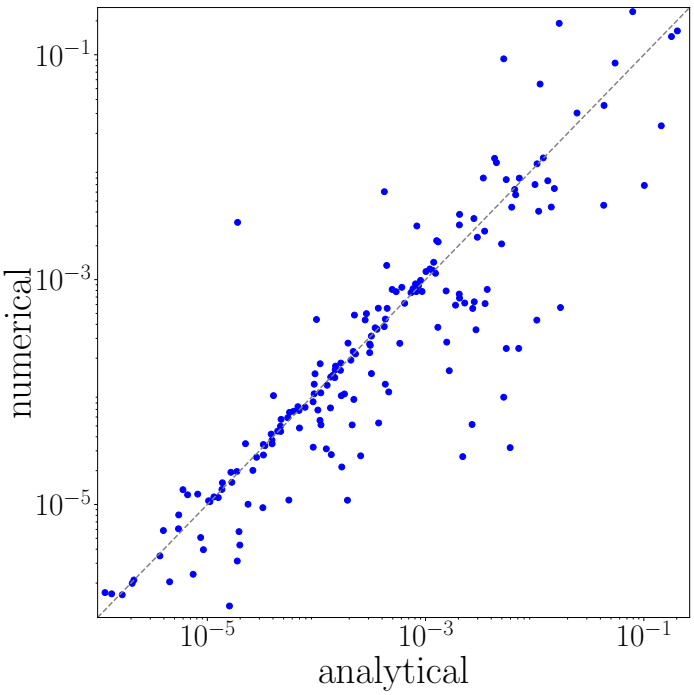

Figure 4.3: Correlation between numerically calculated frequency ω_2 and J_{ab} from equation (4.9) for $L = 16, W = 8, U = 1, d = 4$

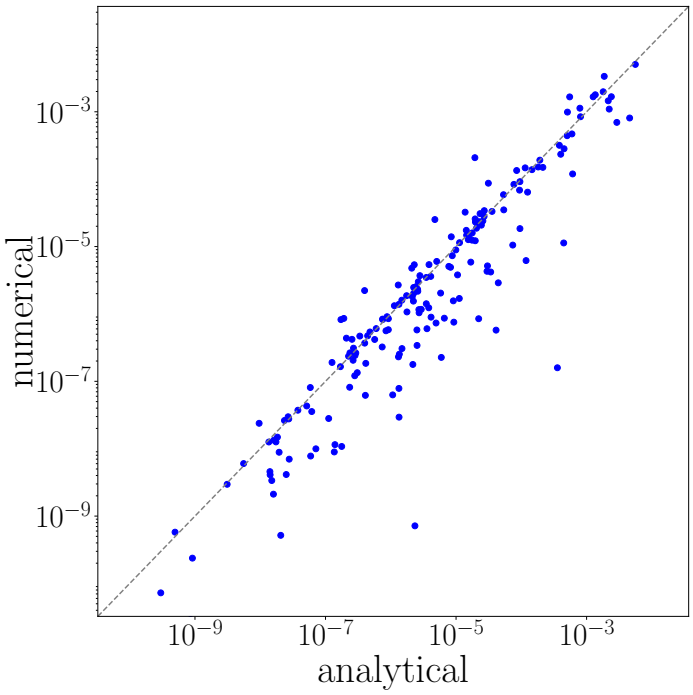

Figure 4.4: Correlation between numerically calculated frequency ω_2 and J_{ab} from equation (4.9) for $L = 16, W = 8, U = 1, d = 6$

4.2.4 Squeezed spin model

Consider the well known problem of placing N points on the line segment of length L. We are interested in the distribution of distances between consecutive points. We start from calculating the probability that any two points are separated by less than x (this is the definition of the cumulative distribution function $F(x)$). This equals to one minus the probability that all points are separated by at least x. If we place first point at one end of the segment then the probability that the next one will be further than x equals $\frac{L-x}{L} = 1 - \frac{x}{L}$. In the limit of $L \to \infty$ we can neglect the fact that the remaining space for placing next point just got smaller because of the previous one and proceed with placing more points. From such procedure we obtain

$$F(x) = \lim_{L\to\infty} 1 - \left(1 - \frac{x}{L}\right)^N = 1 - e^{-x/d}, \tag{4.12}$$

where we used the fact that $\frac{L}{N} = d$. From this we can trivially obtain the probability distribution function of distances between points

$$f(x) = \frac{1}{d} e^{-x/d}. \tag{4.13}$$

While this result was obtained for continuous line segment, in the limit of large d it will also be valid (asymptotically) for discrete space.

From equation (4.11) we get that the smaller the distance between electrons the larger the effective interaction is. We can now compare the probability of randomly picking the distance smaller than some value y with the probability of getting J_{ab} larger than $2Ue^{-y/\lambda}$

$$\int_0^y \frac{1}{d} e^{-x/d} dx = \int_{2Ue^{-y/\lambda}}^{2U} f_J(J) dJ. \tag{4.14}$$

By taking the derivative with respect to y on both sides we get

$$\frac{1}{d} e^{-y/d} = f_J(\underbrace{2Ue^{-y/\lambda}}_{J}) \underbrace{2Ue^{-y/\lambda}}_{J} \frac{1}{\lambda}. \tag{4.15}$$

We used the equation (4.11) here. We then transform both sides into

$$\frac{\lambda}{d} (\underbrace{e^{-y/\lambda}}_{\frac{J}{2U}})^{\frac{\lambda}{d}} = f_J(J) \frac{J}{2U} 2U. \tag{4.16}$$

We now introduce dimensionless variables $\tilde{J} = \frac{J}{2U}$ and $\tilde{\lambda} = \frac{\lambda}{d}$ to obtain probability distribution in the form

$$f(\tilde{J}) = \tilde{\lambda}\tilde{J}^{\tilde{\lambda}-1}, \quad 0 \leq \tilde{J} \leq 1. \tag{4.17}$$

Parameter $\tilde{\lambda}$ is the ratio of the Anderson localization length λ and the average distance between particles d. For large disorder $\lambda \simeq 1$ and low filling $d \gg 1$ we obtain that $\tilde{\lambda} < 1$ and in such case the distribution of $\tilde{J}$ is singular at 0.

To test the formula (4.17) we collect the histogram of distribution of J_{ab} obtained from numerical procedure similar to the one from subsection 4.2.3. We randomize the position of electrons according to the distribution (4.13) but this time we only use the J_{ab} calculated from the equation (4.9). We than plot the distribution of $\tilde{J}f(\tilde{J}) = \tilde{\lambda}\tilde{J}^{\tilde{\lambda}}$ on a log-log scale. As $\log \tilde{\lambda}\tilde{J}^{\tilde{\lambda}} = \log \tilde{\lambda} + \tilde{\lambda} \log \tilde{J}$ we expect that it would form a straight line which is confirmed on plots 4.5 and 4.6. The bump on the right side comes from the fact that the approximation we used holds only for small $\tilde{J}$.

Additionally, by fitting linear function to lines on the plots we estimate the Anderson localization length λ. We get $\lambda \approx 0.75$ for $W = 4$ and $\lambda \approx 0.4$ for $W = 8$. Interesting fact is that although the effective model was derived assuming low filling, the equation (4.17) correctly predicts the distribution of J even for $d = 2$ (half filling).

4.2.5 Spin correlation functions

We define following local spin correlation functions

$$S_L(t) = \langle S_i^z(0) S_i^z(t) \rangle_{dis}, \tag{4.18}$$

where $\langle\rangle_{dis}$ means averaging the results over realisations of disorder. We create the effective Heisenberg model with $\tilde{N}$ spins, randomizing J_i according to the distribution (4.17). Time is expressed in the energy units $1/2U$ and the results are averaged over at least 2000 realisations of disorder.

In figure 4.7 we can see that in the long time, $S_L(t)$ decays with the power law $(2Ut)^{-\alpha}$. The exponent α is approximately equal to $\tilde{\lambda}$ when $\tilde{\lambda} \ll 1$ and ≈ 0.5 for $\tilde{\lambda} = 1$. For small $\tilde{\lambda}$, the finite size effects seem negligible while for larger values of $\tilde{\lambda}$ they start to become more significant but still acceptable. On figure 4.8 we see a summary of the

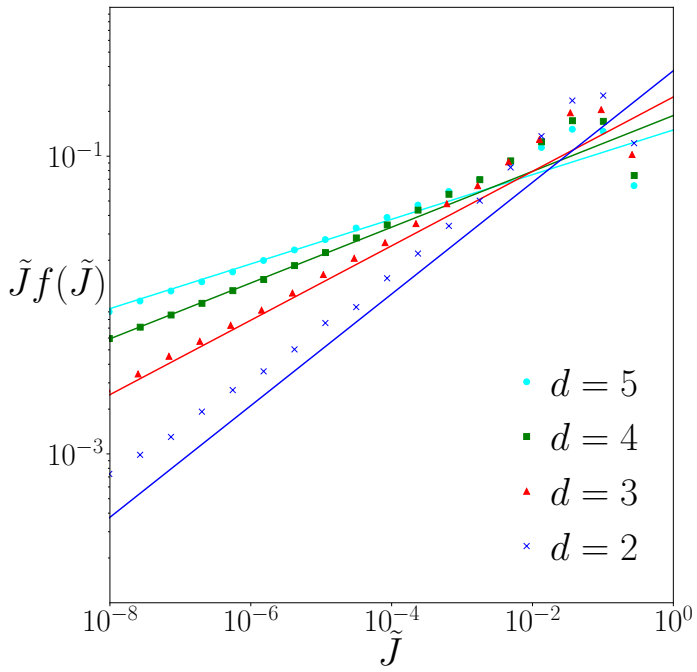

Figure 4.5: Points represent $\tilde{J}f(\tilde{J})$ generated directly from equation (4.9) for various distances d and $W = 4$. Linear function is fitted to obtain λ. There is a single fitting parameter λ for results, i.e. for all values of d.

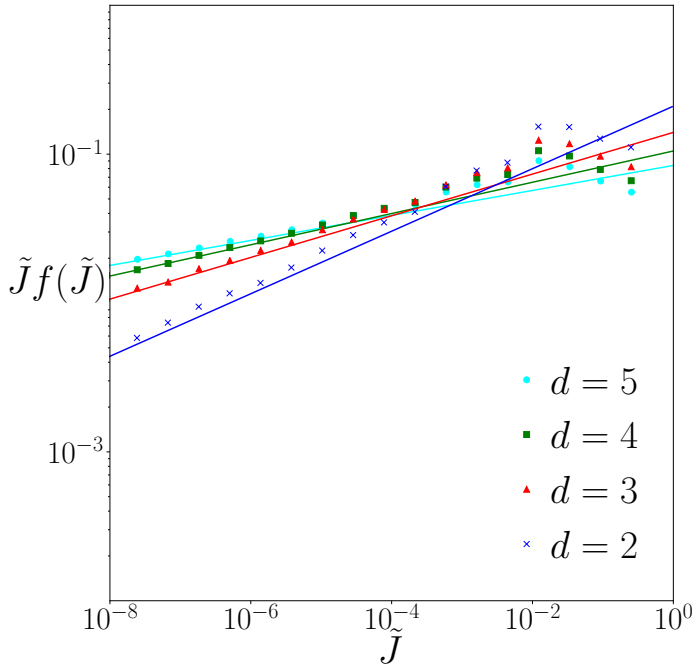

Figure 4.6: Points represent $\tilde{J}f(\tilde{J})$ generated directly from equation (4.9) for various distances d and $W = 8$. Linear function is fitted to obtain λ.

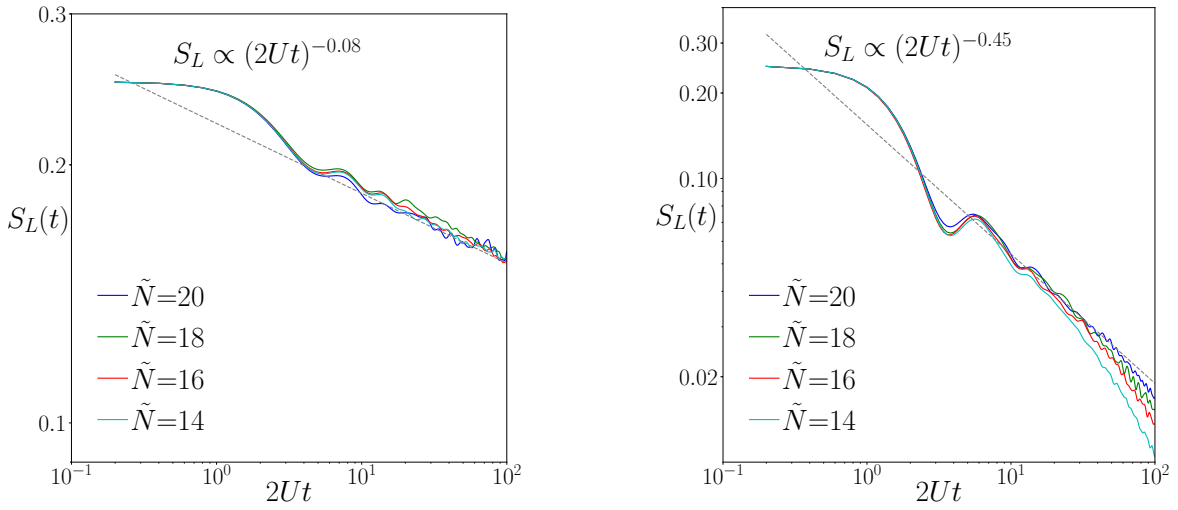

(a) $\tilde{\lambda} = 0.1$ (b) $\tilde{\lambda} = 1.0$

Figure 4.7: Local spin correlation functions for various number of spins $\tilde{N}$. Dashed line represents fit $S_L(t) \sim t^{-\alpha}$ performed for $t \in [10, 50]$.

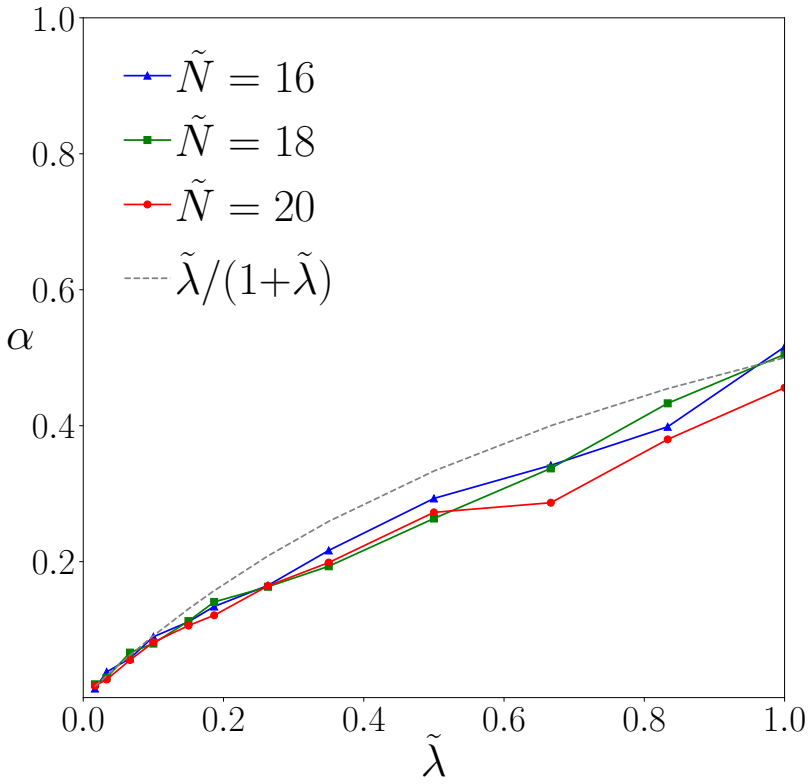

Figure 4.8: Exponent α obtained by the method like in figure 4.7 for different values of $\tilde{\lambda}$.

exponent values for various $\tilde{\lambda}$. The most important observation is that exponent α is non-zero for any non-zero value of $\tilde{\lambda}$. In the next two sections we explain this behaviour from the theoretical point of view.

4.2.6 Single weak link

The subdiffusive spin transport can be explained using similar approach to the one used for spinless particles [64, 115, 116]. In general, the average time of hopping between two sites is inversely proportional to their effective coupling J. This can be taken further, that overall time scale of system evolution is detemined by the smallest of all J-s. We assume that the time necessary for the single excitation to propagate over M sites is

$$t \sim \frac{1}{2UJ_m}, \tag{4.19}$$

where J_m is the smallest out of J_i for $i = 0, 1, 2, ..., M$. We now want to calculate the distribution of J_m and its expectation value. The probability that all J_i are larger than J_m is

$$\left[\int_{\tilde{J}_0}^{1} f(\tilde{J})d\tilde{J}\right]^M = \int_{\tilde{J}_0}^{1} f_m(\tilde{J})d\tilde{J}. \tag{4.20}$$

Using the equation (4.17) and taking derivative with respect to $\tilde{J}_0$ we get

$$M\left[\int_{\tilde{J}_0}^{1} \tilde{\lambda}\tilde{J}^{\tilde{\lambda}-1}d\tilde{J}\right]^{M-1} \tilde{\lambda}\tilde{J}_0^{\tilde{\lambda}-1} = f_m(\tilde{J}_0). \tag{4.21}$$

As

$$\int_{\tilde{J}_0}^{1} \tilde{\lambda}\tilde{J}^{\tilde{\lambda}-1}d\tilde{J} = 1 - \tilde{J}_0^{\tilde{\lambda}}, \tag{4.22}$$

we get the final distribution of the smallest out of $\tilde{J}$

$$f_m(\tilde{J}_0) = M\tilde{\lambda}\tilde{J}_0^{\tilde{\lambda}-1}(1-\tilde{J}_0)^{M-1}. \tag{4.23}$$

We are now interested in the expectation value of the $\tilde{J}_m$. The integration was performed using computer algebra software so we only show final result.

$$\langle\tilde{J}_m\rangle = \int_0^1 \tilde{J}_m f(\tilde{J}_m)d\tilde{J}_m = \frac{M}{\tilde{\lambda}}\frac{\Gamma(\frac{1}{\tilde{\lambda}})\Gamma(M)}{\Gamma(1+M+\frac{1}{\tilde{\lambda}})}. \tag{4.24}$$

Using the property of the Euler gamma function $\Gamma(x+1) = x\Gamma(x)$ we get

$$\langle \tilde{J}_m \rangle = \frac{\Gamma(1+\frac{1}{\tilde{\lambda}})\Gamma(1+M)}{\Gamma(1+M+\frac{1}{\tilde{\lambda}})}. \tag{4.25}$$

Making use of the Gautschi's inequality [117]

$$x^{1-s} < \frac{\Gamma(x+1)}{\Gamma(x+s)} < (x+1)^{1-s}, \tag{4.26}$$

in the limit of large M the following approximation can be made [118]

$$\frac{\Gamma(1+M)}{\Gamma(1+M+\frac{1}{\tilde{\lambda}})} \approx M^{-\frac{1}{\tilde{\lambda}}}, \tag{4.27}$$

so the expectation value of $\tilde{J}_m$ is

$$\langle \tilde{J}_m \rangle = \Gamma(1+\frac{1}{\tilde{\lambda}}) M^{-\frac{1}{\tilde{\lambda}}}. \tag{4.28}$$

The spread of the spin excitation Λ is related to the spin correlation function S_L in the following way $S_L \sim \frac{1}{\Lambda}$ while $\Lambda \sim M \sim (2Ut)^{\tilde{\lambda}}$. Together with equation (4.19) this gives us

$$S_L(t) \sim (2Ut)^{-\tilde{\lambda}}, \tag{4.29}$$

which is the same relation that we obtained from numerical simulations for small $\tilde{\lambda}$, i.e. for very strong disorder.

4.2.7 Multiple weak links

In the case of large $\tilde{\lambda}$ we can no longer assume that dynamics is dominated by the hopping over the link with smallest J. Instead we have a problem known under the name "continuous time random walk" (CTRW) [119, 120]. While it is a classical dynamics, we will show that it correctly captures the studied problem. In order to hop to a neighboring site the particle has to simply wait some amount of time which is randomized from some distribution. The randomization can be performed per each hop, or just once for each link. In our case we have the latter variant of CTRW where each hopping time is randomized just once on "initialization" of a system and then remains constant.

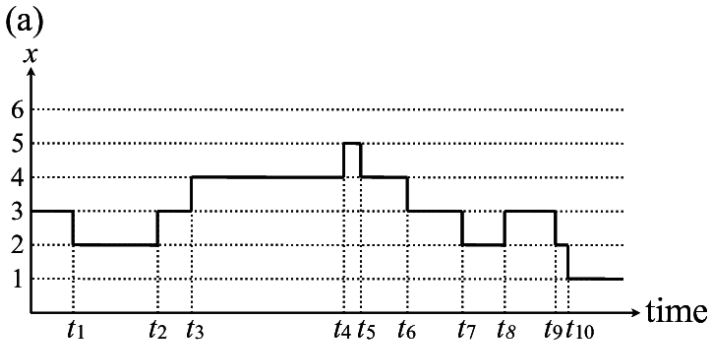

Figure 4.9: Schematic of the standard continuous-time random walk (CTRW) on a one-dimensional lattice. Taken from Physics Reports Volumes 716–717, **22**, 1-58 (2017).

Our hopping time τ is inversely proportional to the coupling J_i thus $\tau_i = \frac{1}{J_i}$ is drawn from the following distribution

$$f_\tau(\tau) = \frac{\tilde{\lambda}}{\tau^{\tilde{\lambda}+1}}, \tag{4.30}$$

obtained straightforwadly from the formula for the distribution of a reciprocal of a random variable [121]. Such problem has been solved in the theoretical context in [122] for the same class of distributions as we have here. The solution for one-dimensional system is

$$\Lambda \sim (2Ut)^\alpha, \tag{4.31}$$

where

$$\alpha = \frac{\tilde{\lambda}}{1+\tilde{\lambda}}. \tag{4.32}$$

This result is consistent with numerical simulations carried on for all $0 \leq \tilde{\lambda} \leq 1$. Also, in the limit of $\tilde{\lambda} \ll 1$ the exponent α is the same as in the weak link scenario.

4.2.8 Back to Hubbard model

At the end we return to the original Hubbard model to verify our findings. We calculate the same spin correlation functions $S_L(t)$ as in the previous sections. Time evolution was performed using microcanonical Lanczos method [103, 104, 105]. From figures 4.5 and 4.6 we obtain relation between disorder W and Anderson localization length λ -

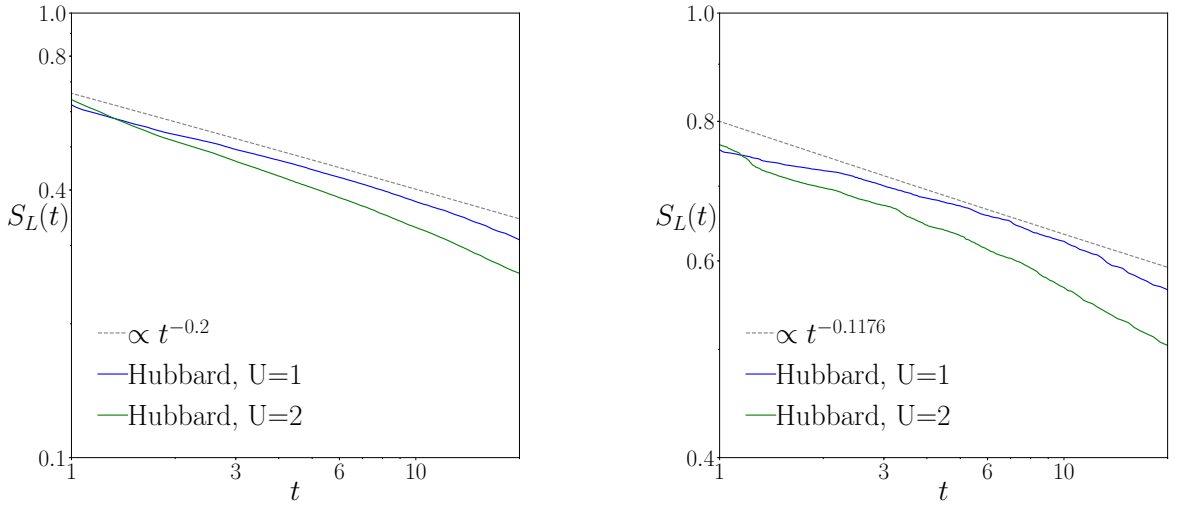

(a) $W = 4$ (b) $W = 8$

Figure 4.10: Local spin correlation functions in full Hubbard model for $L = 18$, $N = 3$ and two values of U. Dashed line represents the theoretical result $S_L(t) \sim t^{-\alpha}$ with $\alpha = \frac{\tilde{\lambda}}{\tilde{\lambda}+1}$ shifted vertically for clarity.

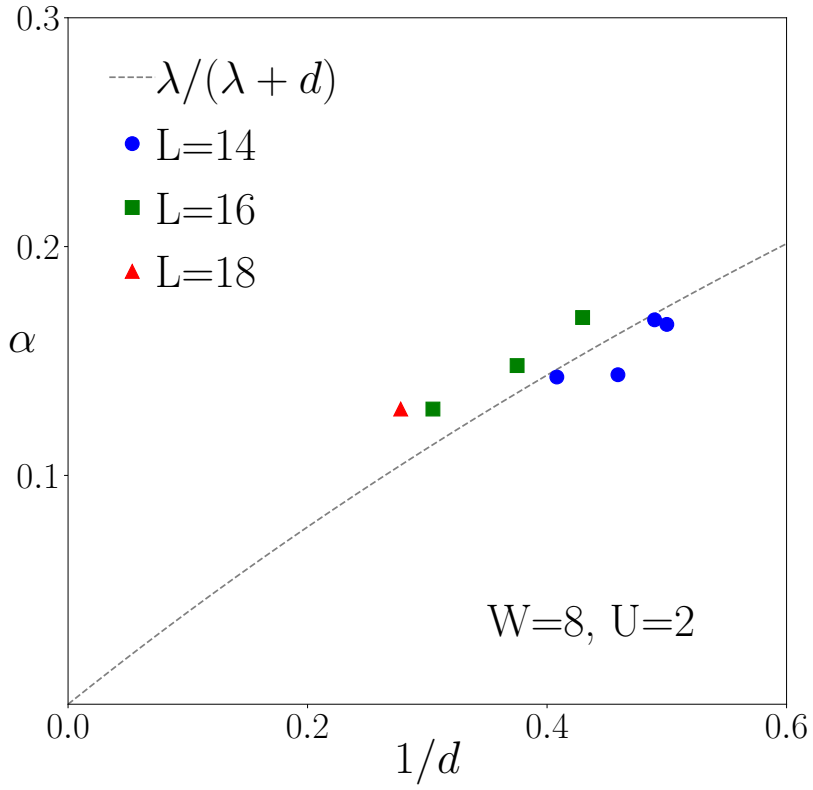

Figure 4.11: Exponent α obtained in the full Hubbard model for a few system sizes. Dashed line is the theoretical value of $\alpha = \frac{\lambda}{\lambda+d}$.

$\lambda \approx 0.75$ for $W = 4$ and $\lambda \approx 0.4$ for $W = 8$. Our system has $L = 18$ sites and $N = 6$ particles which gives average distance $d = \frac{L}{N} = 3$. Results can be seen in figure 4.10 for two values of interaction coefficient U so we observe that the slope does not depend much on it.

Finally we construct plot of exponents α vs $1/d$. In figure 4.11 we see that the results are more or less located near the theoretical predictions (dashed line). Since simulating full Hubbard model was much more computationally challenging we could not go beyond system sizes of $L = 18$. This is why we see non-negligible finite size effects but they do not invalidate our conclusions.

4.3 Summary

In this chapter we considered disordered Hubbard model (4.1). The goal was to show that it is not possible to fully localize spins if the disorder is only in the charge sector.

At first, we studied the situation when there are only two electrons with opposite spins. For sufficiently strong disorder (typically $W = 8$) numerical simulations showed that charges were fully localized, but spin oscillated (figs 4.1 and 4.2). This observation allowed us to create an effective spin model where coupling constant of two spins is equal to the frequency of oscillations. During derivation of the model in equation (4.3), we dropped terms representing coupling between spins and charges. Comparison of the J obtained by two methods is shown in figures 4.3 and 4.4.

This allows for the numerical procedure of creating the effective Hamiltonian. We can now perform simulation with two electrons in full Hubbard model and numerically evalute the oscillation frequency to get value of effective coupling J. However, for this particular case it was possible to calculate the distribution of J analytically. Starting from the distribution of randomly placing of N points on line segment of length L (equation (4.13)) we get to the equation (4.17). Now, instead of randomizing disorder in the Hubbard model, we can directly create effective model by randomizing J. We introduced dimensionless parameter $\tilde{\lambda} = \frac{\lambda}{d}$ as a ratio of Anderson localization length λ to the average distance between particles $d = \frac{L}{N}$. We tested the resulting probability

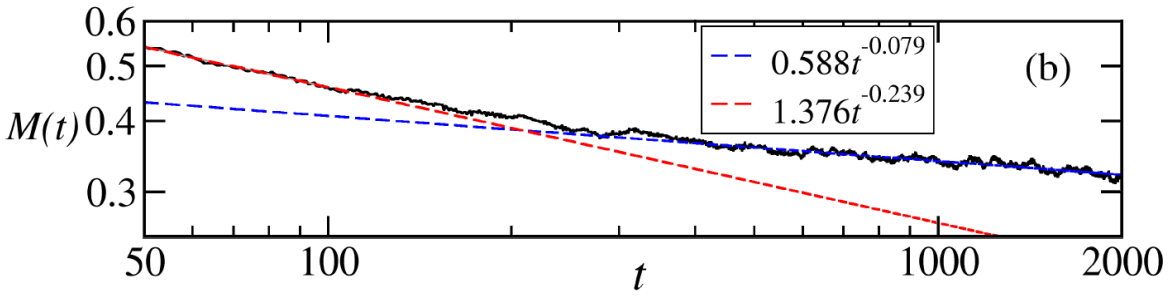

Figure 4.12: Numerical simulation of $M(t)$ correlation funcion (equivalent of ours $S_L(t)$) obtained using t-DMRG in a system with $L = 64$ sites, $U = t_0 = 1$ and disorder strength $W = 16$ averaged over 237 realizations of the disorder. Taken from Phys. Rev. B **98**, 014203 (2018).

distribution (4.17) which can be seen on figures 4.5 and 4.6. Additionally from those plots we obtained relationship between disorder strength W in the original Hubbard model and our new parameter $\tilde{\lambda}$.

We performed numerical simulations and calculated spin correlation function (4.18) for various values of $\tilde{\lambda}$ to estimate the exponent of the decay as shown in figure 4.7. Results for different values of $\tilde{\lambda}$ are combined in figure 4.8 which is the most important plot in this chapter. If it was possible to localize spins, the curve would cross horizontal axis for some non-zero $\tilde{\lambda}$. Since it crosses point (0,0) we see that for any non-zero $\tilde{\lambda}$ the spins would remain delocalized. Just to remind, $\tilde{\lambda} = 0$ can occur only if the Anderson localization length is zero (the limit of infinite disorder), or the average distance between particles is infinite (the limit of empty lattice).

The results we obtained from numerical simulations can be backed with theoretical considerations. We distinguish two cases: low and large values of $\tilde{\lambda}$. In the former case spin transport is limited by the smallest J and it can be shown that the exponent is equal to $\tilde{\lambda}$ (equation (4.29)). On the other hand, for larger values $\tilde{\lambda}$ we obtain different exponent as in equation (4.32) (which is consistent with the previous result for $\tilde{\lambda}$ near zero). In figure 4.8 the dashed line represents the theoretically obtained value and we see that it matches the numerical results.

We also compare the results obtained in effective model to the full Hubbard model

that we had at the beginning. The spin correlation functions are shown in figure 4.10 and their slope is very similar to our predictions. In figure 4.11 we combine the exponents together and while they do not present themselves as accurately as for the effective model, we see that they are close to the theoretical values.

Interestingly, there is a similar work [123] that was published slightly later and supports our results. The authors used DMRG method [124] to numerically simulate full Hubbard model with 64 sites and calculated the same kind of spin correlation functions as we did. For parameters equivalent to our $\tilde{\lambda} \approx 0.125$ they obtained the exponent between 0.239 and 0.079 for short and long times respectively 4.12, the latter value being close to 0.11 that we get from our equation (4.32). This suggests that our systems sizes were large enough and we focused on sufficiently long times for our results to be accurate. Most importantly, advanced numerics in [123] supports our analytical approach.

Chapter 5

Energy transport in disordered Hubbard model

The results presented in this chapter were previously published in *"Suppressed energy transport in the strongly disordered Hubbard chain"*, M. Kozarzewski, M. Mierzejewski, P. Prelovšek, Phys. Rev. B **99**, 241113(R) (2019)

5.1 Motivation

In the previous chapter we showed that spin dynamics in disordered Hubbard model is subdiffusive and that spins are always delocalized. Such conclusions was based on the investigation of an effective spin model. However, it is possible that spin-charge coupling terms (that we neglected) are responsible for charge delocalization in the long time. We now focus on the energy correlation function $C^h(t)$ describing the energy transport and show that it is very different from the one for spin. While the spin correlation function $C_S(t)$ decays to zero (indicating lack of localization in spin sector), $C_h(t)$ saturates on some level suggesting strongly suppressed energy transport. However, detailed study, performed also by other researchers [125], leads us to the hypothesis that in the limit of large system charges are not localized but their delocalization timescale is beyond numerical sumulations.

5.2 Results

5.2.1 Model

Once again we start with the Hubbard model with disorder

$$H = -t_h \sum_{i,\sigma} (c^\dagger_{i+1,\sigma} c_{i,\sigma} + H.c.) + \sum_i \epsilon_i \hat{n}_i + U \sum_i \hat{n}_{i,\uparrow} \hat{n}_{i,\downarrow}, \tag{5.1}$$

where $\hat{n}_i = \hat{n}_{i,\uparrow} + \hat{n}_{i,\downarrow}$ and $\hat{n}_{i,\sigma} = c^\dagger_{i,\sigma} c_{i,\sigma}$ for $\sigma \in \{\uparrow, \downarrow\}$. The system has L sites and total of N particles, hopping integral $t_h = 1$, total spin projection S^z is zero and each ϵ_i is drawn from uniform distribution in range $[-W, W]$.

At first, we want to study the effective model introduced in a previous chapter. It assumes that charges are frozen so any transport properties are a result of the spin fluctuations. Then, we can reduce Hubbard model to Heisenberg model

$$H = -2U \sum_a J_a \bar{S}_a \cdot \bar{S}_{a+1} = \sum_a h_a, \tag{5.2}$$

where h_a is energy density operator. Coefficients J_a are random numbers in the range $[0, 1]$ drawn from probability distribution

$$f(J_a) = \tilde{\lambda} J_a^{\tilde{\lambda}-1}, \quad 0 \leq \tilde{J} \leq 1, \tag{5.3}$$

where $\tilde{\lambda} = \frac{\tilde{\lambda}}{1+\tilde{\lambda}}$ is a ratio of Anderson localization length λ of the non-interacting Hubbard model and average spacing between particles d in the original Hubbard model. For $\tilde{\lambda} < 1$ the distribution is singular at $\tilde{J} = 0$ which is responsible for the anomalous behaviour - subdiffusive spin transport.

5.2.2 Spin and energy correlation functions

We are interested in calculating following spin and energy correlation functions

$$C^S(t) = \left\langle \frac{\langle S^z_a(t) S^z_a(0) \rangle - \langle S^z_a(0) \rangle^2}{\langle S^z_a(0) S^z_a(0) \rangle - \langle S^z_a(0) \rangle^2} \right\rangle_{dis,a}, \tag{5.4}$$

$$C^h(t) = \left\langle \frac{\langle h_a(t) h_a(0) \rangle - \langle h_a(0) \rangle^2}{\langle h_a(0) h_a(0) \rangle - \langle h_a(0) \rangle^2} \right\rangle_{dis,a}, \tag{5.5}$$

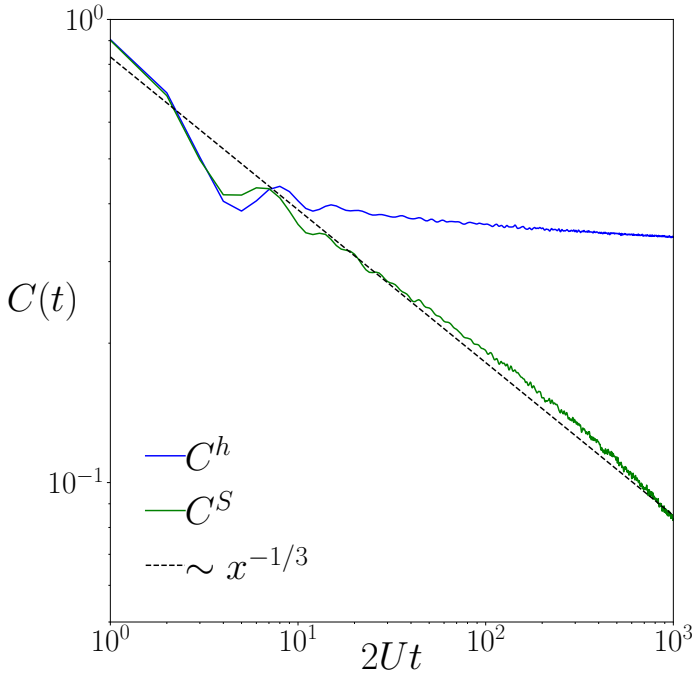

Figure 5.1: Spin and energy correlation functions $C^S(t)$ and $C^h(t)$ in the effective model for $\tilde{\lambda} = 0.5$ and $N = 18$ sites. Dashed line is the analytical prediction as in the equation (4.31).

where $\langle\rangle_{dis,a}$ means averaging over many realisations of disorder and several Anderson states (positions in real space) respectively.

They are generalisations of the spin correlation function we encountered in the previous chapter by making a correction for the initial value. While for C^S the initial value does not matter as total spin is zero, but the energies can differ because of disorder randomization. Using such definitions, both functions are normalized $C^S(0) = C^h(0) = 1$ so we can directly compare them. In figure 5.1 we show a comparison of both functions for $\tilde{\lambda} = 0.5$. While $C^S(t)$ follows the decay predicted by the effective model $t^{-\tilde{\lambda}/(1+\tilde{\lambda})}$, $C^h(t)$ visibly saturates. However, considering the system size and accessible timescale, the shape of the $C^h(t)$ curve leaves us with doubts if the energy stiffness $C^h(t \to \infty)$ is indeed non-zero.

We performed more simulations, two of them being presented in figures 5.2 and 5.3. In both cases we averaged over 2000 distributions of disorder. We plot there several lines of $C^h(t)$ for different system sizes to observe the importance of finite size effects.

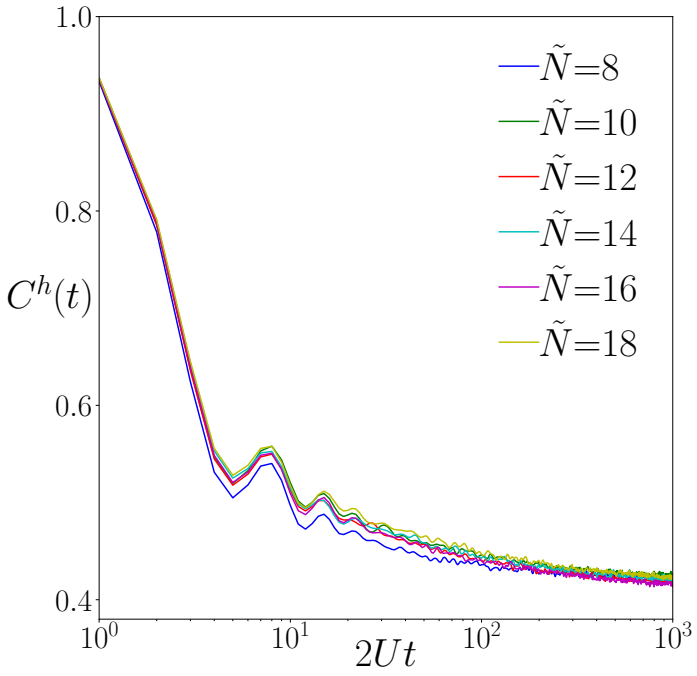

Figure 5.2: Energy correlation functions $C^h(t)$ in the effective model for $\tilde{\lambda} = 0.3$ and various system sizes.

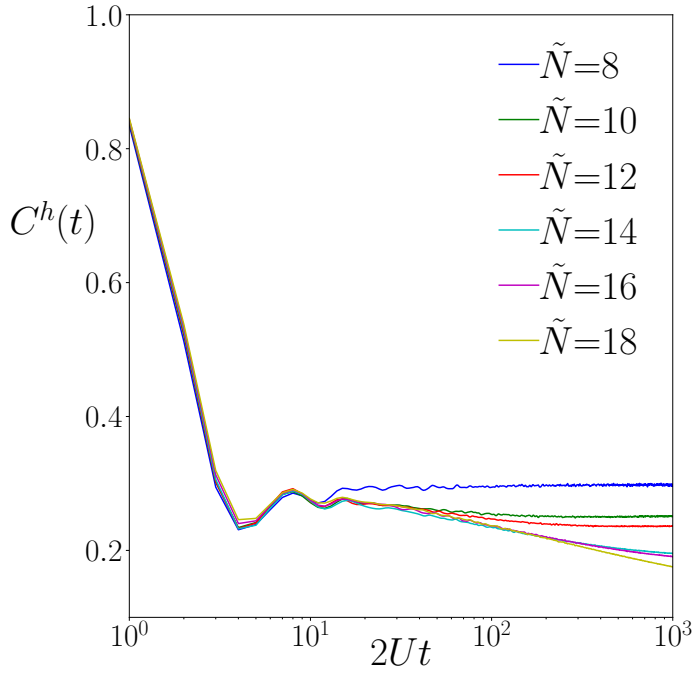

Figure 5.3: Energy correlation functions $C^h(t)$ in the effective model for $\tilde{\lambda} = 1.0$ and various system sizes. The finite-size effects are clearly visible here.

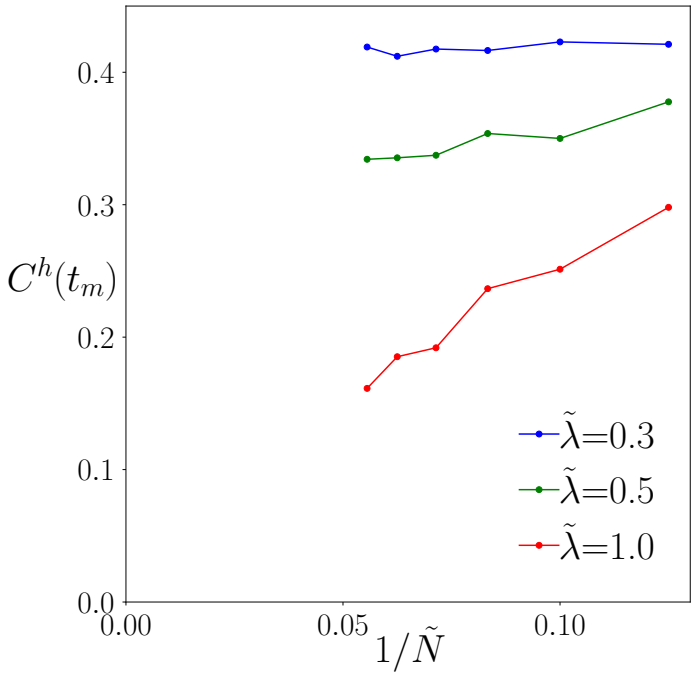

Figure 5.4: Finite-size scaling of C^h for times $2Ut = 10^3$ as in the figure 5.3.

For $\tilde{\lambda} = 0.3$ we see that all curves follow the same decay profile, while for $\tilde{\lambda} = 1$ finite-size effects are significant. Their scaling (together with intermediate $\tilde{\lambda} = 0.5$) in figure 5.4 shows that apparently for low values $\tilde{\lambda}$ energy correlation function relaxes to some non-zero stationary value. We do not try to provide exact value of the stiffness $C^h(t \to \infty)$ because of the randomness in the simulations that was not completely filtered out after averaging.

We can also estimate the infinite time value of $C^h(t)$ using exact diagonalization (ED) approach. In figure 5.5 we have longer times of $2Ut = 10^4$ which seems enough to be more confident about $C^h(t)$ relaxation profile. This time, we average over 10^5 simulations for $\tilde{N} = 10$, $3*10^4$ for $\tilde{N} = 12$ and 10^4 for $\tilde{N} = 14$. Additionally, this allows us to perform more precise finite-size scaling, as shown in figure 5.6. While the lines are more smooth than previously, they have visible negative curvature. It is possible that they all go down to zero for $\tilde{N} \to \infty$ but proving this is beyond the capabilities of our numerical simulations. Similar topic was considered in [125] and it was suggested that delocalization and ergodicity may occur for very large system sizes.

In [125] authors investigated the matrix elements of $\bar{S}_a \cdot \bar{S}_{a+1}$ in the eigenbasis of

a Hamiltonian over two sites a and $a+1$ that are coupled by the largest of all J. In figure 5.7 we see such matrix elements for two realisations of disorder. The elements $\langle n|\, \bar{S}_a \cdot \bar{S}_{a+1}\, |n\rangle$ typically take one of the two values, approximately either -3/4 or 1/4 which correspond to either singlet or triplet state. Both states form a barrier that blocks energy transport in their neighborhood. In cited work there was also similar plot in the ETH phase, where as expected elements have values close to 0.

5.2.3 Conductivity in full Hubbard model

We have to return to original Hubbard model to further test our findings. We study dynamical charge, spin and thermal conductivities at half-filling.

$$\sigma^x(\omega) = \frac{1}{L}\Re \int_0^\infty e^{i\omega t}\langle I_x(t) I_x(0)\rangle dt, \tag{5.6}$$

where x is either c, S or t for charge, spin and thermal conductivities respectively. We define following density of the current

$$I_{j,\sigma} = i\left(c^\dagger_{j+1,\sigma}c_{j,\sigma} - c^\dagger_{j,\sigma}c_{j+1,\sigma}\right), \tag{5.7}$$

then the charge current I_c is straightforwardly

$$I_c = \sum_{j,\sigma} I_{j,\sigma}, \tag{5.8}$$

spin current I_S is

$$I_c = \sum_{j,\sigma} \sigma I_{j,\sigma}, \tag{5.9}$$

and finally the energy current I_t with more complex form

$$I_t = -\sum_{j,\sigma}\left(ic^\dagger_{j+1,\sigma}c_{j-1,\sigma} + H.c.\right) + \sum_{j,\sigma} I_{j,\sigma}\left(\frac{\epsilon_j + \epsilon_{j+1}}{2} + U\frac{n_{j,\sigma} + n_{j+1,\sigma}}{2}\right). \tag{5.10}$$

During derivation of those equation we followed procedure described in [126], especially the supplemental material. For time evolution, we use microcanonical Lanczos method [104, 105] in system with $L = 14$ sites averaging over 30-100 realisations of disorder.

In figure 5.8 (a) and (b) we compare $\bar{\sigma}^S$ and $\bar{\sigma}^t$ for different system sizes to estimate finite-size effects. While for large ω there are some differences, the low frequency regime

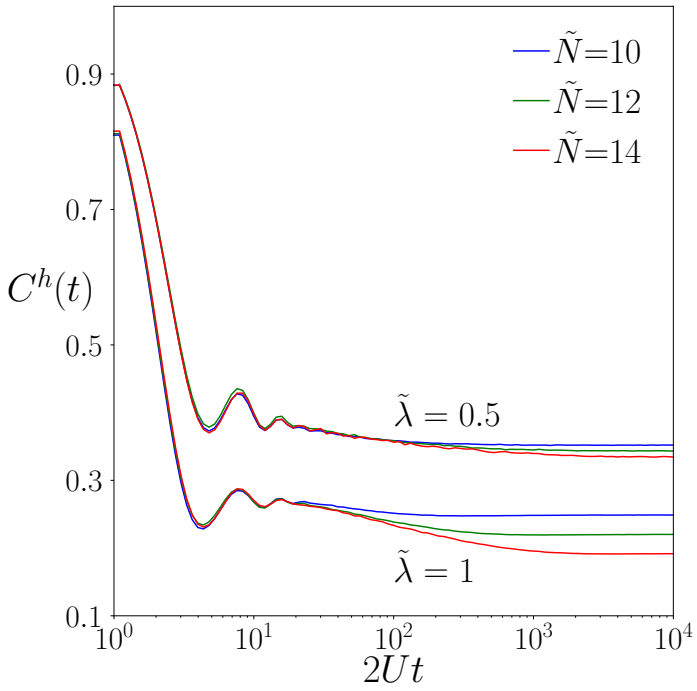

Figure 5.5: $C^h(t)$ as in 5.3 but for longer times.

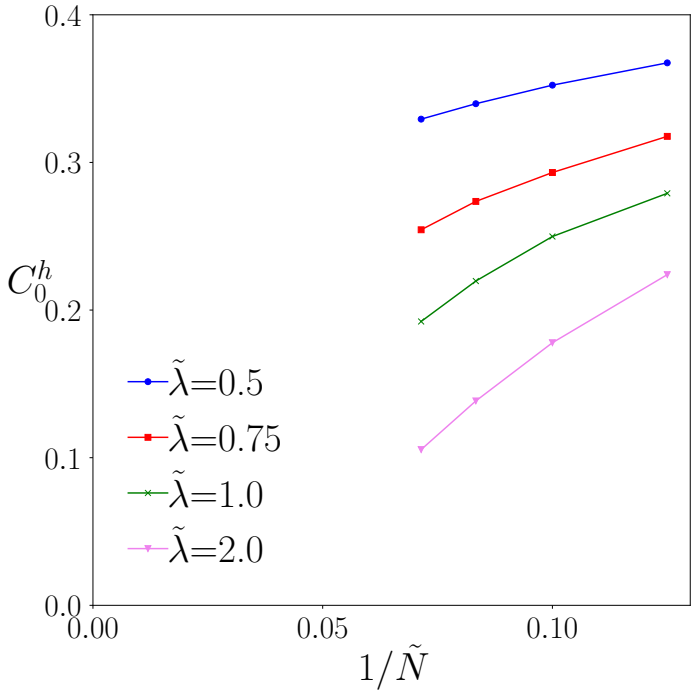

Figure 5.6: Finite-size scaling of the result from figure 5.5 for times $2Ut = 10^4$.

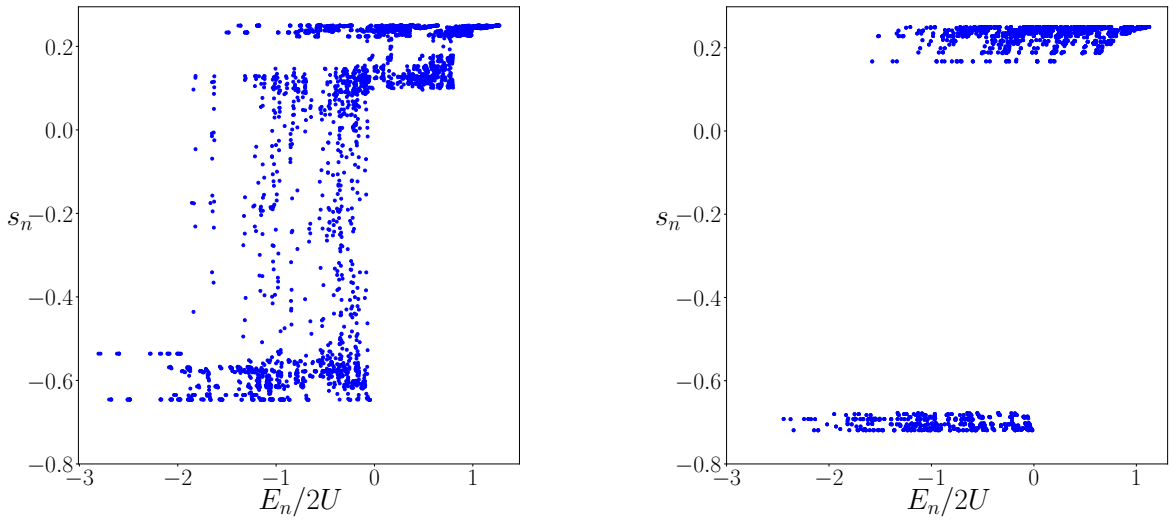

Figure 5.7: Diagonal matrix elements of $s_n = \bar{S}_a \cdot \bar{S}_{a+1}$ vs eigenenergy E_n obtained for a bond with the largest J_a for $\tilde{N} = 14$ and two particular realisations of disorder corresponding to the same $\tilde{\lambda} = 0.5$.

behaves in the same way, fairly independently of L. On panels (c) and (d) we compare the three conductivities for largest accesible system size $L = 14$ and $U = 2, W = 8$ or $U = 4, W = 12$ respectively. We are interested in the exponent α in relation $\sigma^x(\omega) \sim \omega^\alpha$ for low values of ω. We see that for spin, this exponent is smaller than 1, as we already know that spin transport is subdiffusive. On the other hand, for both charge and energy conductivities the exponent is close to 1 which is consistent with other research [65, 66]. However full charge localization should give us exponent strictly larger than 1 [69]. Our results provide another argument for the absence of full MBL for this class of Hamiltonians.

5.3 Summary

In this chapter we focused on energy transport within disordered Hubbard model and its effective spin model. The goal was to find out whether there is an energy transport when we already know that spin transport is subdiffusive.

We define generalised spin and charge correlation functions $C^S(t)$ and $C^h(t)$. The first presented plot 5.1 shows that they have completely different behaviour. Further

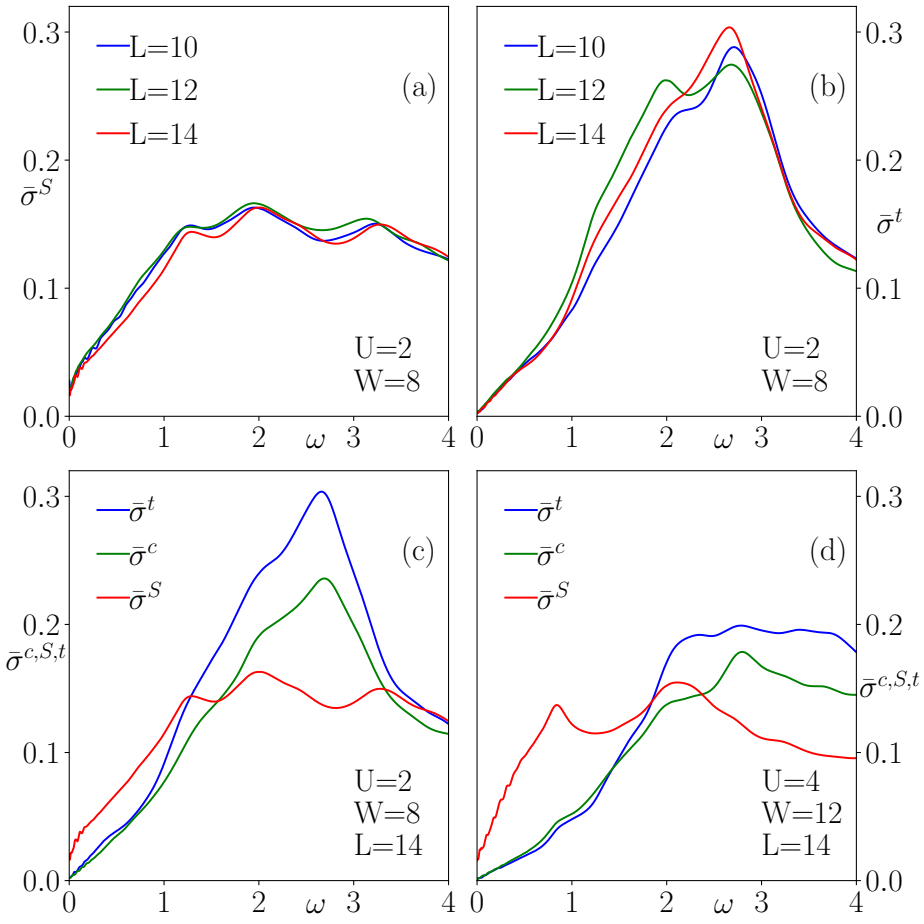

Figure 5.8: Normalized charge, spin, and thermal dynamical conductivities $\bar{\sigma}^c, \bar{\sigma}^S, \bar{\sigma}^t$. (a) and (b) show the finite-size effects of $\bar{\sigma}^S$ and $\bar{\sigma}^t$. (c) and (d) compare the three conductivities for two parameter sets.

analysis reveals that increasing $\tilde{\lambda}$ signifies finite-size effects 5.2 5.3. Using finite-size scaling we conclude that for $\tilde{\lambda} = 1$ (uniform distribution of J) infinite time value of C^h seems to vanish.

Much clearer picture arises when we use exact diagonalization. In figure 5.6 we obtain much smoother curves, their negative slope might be a clue that $C^h(t)$ vanishes in all cases but for systems too large for our numerical simulations.

Then we return to full Hubbard model to calculate optical conductivities. In figure 5.8 we compare three conductivities, for spin, charge and energy. We see that σ^S behaves differently from the other two, around $\omega = 0$ proportionaly to ω^α with $\alpha < 1$

while σ^c and σ^t have the exponent close to 1. Because σ^c and σ^t are very similar to each other and distinct from σ^S we conclude that energy transport is strongly suppressed as it is the case for the particle transport.

Finally, we can explain the suppressed energy transport by calculating matrix elements of $\langle n| \bar{S}_a \cdot \bar{S}_{a+1} |n\rangle$ for the link with the strongest coupling J_a. We see that there are two distinct states, spin singet and triplet. Such configuration blocks transport near this link.

Overall conclusion is that while for finite-size systems the energy transport quickly saturates (quickly when compared to spin transport), there is a possibility that for very large systems and very long time evolution there is no full MBL as the energy transport is strongly suppressed but not fully eliminated.

Conclusions

Many-body localization (MBL) is a relatively new topic of research but its foundations were set several decades earlier by investigations of single particle in a random potential or strongly correlated systems. Perhaps the most significant characteristic of MBL is the lack of thermalization which means they can store information. This information is stored in the form of local integrals of motion (l-bits) which is another important property of MBL systems. We focus on the transport properties, either the particle current in driven spinless system or spin and energy transport in disordered Hubbard model. In this short chapter we summarise the results presented in this thesis.

In the third chapter we wanted to find an experimentally measurable indicator whether the system is already in the MBL phase. Procedure that we simulated numerically, is to apply strong electric field to the system and measure the current response. Such behaviour is known as Bloch oscillations (with no disorder). General observation is that the frequency is proportional to the field and Joule heating will eventually damp the oscillations and the system would no longer conduct electrical current.

Very different picture arises if we include strong disorder. In the numerical simulations we observed that the frequency is constant, independently of the parameters used. While investigating local currents, it became obvious that individual currents do not undergo any damping, suggesting that MBL prevented the system from heating. We formulated and solved local two-site model which supported this observation. The local currents oscillate with frequency inversely proportional to the amplitude. The vanishing of the total current turned out to be an effect of destructive interference of many such local currents, indeed with constant characteristic frequency. These results mean that in the experiments one can distinguish the two phases by simply measuring

the response to the external field. Another implication is that MBL prevented such system from heating.

The two-site model already correctly predicts the oscillation frequency but its weakness is the impossibility to include interactions. Theoretically, we can consider 3-site model with 1 or 2 electrons but this is the largest variant that could be solved analytically (while being much more complicated than 2-site one). However, instead of creating larger local models, one may try the reverse procedure where we start from original full lattice and look for the "weakest link" that divides the system into two subsystems. Then both parts could undergo time evolution separately using some kind of mean field approximation for the interactions over the boundary of the two parts. The task of finding proper division point could be solved using machine learning algorithms, which has recently become very popular direction of research in solid state physics [127].

In the fourth chapter we shifted towards less commonly investigated topic of spin systems, namely the disordered Hubbard model. In such model the disorder can be coupled either to charges or to spins (or both). One of the problems encountered in this area was the apparent lack of localization in the spin sector if disorder is in charge sector. While it was a quite well established conclusion, evidences were mostly based on numerical simulations. In numerical simulations, we noticed that while charges are localized, the spins are not. Basing on this, we created effective Heisenberg model that could be used to analytically show that without disorder coupled to spins it is not possible to localize them (unless the disorder is infinite or the lattice is empty).

In full Hubbard model, we were able to obtain a few more results that support our conclusions about the spin subdiffusion. Our simulations were limited to moderate system sizes but there are another publications that reported subdiffusive transport, both prior and after our work [71, 84, 85, 123]. One thing left out from our considerations is the approximation that neglects all spin-charge coupling terms in the derivation of an effective model. Perhaps, if we include some of them we could analytically show that charges are delocalized, which would be much more direct argument instead of drawing conclusions from the inherently limited numerical simulations.

The fifth chapter expands the fourth one with the investigations of the energy transport. Right from the start we observe that charge correlation function saturates on some level instead of vanishing to zero like the one for spin. We collect several clues that this saturation might be a finite-size effect which was suggested in other research [125] but the final conclusion is still missing. It appears that disorder only in charge sector is not sufficient to cause full localization in such kind of systems.

Another approach to the problem of existence of full MBL in disordered Hubbard model is presented in the appendix to this thesis. We know that non-thermalizing systems posess extensive number of local integrals of motion (LIOM). For given Hamiltonian, we can calculate the exact number of LIOMs that is required for full MBL and compare that with the number of actual LIOMs that exist in this system. We create a procedure of finding all relevant LIOMs, ordered by their "locality". For spinless fermions their number exactly matches the theoretical prediction, which is not surprising as such system is known to exhibit full MBL.

For spin system the number of LIOMs is significantly smaller than required, but larger than in spinless system. On the other hand, if we include random magnetic field the number of LIOMs increases to the value expected for full localization. The only weakness of this method is the necessity of exact diagonalization of a Hamiltonian which restricts applicability of this method to relatively small systems. It does not seem that this requirement could be mitigated in any way, so the only progress that could be made is to use some large scale distributed computation software to slightly increase accessible system sizes.

During the research presented in this thesis we used to start with performing many numerical simulations until we noticed something that allowed us to attack the problem and possibly solve it. I personally found such approach to scientific work to be the most enjoyable.

Appendix A

The results presented in this appendix were previously published in *"Counting local integrals of motion in disordered spinless-fermion and Hubbard chains"*, M. Mierzejewski, M. Kozarzewski, P. Prelovšek, Phys. Rev. B **97**, 064204 (2018)

5.4 Construction of local integrals of motion

Local integrals of motion (LIOM) concept is appealing point of view on the topic of many body localized (MBL) systems. In the first chapter we have already described LIOM approach in terms of so called "l-bits". In general it is known that MBL systems have macroscopic number of local conserved quantities but unfortunately the practical application of "l-bit" concept in numerical simulations is challenging [60, 61, 62, 128]. In this appendix we review our publication where we provide alternative method for finding LIOMs which is an extension and generalisation of a method described in [129, 130]. For Hubbard model with disorder both in spin and charge sector, we can show that it has as many LIOMs as it is predicted theoretically. However, without disorder coupled to spins, number of LIOMs is significantly lower indicating that there is only partial MBL.

We want to construct local operators on M sites in tight-binding Hamiltonian with L sites. At first we enumerate all possible combinations of creation, annihilation and particle number operators on M sites. Then we calculate time averaged operator as in the following equation.

$$\bar{A} = \lim_{\tau\to\infty} \frac{1}{\tau} \int_0^\tau e^{iHt} A e^{-iHt} dt. \tag{5.11}$$

Then we create matrix of stiffnesses.

$$D_{AB} = \langle \bar{A}\bar{B} \rangle = Tr(\bar{A}\bar{B})/Tr(I). \tag{5.12}$$

This matrix is diagonalized with orthogonal matrix U.

$$\sum_{a,b} U^T_{a,\alpha} \langle \bar{O}_a \bar{O}_b \rangle U_{b,\beta} = \lambda_\alpha \delta_{\alpha,\beta}. \tag{5.13}$$

Using this matrix we can change the basis to the orthonormal one, thus having complete and independent set of orthogonal operators O ordered by their locality captured in associated eigenvalue λ_α. Typically operators that we begin the whole procedure with look like following, in this case for $M = 4$ sites

$o_1 = \tilde{n}_1 + \text{H.c.}$ $o_9 = \tilde{n}_2\tilde{n}_4 + \text{H.c.}$ $o_{34} = a_1^\dagger \tilde{n}_2 a_3 + \text{H.c.}$

$o_2 = \tilde{n}_2 + \text{H.c.}$ $o_{10} = \tilde{n}_1\tilde{n}_4 + \text{H.c.}$ $o_{35} = a_2^\dagger \tilde{n}_3 a_4 + \text{H.c.}$

$o_3 = \tilde{n}_3 + \text{H.c.}$ $o_{11} = \tilde{n}_1\tilde{n}_2\tilde{n}_3 + \text{H.c.}$ $o_{36} = \tilde{n}_1 a_2^\dagger a_4 + \text{H.c.}$

$o_4 = \tilde{n}_4 + \text{H.c.}$ ... $o_{37} = a_1^\dagger a_3 \tilde{n}_4 + \text{H.c.}$

$o_5 = \tilde{n}_1\tilde{n}_2 + \text{H.c.}$ $o_{30} = a_1^\dagger a_4 + \text{H.c.}$ $o_{38} = a_1^\dagger \tilde{n}_3 a_4 + \text{H.c.}$

$o_6 = \tilde{n}_2\tilde{n}_3 + \text{H.c.}$ $o_{31} = a_1^\dagger a_2 a_3^\dagger a_4 + \text{H.c.}$

$o_7 = \tilde{n}_3\tilde{n}_4 + \text{H.c.}$ $o_{32} = a_1^\dagger a_2^\dagger a_3 a_4 + \text{H.c.}$

$o_8 = \tilde{n}_1\tilde{n}_3 + \text{H.c.}$ $o_{33} = a_1 a_2^\dagger a_3^\dagger a_4 + \text{H.c.}$ $\tilde{n}_i = a_i^\dagger a_i - \frac{1}{2}.$

5.5 Spinless system

We first focus on model of spinless fermions, similar to the one used in Chapter 3.

$$H = -t_h \sum_{j=0}^{L-1} (c_{j+1}^\dagger c_j + H.c.) + V \sum_{j=0}^{L-1} \hat{n}_j \hat{n}_{j+1} + \sum_{j=0}^{L-1} \hat{n}_j \epsilon_j. \tag{5.14}$$

Here we also consider half filling. In this model we expect that $2^M - 1$ LIOMs will be required for full MBL. The results are summarized in figure 5.9. On panels a-c we can see that increasing disorder creates a visible discontinuity in the progression of λ_α values. The MBL transition appears to occur at $W \approx 4$ which is consistent with previous studies [131, 132]. Model 5.14 exhibits full MBL behaviour which is confirmed

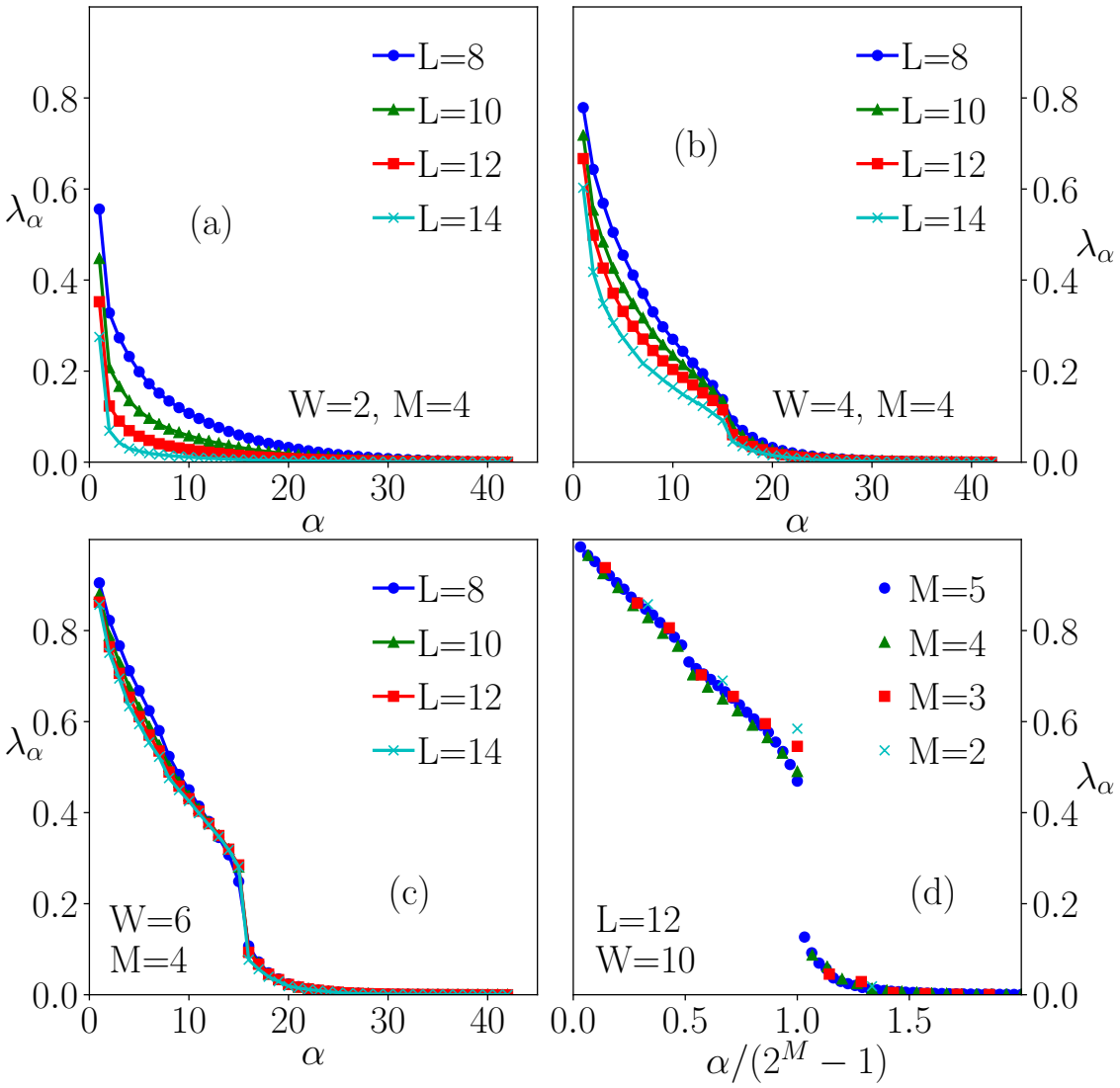

Figure 5.9: Results for disordered chain of spinless fermions. Eigenvalues λ_α corresponding to local components of each LIOM, averaged over disorder for various system sizes L, supports M and different disorders W.

on panel (d) - there are exactly $2^M - 1$ (15 for this case) LIOMs. In figure 5.10 (a) we also check the importance of interactions in the model. We get that the case of $V = 0$ (Anderson insulator) has the same number of conserved quantities as the interacting variant.

It is clear that while the number of LIOMs in MBL phase does not depend on disorder strength W, their combined locality do. This is why we introduce another measure $\Lambda = \sum_\alpha \lambda_\alpha$ which is simply a weighted sum, with LIOM locality as its weight. It is obvious that for perfectly localized system Λ would be equal to the number of local conserved operators. In figure 5.10 (b) we see that increasing disorder makes the Λ closer to the theoretical value of $2^M - 1$. Since construction of LIOMs requires a diagonalization of a Hamiltonian, it is quite an expensive procedure. Because of that, we can only reach relatively moderate system sizes and that calls for finite size scaling analysis. In figure 5.10 (c) we check how Λ changes with system size and conclude that for strong disorder (above $W = 6$) it no longer depends on system size. On the other hand for small W, Λ vanishes in the limit $L \to \infty$ providing another method of finding transition point.

Finally, we distinguish two types of LIOMs, those containing hopping operator ($c_i^\dagger c_{j\neq i}$) and those without hopping. As presented in figure 5.10 (d) it turns out that contribution of 'hopping' LIOMs is almost independent of disorder strength, which means that deep in MBL phase the 'non-hopping' LIOMs will be dominant. Non-hopping operators must be composed solely of number of particles operators $\hat{n}_i$ so for large W they can be used to effectively approximate "l-bits".

5.6 Disordered Hubbard model

We turn to Hubbard model with disorder like in the Chapter 4 and 5 but now the disorder can couple also to spins.

$$H = -t_h \sum_{i,\sigma} (c^\dagger_{i+1,\sigma} c_{i,\sigma} + H.c.) + U \sum_i \hat{n}_{i,\uparrow}\hat{n}_{i,\downarrow} + \sum_i \epsilon_i \hat{n}_i + \sum_i (\hat{n}_{i,\uparrow} - \hat{n}_{i,\downarrow}) h_i. \quad (5.15)$$

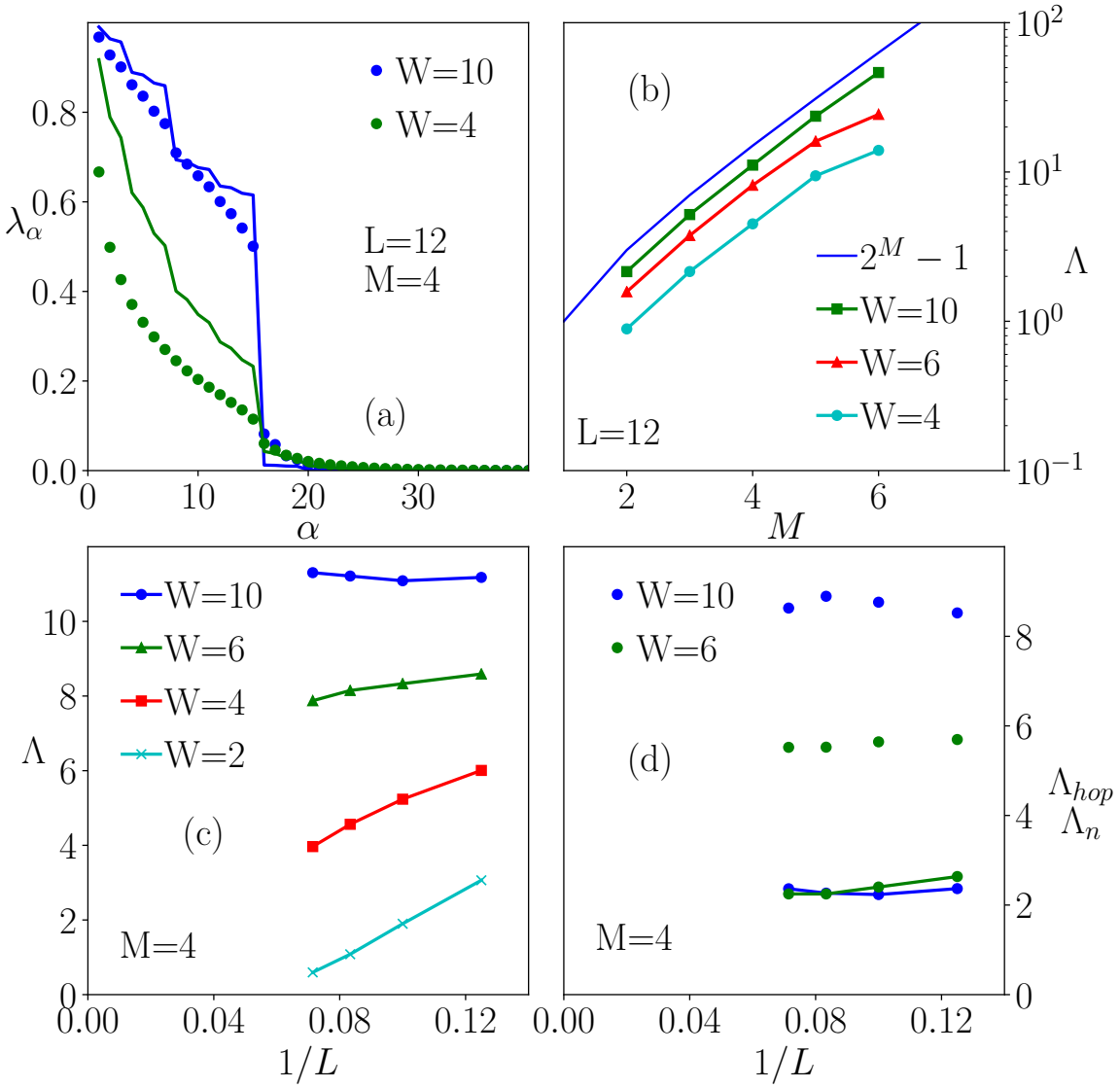

Figure 5.10: Results for disordered chain of spinless fermions. (a) Sorted eigenvalues λ_α (local components of LIOM) for $V = 1$ (points) and for Anderson insulator, $V = 0$ (lines), (b) total weight of LIOM Λ for various supports M and different disorders W, (c) finite–size scaling of Λ with $1/L$ for $M = 4$ and different W, (d) total weights vs $1/L$ constructed from local operators without hopping (Λ_n – points) or with at least one hopping term (Λ_{hop} – points with lines), for $W = 6$ and $W = 10$.

We expect that there should be $4^M - 1$ LIOMs if there is full MBL. At first we consider disorder coupled only to charges, i.e. $h_i = 0$. We jump straight to strong disorder of $W = 15$ to decrease the influence of finite size effects [77, 78].

In figure 5.11 (a) we have total weight Λ for various M where undoubtedly it exceeds the number of LIOMs in the spinless case $2^M - 1$ but seems to be equal approximately $0.4 * 4^M$. This is not enough for full MBL, especially considering results in panel (b). Then, we introduce random magnetic field $h_i \neq 0$ (thus breaking SU(2) symmetry) as a random variable from range $[-W_h, W_h]$. It increased the number of LIOMs to 15 which is the expected value for $M = 2$ exactly as described in [78, 82, 83, 133].

Going back to system without random magnetic field, in figure 5.11 (c) we see that it is not clear where the discontinuity begins. However, the values start to drop much sharper after about $3^M - 1$ operators. To get more insight, we use restriced basis of orthogonal operators O excluding those with hopping terms. As it was stated in previous section, 'non-hopping' operators are dominant in this regime while apparently 'hopping' ones make the plot fuzzy near the discontinuity. As presented on panel (d) the jump is now visible exactly where we suspected it to be. Additionally, when we check even stronger disorder, the jump is slightly better exposed. The 3^M scaling can be explained by the fact that without hopping, every operator O must be composed of the only three single-site, SU(2) invariant operators: identity I_i, $\sqrt{2}(\hat{n}_{i,\uparrow} + \hat{n}_{i,\downarrow} - 1)$ or $(2\hat{n}_{i,\uparrow} - 1)(2\hat{n}_{i,\downarrow} - 1)$.

5.7 Conclusions

We showed that using new method for creating LIOMs for given Hamiltonian we can decide whether this system exhibits MBL behaviour or not. For spinless systems we got exactly the expected number of LIOMs $2^M - 1$ indicating full MBL. On the other hand, for disordered Hubbard model the number of LIOMs is insufficient, $3^M - 1$ against required $4^M - 1$, so unless we have disorder both in charge and spin sector, the localization is not complete.

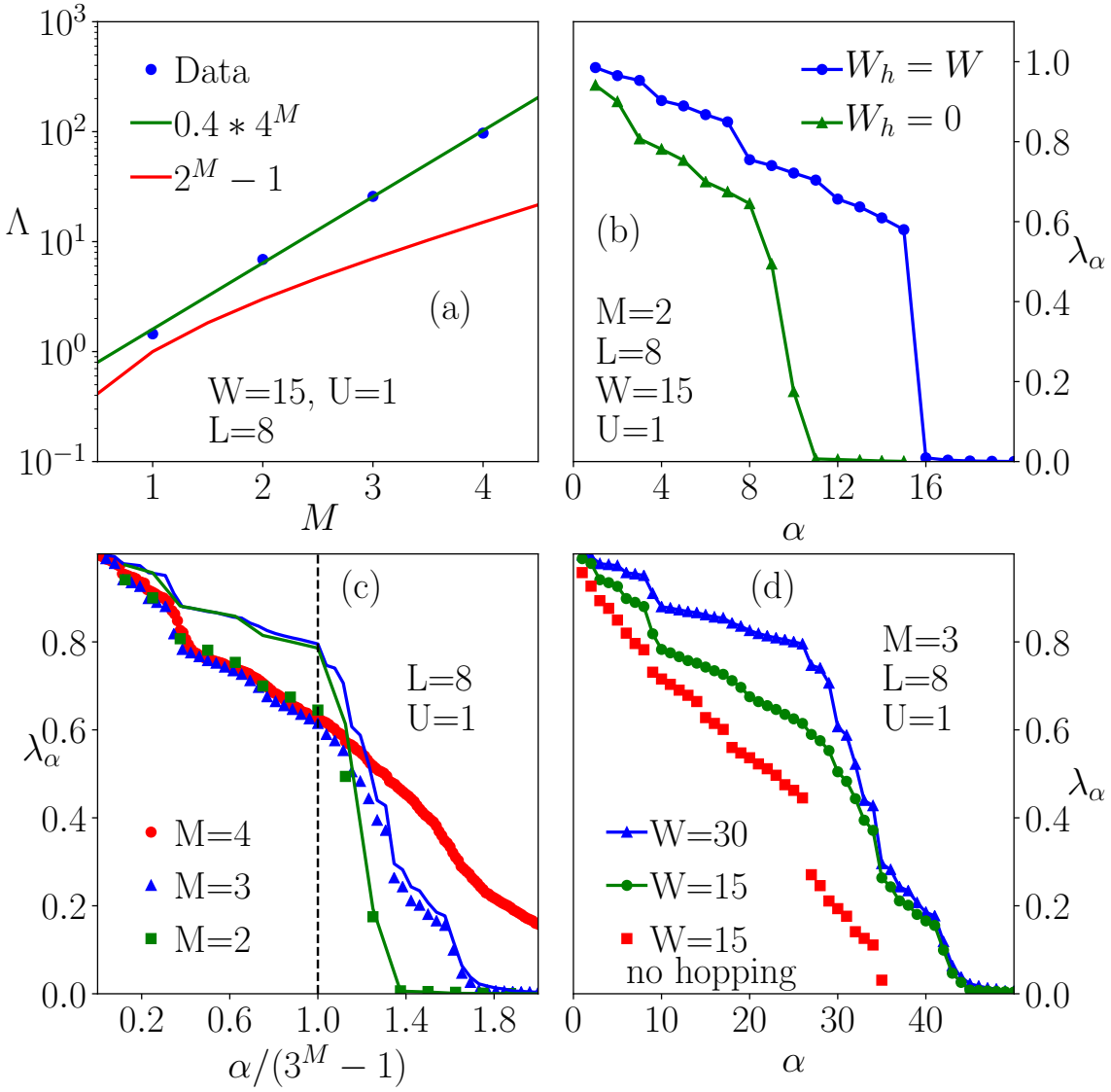

Figure 5.11: Results for disordered Hubbard chain. (a) total weight Λ of LIOM (points) for various supports M together with two different estimates; (b),(c),(d): sorted averaged eigenvalues λ_α of LIOM. (b) results for LIOM constructed for Hubbard chain without and with random magnetic field, respectively. Points and lines in (c) show results for $W = 15$ and $W = 30$, respectively. (d) LIOM constructed from local operators with and without hopping terms, respectively.

List of publications

1. M. Kozarzewski, P. Prelovšek, M. Mierzejewski, *"Distinctive response of many-body localized systems to strong electric field"*, Phys. Rev. B **93**, 235151 (2016)

2. M. Mierzejewski, M. Kozarzewski, P. Prelovšek, *"Counting local integrals of motion in disordered spinless-fermion and Hubbard chains"*, Phys. Rev. B **97**, 064204 (2018)

3. M. Kozarzewski, P. Prelovšek, M. Mierzejewski, *"Spin Subdiffusion in the Disordered Hubbard Chain"*, Phys. Rev. Lett. **120**, 246602 (2018)

4. M. Kozarzewski, M. Mierzejewski, P. Prelovšek, *"Suppressed energy transport in the strongly disordered Hubbard chain"*, Phys. Rev. B **99**, 241113(R) (2019)

Bibliography

[1] J. Moore, *"The birth of topological insulators."*, Nature **464**, 194–198 (2010)

[2] J. H. de Boer, E. J. W. Verwey, *"Semiconductors with partially and with completely filled 3d-lattice bands"*, Proceedings of the Physical Society, Volume **49**, Number 4S (1937)

[3] N. F. Mott, *"The basis of the electron theory of metals, with special reference to the transition metals"*, Proceedings of the Physical Society. Section A, Volume **62**, Number 7 (1949)

[4] Y. Taguchi, T. Matsumoto, Y. Tokura, *"Dielectric breakdown of one-dimensional Mott insulators Sr_2CuO_3 and $SrCuO_2Y$ "*, Phys. Rev. B, **62** 7015 (2000)

[5] C. Vaju, L. Cario, B. Corraze, E. Janod, V. Dubost, T. Cren, D. Roditchev, D. Braithwaite, O. Chauvet, *"Electric-pulse-driven electronic phase separation, insulator–metal transition, and possible superconductivity in a mott insulator"*, Advanced Materials **20**, 2760 (2008)

[6] T.-L. Wi, L. Whittaker, S. Banerjee, G. Sambandamurthy, *"Temperature and voltage driven tunable metal-insulator transition in individual $W_xV_{1-x}O_2$ nanowires"*, Phys. Rev. B **83**, 073101 (2011)

[7] V. Guiot, L. Cario, E. Janod, B. Corraze, V. T. Phuoc, M. Rozenberg, P. Stoliar, T. Cren, D. Roditchev, *"Avalanche breakdown in $GaTa_4Se_{8-x}Te_x$ narrow-gap Mott insulators"*, Nature communications **4**, 1722 (2013)

[8] P. W. Anderson, *"Absence of diffusion in certain random lattices"*, Phys. Rev. **109**, 1492 (1958)

[9] E. Abrahams, P. W. Anderson, D. C. Licciardello, T. V. Ramakrishnan, *"Scaling Theory of Localization: Absence of Quantum Diffusion in Two Dimensions"*, Phys. Rev. Lett. **42**, 673 (1979)

[10] S. Yoshino, M. Okazaki, *"Numerical Study of Electron Localization in Anderson Model for Disordered Systems: Spatial Extension of Wavefunction"*, Journal of the Physical Society of Japan, Vol. 43, No. 2 : pp. 415-423 (1977)

[11] A. MacKinnon, B. Kramer, *"One-Parameter Scaling of Localization Length and Conductance in Disordered Systems"*, Phys. Rev. Lett. **47**, 1546 (1981)

[12] D. S. Wiersma, P. Bartolini, A. Lagendijk, R. Righini, *"Localization of light in a disordered medium."*, Nature **390**, 671–673 (1997)

[13] M. Störzer, P. Gross, C. M. Aegerter, G. Maret, *"Observation of the Critical Regime Near Anderson Localization of Light"*, Phys. Rev. Lett. **96**, 063904 (2006)

[14] T. Schwartz, G. Bartal, S. Fishman, M. Segev, *"Transport and Anderson localization in disordered two-dimensional photonic lattices"*, Nature **446**, 52–55 (2007)

[15] Yoav Lahini, Assaf Avidan, Francesca Pozzi, Marc Sorel, Roberto Morandotti, Demetrios N. Christodoulides, and Yaron Silberberg, *"Anderson Localization and Nonlinearity in One-Dimensional Disordered Photonic Lattices"*, Phys. Rev. Lett. **100**, 013906 (2008)

[16] S. Karbasi, R. J. Frazier, K. W. Koch, T. Hawkins, J. Ballato, A. Mafi, *"Image transport through a disordered optical fibre mediated by transverse Anderson localization."*, Nat Commun **5**, 3362 (2014)

[17] J. Chabé, G. Lemarié, B. Grémaud, D. Delande, P. Szriftgiser, J. C. Garreau, *"Experimental Observation of the Anderson Metal-Insulator Transition with Atomic Matter Waves"*, Phys. Rev. Lett. **101**, 255702 (2008)

[18] G. Roati, C. D'Errico, L. Fallani, M. Fattori, C. Fort, M. Zaccanti, G. Modugno, M. Modugno, M. Inguscio , *"Anderson localization of a non-interacting Bose–Einstein condensate."*, Nature **453**, 895–898 (2008)

[19] J. Billy, V. Josse, Z. Zuo, A. Bernard, B. Hambrecht, P. Lugan, D. Clément, L. Sanchez-Palencia, P. Bouyer, A. Aspect, *"Direct observation of Anderson localization of matter waves in a controlled disorder"*, Nature volume **453**, pages 891–894 (2008)

[20] J. W. Goodman, *"Speckle Phenomena in Optics"*, ISBN 0-9747077-9-1. Published by Roberts and Company, Greenwood Village, CO USA, (2007)

[21] R. Dalichaouch, J. P. Armstrong, S. Schultz, P. M. Platzman, S. L. McCall, *"Microwave localization by two-dimensional random scattering."*, Nature **354**, 53–55 (1991)

[22] R.L.Weaver, *"Anderson localization of ultrasound"*, Wave Motion Volume **12**, Issue 2, Pages 129-142 (1990)

[23] L. Fleishman and P. W. Anderson, *"Interactions and the Anderson transition"*, Phys. Rev. B **21**, 2366 (1980)

[24] I. V. Gornyi, A. D. Mirlin, D. G. Polyakov, *"Interacting Electrons in Disordered Wires: Anderson Localization and Low-T Transport"*, Phys. Rev. Lett. **95**, 206603 (2005)

[25] R. Vosk, D. A. Huse, E. Altman, *"Theory of the Many-Body Localization Transition in One-Dimensional Systems"*, Phys. Rev. X **5**, 031032 (2015)

[26] P. Jordan, E. Wigner, *"Über das Paulische Äquivalenzverbot."*, Z. Physik **47**, 631–651 (1928)

[27] D. M. Basko, I. L. Aleiner, B. L. Altshuler, *"Possible experimental manifestations of the many-body localization"*, Phys. Rev. B 76, 052203 (2007)

[28] V. Oganesyan, D. A. Huse, *"Localization of interacting fermions at high temperature* Physical Review B, **75** 155111 (2007)

[29] A. Pal, D. A. Huse, *"Many-body localization phase transition"*, Phys. Rev. B **82**, 174411 (2010)

[30] D. J. Luitz, N. Laflorencie, F. Alet, *"Many-body localization edge in the random-field Heisenberg chain"*, Phys. Rev. B **91**, 081103(R) (2015)

[31] Y. Y. Atas, E. Bogomolny, O. Giraud, G. Roux, *"Distribution of the Ratio of Consecutive Level Spacings in Random Matrix Ensembles"*, Phys. Rev. Lett. **110**, 084101 (2013)

[32] Y. Geng, T. Hu, K. Xue, H. Li, H. Zhao, X. Li, H. Ren, *"Many-Body Localization Transition in the Heisenberg Ising Chain."*, Int J Theor Phys **59**, 1330–1337 (2020)

[33] R. Yao, J. Zakrzewski, *"Many-body localization in the Bose-Hubbard model: Evidence for mobility edge"*, Phys. Rev. B **102**, 014310 (2020)

[34] T. Chanda, P. Sierant, J. Zakrzewski, *"Many-body localization transition in large quantum spin chains: The mobility edge"*, Phys. Rev. Research **2**, 032045(R) (2020)

[35] A. Samanta, K. Damle, R. Sensarma, *"Tracking the many-body localized to ergodic transition via extremal statistics of entanglement eigenvalues"*, Phys. Rev. B **102**, 104201 (2020)

[36] A. Maksymov, P. Sierant, J. Zakrzewski, *"Many-body localization in one dimensional optical lattice with speckle disorder"*, https://arxiv.org/abs/2008.00219

[37] E. Chertkov, B. Villalonga, B. K. Clark, *"Numerical evidence for many-body localization in two and three dimensions"*, https://arxiv.org/abs/2007.02959

[38] P. Sierant, J. Zakrzewski, *"Level statistics across the many-body localization transition"*, Phys. Rev. B **99**, 104205 (2019)

[39] P. Sierant, J. Zakrzewski, *"Model of level statistics for disordered interacting quantum many-body systems"*, Phys. Rev. B **101**, 104201 (2020)

[40] J. M. Deutsch, *"Quantum statistical mechanics in a closed system"*, Phys. Rev. A **43**, 2046 (1991)

[41] M. Srednicki, *"Chaos and quantum thermalization"*, Phys. Rev. E **50**, 888 (1994)

[42] L. F. Santos, M. Rigol, *"Localization and the effects of symmetries in the thermalization properties of one-dimensional quantum systems"*, Phys. Rev. E **82**, 031130 (2010); Erratum Phys. Rev. E **87**, 029904 (2013)

[43] M. Rigol, *"Quantum quenches and thermalization in one-dimensional fermionic systems"*, Phys. Rev. A **80**, 053607 (2009); Erratum Phys. Rev. A **87**, 029902 (2013)

[44] R. Steinigeweg, J. Herbrych, P. Prelovšek, *"Eigenstate thermalization within isolated spin-chain systems"*, Phys. Rev. E **87**, 012118 (2013)

[45] H. Kim, T. N. Ikeda, D. A. Huse, *"Testing whether all eigenstates obey the eigenstate thermalization hypothesis"*, Phys. Rev. E **90**, 052105 (2014)

[46] J. Smith, A. Lee, P. Richerme, et al., *"Many-body localization in a quantum simulator with programmable random disorder"*, Nature Phys **12**, 907–911 (2016)

[47] J. A. Kjäll, J. H. Bardarson, F. Pollmann, *"Many-Body Localization in a Disordered Quantum Ising Chain"*, Phys. Rev. Lett. **113**, 107204 (2014)

[48] D. J. Luitz, N. Laflorencie, F. Alet, *"Extended slow dynamical regime close to the many-body localization transition"*, Phys. Rev. B **93**, 060201(R) (2016)

[49] V. Khemani, S. P. Lim, D. N. Sheng, D. A. Huse, *"Critical properties of many-body localization transition"*, Phys. Rev. X **7**, 021013 (2017)

[50] J. Eisert, M. Cramer, M. B. Plenio, *"Area laws for the entanglement entropy"*, Rev. Mod. Phys. **82**, 277 (2010)

[51] A. M. Kaufman, M. E. Tai, A. Lukin, M. Rispoli, R. Schittko, P. M. Preiss, M. Greiner, *"Quantum thermalization through entanglement in an isolated many-body system"*, Science 353 **794**, 00081 (2016)

[52] R. Islam, R. Ma, P. M. Preiss, M. Eric Tai, A. Lukin, M. Rispoli, M. Greiner, *"Measuring entanglement entropy in a quantum many-body system"*, Nature 528 **77**, 00151 (2015)

[53] M. Žnidarič, T. Prosen, P. Prelovšek, *"Many-body localization in the Heisenberg XXZ magnet in a random field"*, Phys. Rev. B **77**, 064426 (2008)

[54] J. H. Bardarson, F. Pollmann, J. E. Moore, *"Unbounded Growth of Entanglement in Models of Many-Body Localization"*, Phys. Rev. Lett. **109**, 017202 (2012)

[55] M. Serbyn, Z. Papić, D. A. Abanin, *"Universal Slow Growth of Entanglement in Interacting Strongly Disordered Systems"*, Phys. Rev. Lett. **110**, 260601 (2013)

[56] D. J. Luitz, Y. Bar Lev, *"Absence of slow particle transport in the many-body localized phase"*, Phys. Rev. B **102**, 100202(R) (2020)

[57] M. Serbyn, Z. Papić, D. A. Abanin, *"Criterion for Many-Body Localization-Delocalization Phase Transition"*, Phys. Rev. X **5**, 041047 (2015)

[58] M. Serbyn, Z. Papić, D. A. Abanin, *"Local Conservation Laws and the Structure of the Many-Body Localized States"*, Phys. Rev. Lett. **111**, 127201 (2013)

[59] D. A. Huse, R. Nandkishore, V. Oganesyan, *"Phenomenology of fully many-body-localized systems"*, Phys. Rev. B **90**, 174202 (2014)

[60] L. Rademaker, M. Ortuño, *"Explicit Local Integrals of Motion for the Many-Body Localized State"*, Phys. Rev. Lett. **116**, 010404 (2016)

[61] A. Chandran, I. H. Kim, G. Vidal, D. A. Abanin, *"Constructing local integrals of motion in the many-body localized phase"*, Phys. Rev. B **91**, 085425 (2015)

[62] S. Inglis, L. Pollet, *"Accessing Many-Body Localized States through the Generalized Gibbs Ensemble"*, Phys. Rev. Lett. 117, 120402 (2016)

[63] O. S. Barišić, P. Prelovšek, *"Conductivity in a disordered one-dimensional system of interacting fermions"*, Phys. Rev. B **82**, 161106(R) (2010)

[64] K. Agarwal, S. Gopalakrishnan, M. Knap, M. Müller, E. Demler, *"Anomalous Diffusion and Griffiths Effects Near the Many-Body Localization Transition"*, Phys. Rev. Lett. **114**, 160401 (2015)

[65] R. Steinigeweg, J. Herbrych, F. Pollmann, W. Brenig, *"Typicality approach to the optical conductivity in thermal and many-body localized phases"*, Phys. Rev. B **94**, 180401(R) (2016)

[66] O. S. Barišić, J. Kokalj, I. Balog, P. Prelovšek, *"Dynamical conductivity and its fluctuations along the crossover to many-body localization"*, Phys. Rev. B **94**, 045126 (2016)

[67] D. J. Luitz, Y. Bar Lev, *"The ergodic side of the many-body localization transition"*, Ann. Phys. (Berlin) **529**, No. 7, 1600350 (2017)

[68] P. Prelovšek, M. Mierzejewski, O. Barišić, J. Herbrych, *"Density correlations and transport in models of many-body localization"*, Ann. Phys. (Berlin) **529**, No. 7, 1600362 (2017)

[69] S. Gopalakrishnan, M. Müller, V. Khemani, M. Knap, E. Demler, D. A. Huse, *"Low-frequency conductivity in many-body localized systems"*, Phys. Rev. B **92**, 104202 (2015)

[70] M. Kozarzewski, P. Prelovšek, M. Mierzejewski, *"Distinctive response of many-body localized systems to strong electric field"*, Phys. Rev. B **93**, 235151 (2016)

[71] M. Žnidarič, A. Scardicchio, V. K. Varma, *"Diffusive and Subdiffusive Spin Transport in the Ergodic Phase of a Many-Body Localizable System"*, Phys. Rev. Lett. **117**, 040601 (2016)

[72] M. Schreiber, S. S. Hodgman, P. Bordia, H. P. Lüschen, M. H. Fischer, R. Vosk, E. Altman, U. Schneider, and I. Bloch, *"Observation of many-body localization of interacting fermions in a quasi-random optical lattice"*, Science **349**, 842 (2015)

[73] P. Bordia, H. P. Lüschen, S. S. Hodgman, M. Schreiber, I. Bloch, U. Schneider, *"Coupling Identical one-dimensional Many-Body Localized Systems"*, Phys. Rev. Lett. **116**, 140401 (2016)

[74] H. P. Lüschen, P. Bordia, S. Scherg, F. Alet, E. Altman, U. Schneider, I. Bloch, *"Observation of Slow Dynamics near the Many-Body Localization Transition in One-Dimensional Quasiperiodic Systems"*, Phys. Rev. Lett. **119**, 260401 (2017)

[75] S. Iyer, V. Oganesyan, G. Refael, D. A. Huse, *"Many-body localization in a quasiperiodic system"*, Phys. Rev. B **87**, 134202 (2013)

[76] V. P. Michal, B. L. Altshuler, G. V. Shlyapnikov, *"Delocalization of Weakly Interacting Bosons in a 1D Quasiperiodic Potential"*, Phys. Rev. Lett. **113**, 045304 (2014)

[77] R. Mondaini and M. Rigol, *"Many-body localization and thermalization in disordered Hubbard chains"*, Phys. Rev. A **92**, 041601(R) (2015)

[78] P. Prelovšek, O. S. Barišić, M. Žnidarič, *"Absence of full many-body localization in the disordered Hubbard chain"*, Phys. Rev. B 94, 241104(R) (2016)

[79] M. Mierzejewski, M. Kozarzewski, P. Prelovšek, *"Counting local integrals of motion in disordered spinless-fermion and Hubbard chains"*, Phys. Rev. B **97**, 064204 (2018)

[80] R. Vasseur, A. C. Potter, S. A. Parameswaran, *"Quantum Criticality of Hot Random Spin Chains"*, Phys. Rev. Lett. **114**, 217201 (2015)

[81] R. Vasseur, A. J. Friedman, S. A. Parameswaran, A. C. Potter, *"Particle-hole symmetry, many-body localization, and topological edge modes"*, Phys. Rev. B **93**, 134207 (2016)

[82] A. C. Potter, R. Vasseur, *"Symmetry constraints on many-body localization"*, Phys. Rev. B **94**, 224206 (2016)

[83] I. V. Protopopov, W. W. Ho, D. A. Abanin, *"Effect of SU(2) symmetry on many-body localization and thermalization"*, Phys. Rev. B **96**, 041122(R) (2017)

[84] S. Gopalakrishnan, K. R. Islam, M. Knap, *"Noise-Induced Subdiffusion in Strongly Localized Quantum Systems"*, Phys. Rev. Lett. **119**, 046601 (2017)

[85] Y. Bar Lev, D. M. Kennes, C. Klöckner, D. R. Reichman, C. Karrasch, *"Transport in quasiperiodic interacting systems: From superdiffusion to subdiffusion"*, EPL (Europhysics Letters), Volume **119**, Number 3 (2017)

[86] P. Prelovšek, J. Bonča, M. Mierzejewski, *"Transient and persistent particle subdiffusion in a disordered chain coupled to bosons"*, Phys. Rev. B **98**, 125119 (2018)

[87] M. Kozarzewski, P. Prelovšek, M. Mierzejewski, *"Spin Subdiffusion in the Disordered Hubbard Chain"*, Phys. Rev. Lett. **120**, 246602 (2018)

[88] M. Kozarzewski, M. Mierzejewski, P. Prelovšek, *"Suppressed energy transport in the strongly disordered Hubbard chain"*, Phys. Rev. B **99**, 241113(R) (2019)

[89] Negele, J.W. and Orland, H., *Quantum Many-particle Systems*, ISBN:9780786743179, Advanced Books Classics, (2008), Westview Press

[90] Combinatorial Number System at Wikipedia

[91] Ivan P. Stanimirović, Milan B. Tasić, *Performance comparisons of storage formats for sparse matrices*, Facta Universitatis, Ser. Math. Inform. **24** (2009), 39-51

[92] J. G. F. Francis, *" The QR Transformation A Unitary Analogue to the LR Transformation—Part 1"* The Computer Journal, Volume **4**, Issue 3, Pages 265–271 (1961)

[93] J. G. F. Francis, *"The QR Transformation—Part 2"*, The Computer Journal, Volume **4**, Issue 4, Pages 332–345 (1962)

[94] V.N.Kublanovskaya, *"On some algorithms for the solution of the complete eigenvalue problem"*, USSR Computational Mathematics and Mathematical Physics, Volume **1**, Isssue 3, Pages 637-657 (1962)

[95] Alston Householder, *"Unitary triangularization of a nonsymmetric matrix"*, Journal of the ACM(JACM), Association for Computing Machinery (1958)

[96] Inderjit Singh Dhillon, *"A New $O(n^2)$ Algorithm for the Symmetric Tridiagonal Eigenvalue Eigenvector Problem"*, PhD thesis, University of California, Berkeley

[97] James T. Albrecht, Cy P. Chan, and Alan Edelman, *"Sturm sequences and random eigenvalue distributions"*, Foundations of Computational Mathematics, Volume **9**, Issue 4, pp 461-483 (2009)

[98] W. Barth, R. S. Martin and J. H. Wilkinson, *"Calculation of the eigenvalues of a symmetric tridiagonal matrix by the method of bisection"*, Numerische Mathematik, Volume **4**, Issue 1, pp 362-367 (1962)

[99] Ilse C. F. Ipsen, *"Computing an eigenvector with inverse iteration"*, SIAM Rev., **39**, 254–291 (1997)

[100] W. T. Lee, *"Tridiagonal Matrices: Thomas Algorithm"*, `http://www3.ul.ie/wlee/ms6021_thomas.pdf`

[101] Andre Leger, *"Lanczos method seminar for eigenvalue reading group"*, `http://people.bath.ac.uk/mamamf/talks/lanczos.pdf`

[102] H. D. Simon, *"Analysis of the symmetric Lanczos algorithm with reorthogonalization methods"*, Linear Algebra and its Applications Volume **61**, Pages 101-131 (1984)

[103] M. W. Long, P. Prelovšek, S. El Shawish, J. Karadamoglou, X. Zotos, *"Finite-temperature dynamical correlations using the microcanonical ensemble and the Lanczos algorithm"*, Phys. Rev. B **68**, 235106 (2003)

[104] X. Zotos, *"Microcanonical Lanczos method"*, Philosophical Magazine, **86** 17-18, 2591-2601 (2006)

[105] P. Prelovšek, J. Bonča, *"Ground State and Finite Temperature Lanczos Methods"*, Strongly Correlated Systems. Springer Series in Solid-State Sciences, vol **176** Springer, Berlin, (2013)

[106] DLMF: 3.7 - Ordinary Differential Equations

[107] H. Tal-Ezer, R. Kosloff, *"An accurate and efficient scheme for propagating the time dependent Schrödinger equation"*, The Journal of Chemical Physics, **81** 9, pages 3967-3971 (1984)

[108] Jun Jing, H.R. Ma, *"Polynomial scheme for time evolution of open and closed quantum systems"*, Phys. Rev. E, **75** 016701 (2007)

[109] Martin Kreh, *"The Bessel Functions §1 The Bessel differential equation"*, `http://www.math.psu.edu/papikian/Kreh.pdf`

[110] Subroto Mukerjee, Vadim Oganesyan, David Huse, *"Statistical theory of transport by strongly interacting lattice fermions"*, Physical Review B, **73** 035113 (2006)

[111] M. Mierzejewski, T. Prosen, D. Crivelli, P. Prelovsek, *"Eigenvalue Statistics of Reduced Density Matrix during Driving and Relaxation"*,Phys. Rev. Lett. **110**, 200602 (2013)

[112] M. Mierzejewski, P. Prelovsek, *"Nonlinear Current Response of an Isolated System of Interacting Fermions"*, Phys. Rev. Lett. **105** 186405 (2010)

[113] D. L. Shelepyanski, *"Coherent propagation of two interacting particles in a random potential"*, Phys. Rev. Lett. **73**, 2607 (1994)

[114] Ph. Jacquod, D. L. Shepelyansky, *"Two interacting quasiparticles above the Fermi sea"*, Phys. Rev. Lett. **78**, 4986 (1997)

[115] K. Agarwal, E. Altman, E. Demler, S. Gopalakrishnan, D. A. Huse, M. Knap, *"Rare region effects and dynamics near the many body localization transition"*, Annalen der Physik **529**, 1600326 (2017)

[116] Pranjal Bordia, Henrik Lüschen, Sebastian Scherg, Sarang Gopalakrishnan, Michael Knap, Ulrich Schneider, and Immanuel Bloch , *"Probing slow relaxation and many-body localization in two-dimensional quasiperiodic systems"*, Phys. Rev. X **7**, 041047 (2017)

[117] DLMF: 5.6.4 - Inequalities

[118] DLMF: 5.11.12 - Asymptotic Expansions

[119] B. Baeumer, M. M. Meerschaert, *"Properties of contiuous time random walks with waiting times."*

[120] N. Masudaa, M. A. Porter, R. Lambiottec, *"Random walks and diffusion on networks"*, Physics Reports Volumes 716–717, **22**, 1-58 (2017)

[121] Inverse distribution - Wikipedia

[122] J.-P. Bouchaud, A. Georges, *"Anomalous diffusion in disordered media: Statistical mechanisms, models and physical applications"*, Physics Reports **195**, 173 – 175 (1990)

[123] J. Zakrzewski, D. Delande, *"Spin-charge separation and many-body localization"*, Phys. Rev. B **98**, 014203 (2018)

[124] S. R. White, *"Density matrix formulation for quantum renormalization groups"*, Phys. Rev. Lett. 69, 2863 (1992)

[125] I. V. Protopopov, R. K. Panda, T. Parolini, A. Scardicchio, E. Demler, D. A. Abanin, *"Non-Abelian Symmetries and Disorder: A Broad Nonergodic Regime and Anomalous Thermalization"*, Phys. Rev. X 10, 011025 (2020)

[126] C. Karrasch, D. M. Kennes, F. Heidrich-Meisner, *"Thermal Conductivity of the One-Dimensional Fermi-Hubbard Model"*, Phys. Rev. Lett. 117, 116401 (2016)

[127] J. Schmidt, M. R. G. Marques, S. Botti, M. A. L. Marques, *"Recent advances and applications of machine learning in solid-state materials science"*, npj Computational Materials volume 5, Article number: 83 (2019)

[128] T. E. O'Brien, D. A. Abanin, G. Vidal, Z. Papić, *"Explicit construction of local conserved operators in disordered many-body systems"*, Phys. Rev. B **94**, 144208 (2016)

[129] M. Mierzejewski, P. Prelovšek, T. Prosen, *"Identifying Local and Quasilocal Conserved Quantities in Integrable Systems"* hrefhttps://journals.aps.org/prl/abstract/10.1103/PhysRevLett.114.140601Phys. Rev. Lett. **114**, 140601 (2015)

[130] M. Mierzejewski, T. Prosen, P. Prelovšek, *"Approximate conservation laws in perturbed integrable lattice models"*, Phys. Rev. B **92**, 195121 (2015)

[131] Y. Bar Lev, G. Cohen, D. R. Reichman, *"Absence of Diffusion in an Interacting System of Spinless Fermions on a One-Dimensional Disordered Lattice"*, Phys. Rev. Lett. **114**, 100601 (2015)

[132] M. Mierzejewski, J. Herbrych, P. Prelovšek, *"Universal dynamics of density correlations at the transition to the many-body localized state"*, Phys. Rev. B **94**, 224207 (2016)

[133] A. Chandran, V. Khemani, C. R. Laumann, S. L. Sondhi, *"Many-body localization and symmetry-protected topological order"*, Phys. Rev. B **89**, 144201 (2014)